Chapter 4. Absorption and radiation of Electromagnetic radiations by surface active films

Crude oil slicks, and silicone oil films used in evaporating reducing films, have an amorphous structure which allows the formation of a surface film of any thickness. For example, the commercially available product; “Aquatain”, with a recommended thickness of around 1 μm (2008), is relatively easy to detect by optical methods, having a thickness comparable to the wavelength of visible light. In contrast, self-assembling monolayers exist in layers the thickness of one molecule, at around 2-3 nm, three orders of magnitude smaller than the thickness of silicone oils and much smaller than the wavelength of visible light. While the evaporation resistance depends on the thickness for silicone oils, it depends on surface pressure (reduction in surface tension) for monolayers (see Section 1.8.2). Despite the considerable differences between the thicknesses of surface films such as Aquatain and monolayers, there remains the possibility of employing sensors that rely on the emission or scattering electromagnetic radiation. Consequently a brief discussion of relevant electromagnetic interaction properties of both surface active films and monolayers will follow. Where possible, with the discussion will be informed by relevant experimental data produced.

Nomenclature

Reflectivity (*R*) - The fraction of intensity of reflected radiation, compared with incident radiation for a particular wavelength or region of wavelengths for thick objects where the thickness will not affect the reflectivity. Relative or percentage reflectivity is then the ratio of reflected radiation intensity compared to incident radiation.

Reflectance - Similar to reflectivity, however the International Commission of Illumination (2010) restrict the application of reflectance to thin objects, where internal reflections may cause the reflectance to vary with thickness. This term would certainly be useful in describing reflection intensity from a surface active layer, however not a clear water surface.

To avoid calling reflection ratios from the water reflectivity and from monolayers reflectance, only the term reflectivity will be used and it will be assumed it is known that it may vary with the thickness of the surface active layer.

4.1.1 Wavelength dependent surface emission characteristics

The amount of blackbody radiation radiated by a surface is dependent on the temperature and the emissivity according to the relationship:

$$P = \varepsilon \sigma T^4 \qquad (4.1)$$

where P is the radiant energy Wm^{-2}, σ is the Stefan-Boltzmann constant = 5.67032×10^{-8} $Wm^{-2}T^4$, T is the temperature in K, ε is the emissivity.

In the IR region, the absorption of radiation α by a film is related to reflection R and transmission T by the following:

$$\alpha = 1 - R - T \qquad (4.2)$$

as incoming radiation must be either transmitted, radiated or absorbed. If the surface is at thermal equilibrium Kirchhoff's second law holds (Pigeat, Rouxel, & Weber 1998) stating the radiant energy is equal to that absorbed. Therefore:

$$\varepsilon = \alpha \qquad \text{so:} \qquad \varepsilon = 1 - R - T \qquad (4.3)$$

However, if just the top surface in contact with air is considered, the water body (with or without film) can be considered opaque and totally absorbing and this relationship reduces to (Konda *et al.* 1994; Shih & Andrews 2008):

$$\varepsilon = 1 - R \qquad (4.4)$$

showing the emissivity can be calculated by measuring the reflectance under thermal equilibrium conditions. This relationship however is limited in its practical use as the water surface is rarely at thermal equilibrium with the surrounding air.

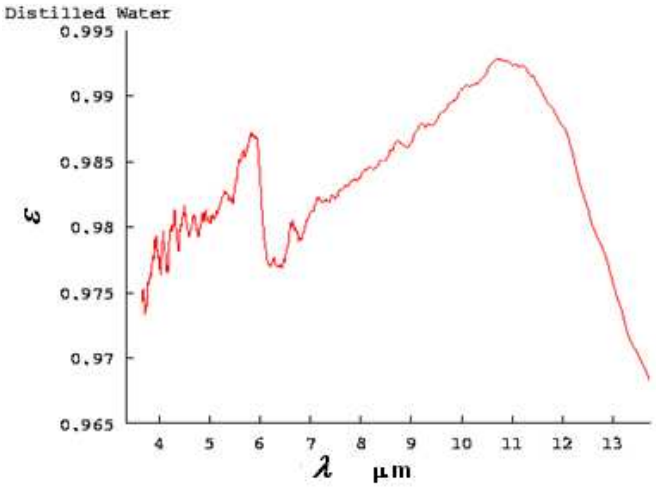

Figure 4.1 Emissivity ε of water in the infrared region. Source; Zhang (1999).

The emissivity of distilled water is shown in Figure 4.1, as determined under laboratory conditions by Zhang (1999), showing values in the IR region (4-14 μm) are between 0.970-0.993. This is the wavelength region where the water emissivity is highest, creating maximum contrast between water and the oil slick (Andreev, Gurov, & Khundzhua 1976; Daniels & Hover 1994; Ivanov, He, & Fang 2002); the latter possessing a slightly lower emissivity (Salisbury & D'Aria 1994).

An average value of 0.980 has been determined for distilled water by Robinson & Davies (1972) using an IR thermometer filter (8-14 μm) to find the value detected by an IR thermometer. They found virtually no difference in emissivity between distilled water, tap water and lake water (Lake Ontario). Oil slicks showed a reduction however, with machine oil of thickness 1-3 mm showing an emissivity of 0.960. Crude oil showed a value lower still, at 0.954.

The net radiation flux between the water surface and atmosphere into the water is given by:

$$Q = \varepsilon\sigma(T_{ws}^4 - T_{sky}^4) \tag{4.5}$$

where T_{WS} is the water surface temperature and T_{sky} is the effective sky temperature. The sky temperature is lower than the ambient air temperature, ranging from 10 ºC below ambient temperature for hot humid conditions, to 30 ºC below for dry cool conditions ((Smith 1994) quoting (Bliss 1961)).

Substituting a water surface at 293K into this equation reveals that for a 1 °C temperature rise to 294 K the radiated energy increases by 1.37% for the water surface term. If the sky is assumed to be an average of 20 ºC below the water temperature the increase in radiance would be 3.1% for a single degree rise in surface temperature.

The wavelength-dependent emission is described by the Stefan-Boltzmann Law, with a peak emission wavelength determined by temperature according to Wien's Displacement Law:

$$\lambda_m T = b \tag{4.6}$$

where λ_m is the peak emission wavelength, T is the temperature (K), and b is the constant of proportionality = 2.8978×10^{-3} m K. Substituting water at 20 °C produces a maximum radiation of:

$$\lambda = \frac{2.8978 \times 10^{-3}}{293} = 9.89\mu m \tag{4.7}$$

This is conveniently at the centre of the atmospheric window used by many IR radiometers, with ranges of 8-12 μm.

With increasing temperature the intensity of the radiant energy increases peak of the wavelength moves towards the higher energy, smaller wavelength end of the spectrum. IR measurements for determination of temperature of water surfaces generally suffer from ambient conditions for the sensor being at a higher temperature than the cooler water surface. This is often overcome either by calibrating the instrument for ambient air temperature, or by cooling the receiver to minimize background noise (Viehmann & Eubanks 1972).

4.2 Visual observations

The effects of monolayers on the surface of water storages are often conspicuous due to wave damping characteristics (examined in Chapter 2). For detection there either needs to be absorption at specific wavelengths as part of a characteristic absorption spectra (Section 4.40) or a change to the reflectivity of the surface, either by reflection from the upper surface due to a change in

emissivity, or interference from reflections from both top and lower surfaces of the surface active layer.

Highly reflective surface active layers would have the effect of lowering the water temperature by reflecting incident radiation. Gainer *et al.* (1969) measured the reflectivity on a large storage using solar radiation on monolayers, motor oils and silicone oils. They found the reflectivity to alter very little for monolayers, whereas thicker films such as aviation oil or silicone oils exhibit between 30% and 70% higher relative *R*, defined by:

$$\text{Relative}\, R = \frac{R_{film}}{R_w} \qquad (4.8)$$

where R_{film} is the reflectivity of the surface layer and R_w is the reflectivity of water (Table 4.1).

Table 4.1 Relative *R* of sample surface active layers. Source; Gainer *et al.* (1969)

Film	Relative *R*
Hecadecanol	0.94
Octanoic Acid	0.97
Linolic Acid	1.00
Aviation Oil *#65*	Immediately 1.81 Later 1.52 Still Later 1.30
Yellow silicone oil film	1.7

The lower relative *R* of hexadecanol would probably be from another cause and not a change in reflectivity. The wide variation in aviation oil of the same sample shows some of the difficulties in assigning an emissivity value to oils. Not only are there many types of oils, but for a particular oil, the emissivity may change with time. Interestingly the commercial product, “yellow silicone oil” (whose complete composition was unknown), shows a very high reflectance, and would probably be quite useful in lowering water temperature. Aquatain may also possess a reflectivity high enough to reduce water temperature. Gainer *et al.* found that monolayers are unfortunately generally colourless, with only linoleic acid and 10-undecenoic acid exhibiting observable colour.

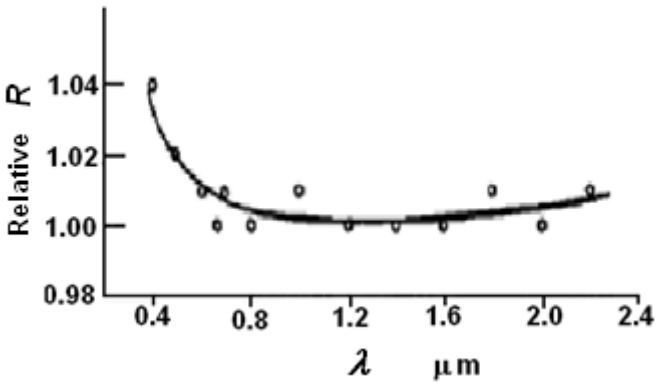

Figure 4.2 Relative *R* of hexadecanol monolayer when unpolarised monochromatic energy is incident at 20 °C. Adapted from Beard & Wiebelt (1966).

Accurate laboratory measurements of wavelength dependant relative *R* from a hexadecanol monolayer (Figure 4.2) were carried out by Beard and Wiebelt (1966), using a selected wavelength from a monochromator, and measuring the reflected intensity using a gonioreflectometer at an angle of 20 º. The results show a -1% decrease to 4% increase in relative reflectivity depending on the incident wavelengths. Over the range 0.4-2.2 µm, there is an increase towards the smaller wavelength end of the spectrum. This is convenient in field use in evaporation reduction as the highest relative *R*, and therefore highest effect on cooling water is around the peak of the solar radiation, at 0.5 µm. Despite this clear difference under controlled conditions, they still came to the conclusion that there was no significant 'observable' changes in reflection under field conditions when hexadecanol monolayer is added to a smooth lake.

4.2.1 Theoretical reflectivity *R* from top surface of surface active layer

Reflectance is also dependent on the angle of incidence and the polarisation of light used and this may be usable in detecting monolayers.

The polarisation-dependent surface reflectivity of water can be determined using the Fresnel reflection coefficients and refractive index of water:

$$R_p = \left(\frac{n_1 \cos\theta_1 - n_2 \cos\theta_2}{n_1 \cos\theta_1 + n_2 \cos\theta_2} \right)^2 = \left(\frac{\tan(\theta_2 - \theta_1)}{\tan(\theta_2 + \theta_1)} \right)^2 \qquad (4.9)$$

$$R_S = \left(\frac{n_1 \cos\theta_2 - n_2 \cos\theta_1}{n_1 \cos\theta_2 + n_2 \cos\theta_1} \right)^2 = \left(\frac{\sin(\theta_2 - \theta_1)}{\sin(\theta_2 + \theta_1)} \right)^2 \qquad (4.10)$$

where subscripts *p* and *s* denote vertical and horizontal planes of polarisation respectively, n_1 is the refractive index of air, n_2 is the refractive index of water and θ_1 is the angle of incidence measured from perpendicular to the water surface. θ_2 can be calculated using Snell's law.

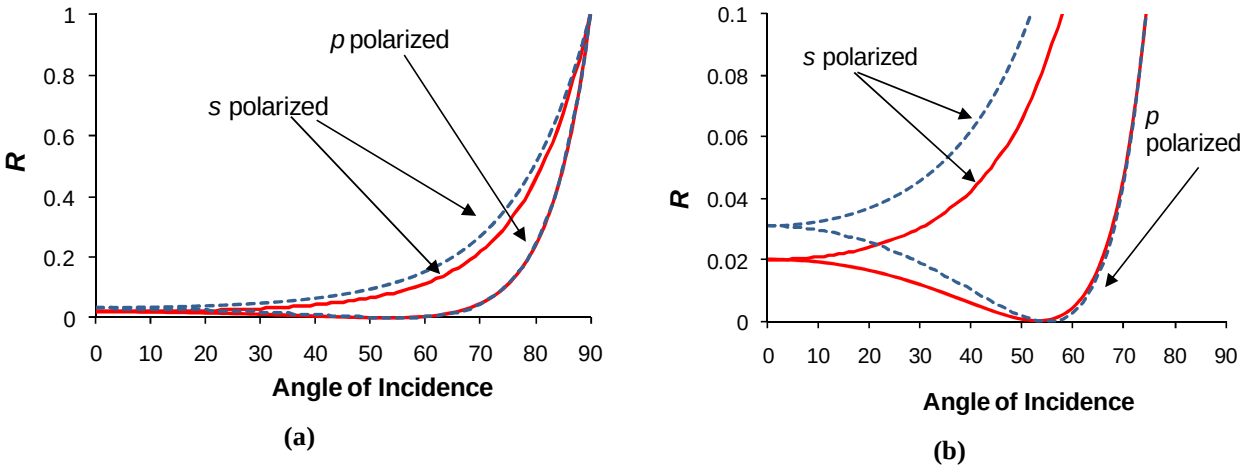

Figure 4.3(a) Theoretical Reflectivity *R* for horizontally (*s*) and vertically (*p*) polarized reflection from water n=1.33; solid line and monolayer n= 1.4283 (Weast 1974) for hexadecanol; dashed line. The difference in *R* for normal angles can be seen in (b) with expanded y axis.

The theoretical predictions for both *s* and *p* polarized reflections in Figure 4.3(a) shows a general higher reflection intensity for the *s* polarized radiation. There is a generally higher reflection for a monolayer. The vertically polarized radiation shows very little difference between clear water surface and monolayer, except for the crucial difference in Brewster angle, discussed later in this chapter. Figure 4.3(b) shows the same data with an expanded y axis so the increase of difference in reflectivity for the normal angle of incidence can be seen.

At a normal angle of incidence (0º), both directions of polarization are reflected equally and the Fresnel reflection intensity calculated in Equations 4.9 and 4.10 can be simplified to:

$$R_{\perp} = \left(\frac{n_2 - n_1}{n_2 + n_1} \right)^2 \qquad (4.11)$$

For water surface, $n_1 = 1$ and $n_2 = 1.33$, so the reflection intensity is predicted to be:

$$R = \left(\frac{0.33}{2.33} \right)^2 = 0.0201 \qquad (4.12)$$

Thus the reflection from a water surface would be close to 2.0% of the incident radiation. This compares fairly well with 2.53% for the sea surface and 2.51% for distilled water in the 2-5 µm range (Salisbury & D'Aria (1994).

The refractive index of water decreases by 0.02 across the visible spectrum from 400-700 nm and decreases by 0.01 when the temperature increases from 20 – 40 ºC (Segelstein 1981). These changes to refractive index should be minimized by using consistent wavelength (laser) and stable laboratory temperature 17-20ºC. Substituting the refractive index of hexadecanol produces a normal reflectivity of 0.0311. So an increase in reflectivity of 50% could be expected with the addition of hexadecanol, due to the higher refractive index at the surface.

The reflectivity of vertically (*p*) polarized radiation vanishes at an angle of incidence called the Brewster angle. The Brewster angle of incidence corresponds to the angle where the sum of the

angles of incidence and refraction is 90º. Using Snell's law for an air water interface where, n_1 =1 n_2 =1.33 this angle can be found using:

$$\theta_B = \tan^{-1}\left(\frac{n_2}{n_1}\right) = \tan^{-1}(1.33) \qquad (4.4)$$
$$= 53.06^0 \text{ for the air water surface.}$$

The reflectivity for water, at angles around the Brewster angle is shown (red) in Figure 4.5 substituting angles around the Brewster angle into the p-polarized surface reflectivity (Equation 4.9). For comparison hexadecanol in this region is also plotted using a refractive index of 1.4283 (Weast 1974). Substituting this into Equation 4.4 reveals the Brewster angle is 55.0°, creating a theoretical increase in the Brewster angle of 1.94°.

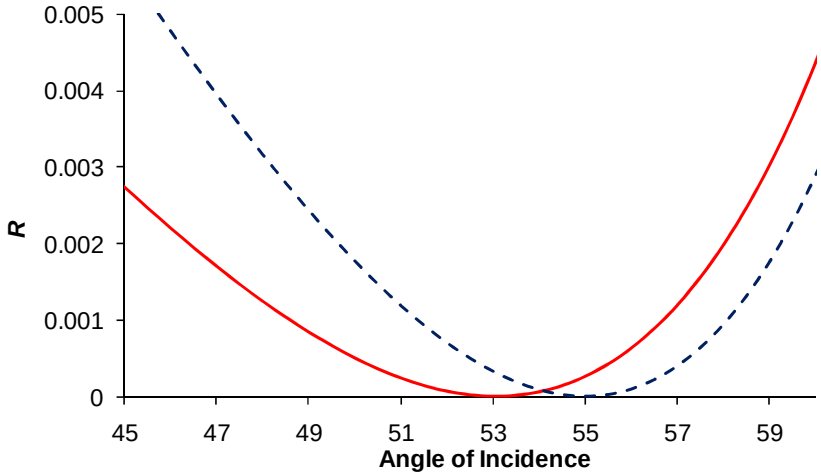

Figure 4.5 Theoretical reflectivity from air to water (n = 1 to 1.33); red solid line, and air to hexadecanol n = 1 to 1.4283, blue dashed line. The Brewster's angle increases by 1.94°.

This change in Brewster angle is measureable under controlled laboratory equipment using still samples and precise equipment; however it is not easy to detect these small angle changes in the field. Brewster angle detection for monolayers has been used by Somasundaran (2006), who also found the contrast between used a polarizing imaging system to observe the contrast between water and monolayer. O'Neil (1983) also found that the contrast can be improved by up to 100% using a crossed polariser technique. A filter with band-pass below 450 nm can also be used to improve contrast according to Fingas (2007). These field techniques however, relied on natural sunlight which constrains observations to daylight hours, with the magnitude of the effect being dictated by the incident sun angle. Reflectivity R due to incident wave interference between reflections from upper and lower surfaces of monolayers

The addition of film on the surface alters the reflectivity of the surface due to interference between the radiation reflected at the air-film and film-water interfaces. Heavens (1955:48) derived the reflection from multiple reflections as:

$$R = \frac{R_1^2 + 2R_1R_2\cos 2\delta_1 + R_2^2}{1 + 2R_1R_2\cos 2\delta_1 + R_1^2R_2^2} \qquad (4.13)$$

where R_1 and R_2 refer to the reflections from the film/air surface and film/water surface respectively, and δ is the phase change on traversing the film:

$$\delta = \frac{2\pi n_1 d}{\lambda}\cos\phi \qquad (4.14)$$

where n_1 is the refractive index of the film and ϕ is the incident angle of radiation. This can be simplified with conditions that the layer is transparent (to reduce the complex part of the refractive index) and the wavelength is much larger than the film thickness. Also if the incident radiation is in the normal direction, then $R = R_p = R_s$. and the following relationship can be used to determine the relative reflection intensity R that occurs with the addition of monolayer (Marple & Vanderslice 1960):

$$Relative\ R = \frac{\Delta R}{R_w} = \frac{4R_1R_2\delta^2}{R_1^2 + 2R_1R_2 + R_2^2} \qquad (4.15)$$

Theory predicts that the relative R would be proportional to the number of carbon atoms in the monolayer squared, as can be seen on inspection of Equations 4.14 and 4.15, as suggested by Marple and Vanderslice (1960). The differences between the heads of the fatty acids and alcohols should make minimal difference to the reflectivity, and therefore it is considered that these results apply equally to alcohols.

Even though Marple and Vanderslice performed experiments in the ultraviolet region (254 and 400 nm), probably to maximise the chances of a detectable response, their results indicated the angle of incidence made no detectable difference to the change in reflection.

Moreover, their results shown in Figure 4.6, taken with incident light at 400 nm (this small visible wavelength increases the ΔR% when substituted into Equation 4.14) showed that for monolayers the change in reflection intensity would be no more than ~ 1.2%.

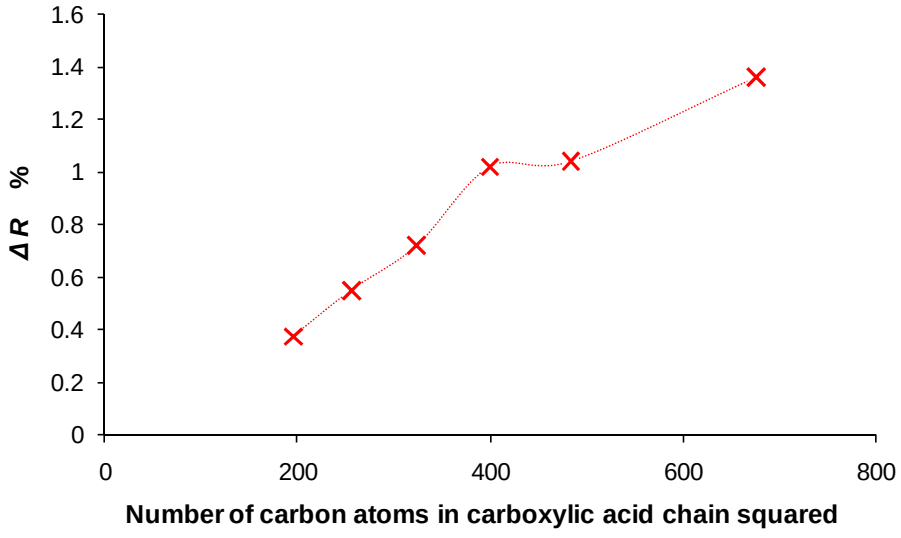

Figure 4.6 Reflectivity difference for carboxylic acid monolayers plotted against number of carbon atoms in chain squared at 400nm. Adapted from experimental data collected by Marple and Vanderslice (1960).

4.3 Experimental detection at visible wavelengths

A check of the reflectivity at various angles (as in Figure 4.3) and a test to determine whether simple laboratory equipment and laser light is accurate enough to detect the small expected changes in emissivity was carried out.

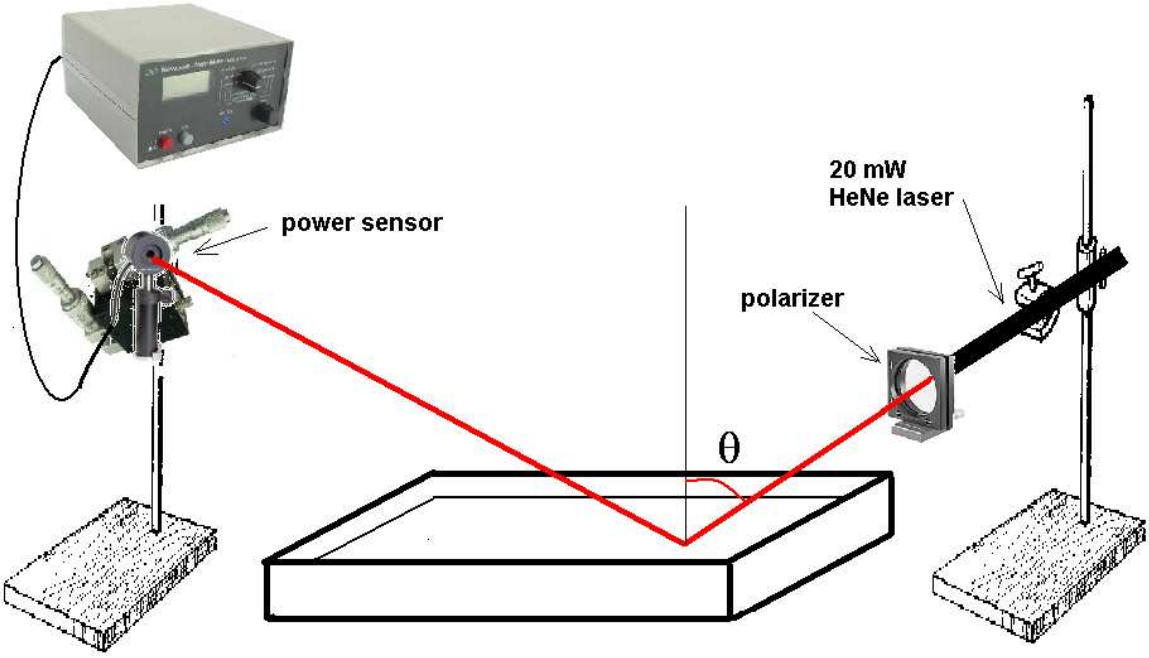

Figure 4.7 Arrangement for measurement of reflection intensity *R*.

Materials and methods

The reflectance values were measured from a 20 mW He-Ne laser (λ=632.9 nm, 1135P Spectra-Physics, Oregon USA) laser orientated to provide incidence angles between 0° (normal to the water surface) to a maximum of 85° as depicted in Figure 4.7. The reflection intensity was measured with a power meter (Model 1815-C, Newport Corporation, USA). The detector head was screwed to a mounting which was adjustable in both lateral directions, so that the signal could be maximised to determine ideal position. A polarizer with an extinction ratio ~0.001 was attached to the output of the laser so that directions of polarization could be observed separately. The trough was a stainless steel baking tray, which when filled to a standard ridge had a surface area; 28 × 50 cm and depth 4.5 cm with ambient temperatures of 16-20 ºC during measurements. Trials of clear tap water with and without a full pressure hexadecanol monolayer were conducted, with the monolayer being added to the surface in the usual way by dropping several crystals onto the surface. The reflectivity intensity ratio was calculated by comparing the intensity of the reflected beam, with the incident beam, both measured using the power meter.

$$R = \frac{I_{\text{Reflection}}}{I_{\text{Incident}}} \qquad (4.16)$$

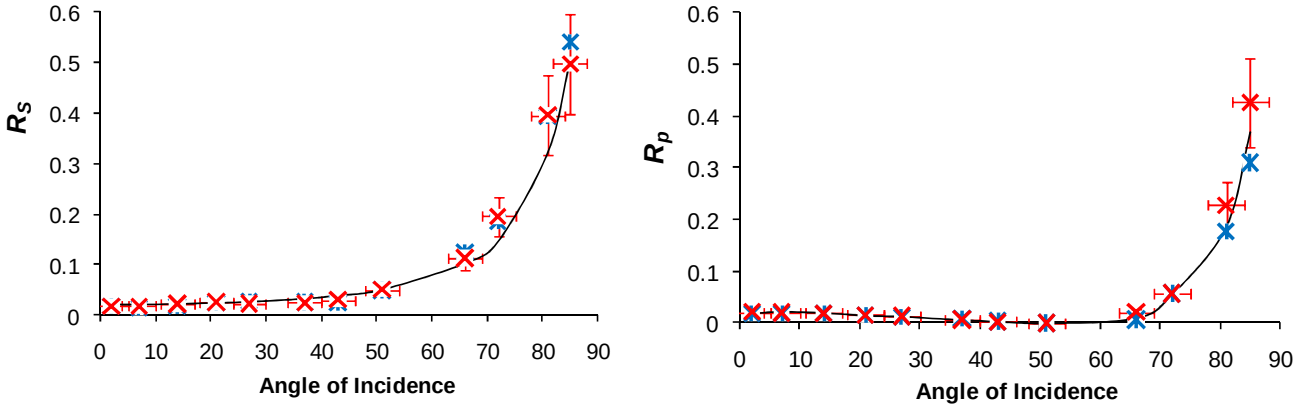

Figure 4.8 Experimentally determined reflectivity *R* for (a) *s* polarization and (b) *p* polarization for water (×) with error bars, and hexadecanol (∗). Theoretical values for water (Solid black line).

Results and Discussion

Graphs of the reflectivity *R* are plotted as a function of angle of incidence for both directions of polarization; the *s* (horizontal) and *p* (vertical) polarization orientations in Figure 4.8. Within the experimental uncertainties indicated by the error bars, the results show no significant difference in the *R* between the clear water surface and hexadecanol surface. The error bars, show the estimation of uncertainty of 20% in intensity, and 3° due to positioning angle. The major cause of a lack of accuracy would undoubtedly be due to alignment accuracy, as both the laser and detector needed to be repositioned for each measurement.

The intensity resolution needed for hexadecanol detection would need to be < 2%, according to Marple & Vanderslice (1960) and Beard & Wiebelt (1966). This was well below the estimated accuracy of this equipment. The use of a goniometer accurate to 0.1° could improve results, and perhaps make detection possible. This equipment however was not pursued as these measurements were considered impractical in the field, with a combination of the difficulty in providing a stable platform affecting the incident angle and water level problems affecting detector position.

4.3.1 Microwave radiometer measurements

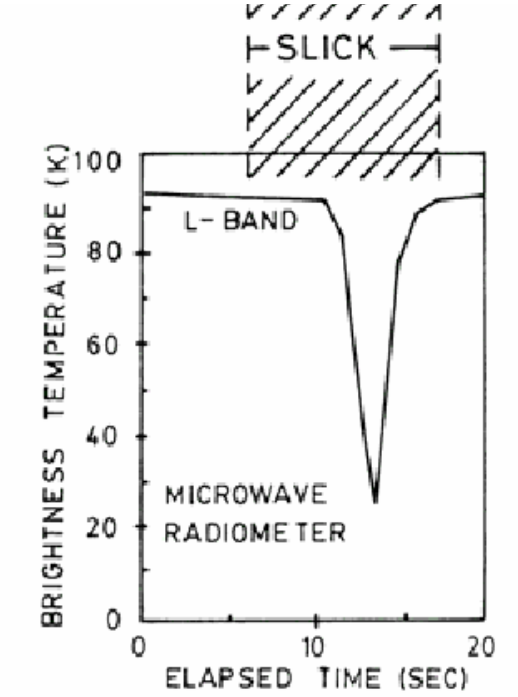

Figure 4.9 Reduction in brightness temperature in the L band (peaking at 1.43 GHz) when observing an oleyl alcohol slick. Source; (Hühnerfuss 2006).

Aerial passive L band microwave detection has been successfully used by Hühnerfuss (2006) to detect oleyl alcohol by comparing the signal with that of backscatter of clean seas (Figure 4.9). Similar detection in the S band, however produced little reduction in signal strength. The intensity of the signal received, known as ***brightness temperature***, showed a large decrease, with a peak reduction at 1.43 GHz noticed in six over flights over an ocean area which was covered.

The cause of the reduction is thought to be a change in the complex dielectric constant in the skin of the ocean, perhaps by clathrate like structures that form near the surface leading to a significant increase in the relaxation time of the surface molecules by an order of magnitude (Hühnerfuss 2006).

This detection method uses a comparison with background water to determine monolayer presence, and this is not always available. The expense involved in investigating these results was considered out of the range of this work; however these results do show some justification for future monolayer detection work.

4.4 IR observations

From the 1970's onwards, air and space-borne radiometers have been used extensively as a cost effective method of determining sea surface temperatures (for example (Smith *et al.* 1970)). The use of such tools has been motivated by the need to assess long term environmental changes (Gurney, Foster, & Parkinson 1993), as well as measuring the net heat flux radiated from the surface for use in predictions of weather, such as the El Niño effect (Rasmusson & Carpenter 1982). It has been determined that in order to calculate the net heat flux with a necessary precision of 10 Wm^{-2} to

monitor such effects, the sea surface temperature has to be measured to within 0.2 °C (Fairall *et al.* 1996).

Radiometers average the radiation from the molecules at and near the surface, with the exact depth being sampled depending on the wavelength range. IR thermometers operate in a region (usually 8-14 μm) where the effective optical depth is at a minimum, at around 10 μm (see Figure 4.26). Therefore the depth of interrogation of the sensor would be the top 25 μm (Saylor, Smith, & Flack 2000) and in a wavelength region where an "atmospheric window", exists to minimise absorption by water vapour (Robinson 1973:91). Thus IR radiometric sensors actually view through surface films such as Aquatain (thickness ~1 μm), and most certainly do so for monolayer (thickness ~ 2 μm). However the interrogation depth of IR radiometers is well within the skin thickness of the water column itself, which is 0.1-1 mm (Chapter 3). In effect the skin temperature is being measured. This poses major challenges in measuring ocean temperatures using satellites when more stable subsurface temperatures are needed. Sea surface temperature algorithms combined with multichannel satellites have been developed to look through atmospheric water vapour and determine the true subsurface ocean temperature below the skin layer (Emery *et al.* 2001; Smith *et al.* 1970; Suarez, Emery, & Wick 1997).

4.4.1 IR Imaging of the surface

The surface of water is considered to be shear -free. However when monolayer is added, the surface changes to assume the property of being able to support shear forces, acting to increase the surface viscosity. The hydrodynamics of the subsurface is affected by this viscosity, which in turn changes the surface temperature field (Saylor, Smith, & Flack 2000), as discussed in Chapter 3.

An imaging IR camera was used by Saylor *et al* (2000) to determine the temperature changes caused by the altered sub skin cold thermals, since temperature differences are in turn conducted through the skin layer, where they can be imaged. A nitrogen cooled Raytheon-Amber CCD camera with a 256 pixel square InSb array using 12 bit intensity resolution was used. The images, which covered an area of surface of around 16 cm on each side show a general decrease in the root mean squared value from the surface temperature with the addition of monolayer shown in Figure 4.10. This reduction in temperature variation for the full range of heat flux tested would tend to indicate an effective thickening of the skin layer and a slowing of the convection currents.

Saylor's images for low heat flux conditions are shown for clear surface in Figure 4.10(a) and hexadecanol surface in Figure 4.10(b). There are slight differences, mostly in enlarging the convection currents, due to increased viscosity. For higher heat fluxes, shown for clear surface in Figure 4.10(c) and oleyl alcohol surface in Figure 4.10(d) show a larger spatial temperature variation for both, however the covered surface has an elimination of small scale variations. This led the group to speculate that, "IR imagery can effectively determine the presence of a surfactant".

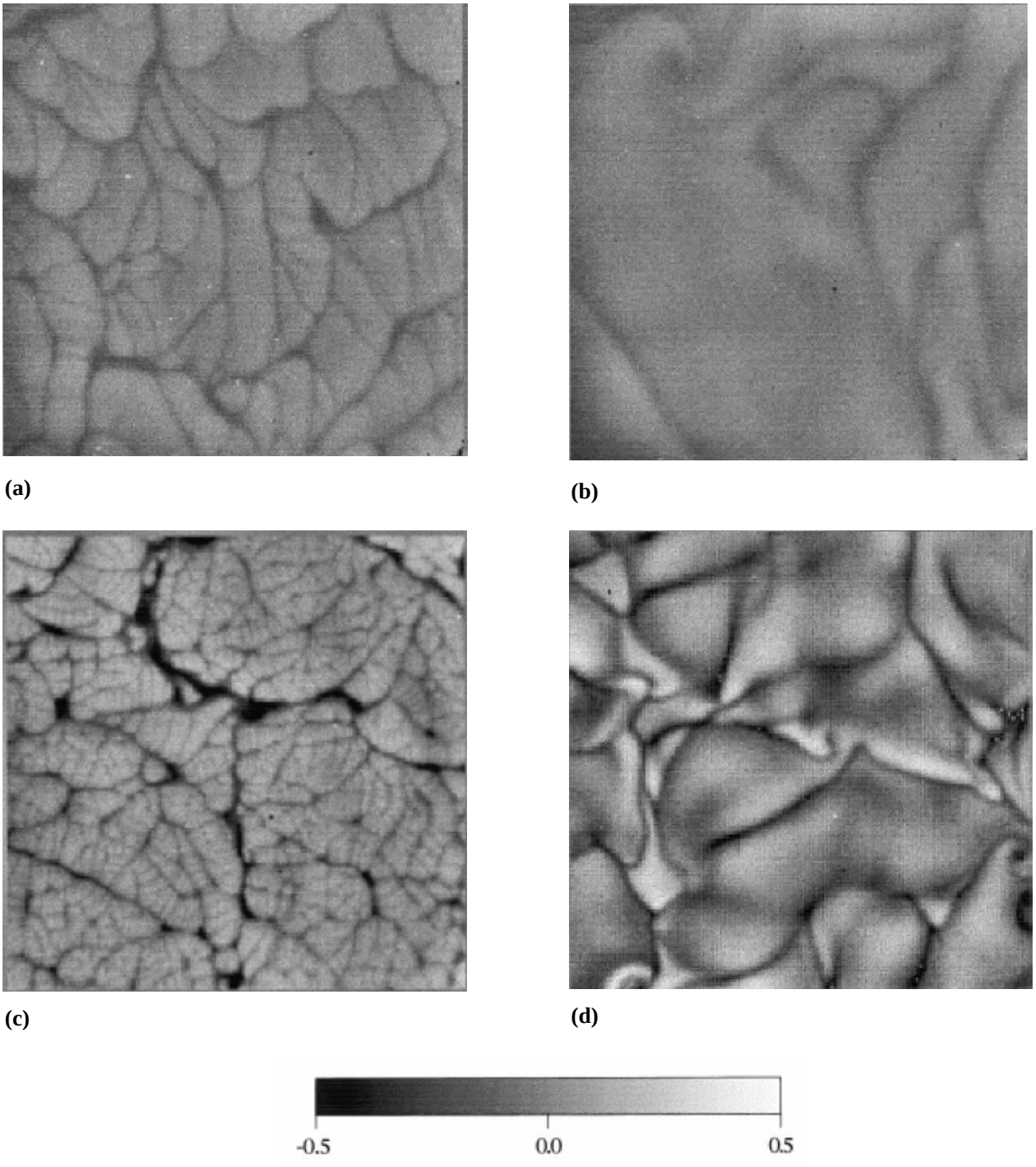

Figure 4.10(a) Clean water at room temperature with a calculated heat flux of 38 Wm^{-2}. (b) Addition of oleic alcohol monolayer. (c) Clear heated water with a heat flux of 480 Wm^{-2}.(d) Addition of oleic acid monolayer (e) Intensity correlation for 1 °C for the above images. Source; Saylor *et al* (2000).

4.4.2 Wavelength-dependent absorption characteristics

The thickness of surface films will determine how easy they are to detect using reflected or scattered radiation.

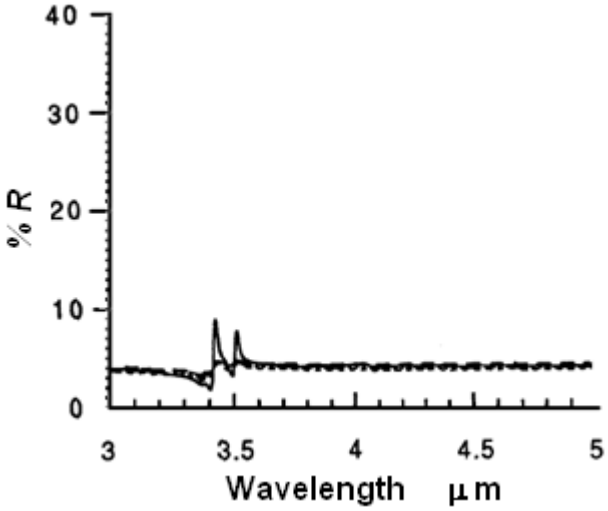

Figure 4.11 Reflectivity of 5 different samples of crude oil, each 2-3 mm thick showing spikes corresponding to the C-H stretching bands occurring around 3.5 µm. Source; Salisbury & D'Aria (1994).

The reflectance spectrum of oil slicks of thickness 2-3 mm in the 3-5 µm range measured by Salibury & D'Aria (1994) shown in Figure 4.11 show a reflectance of 4% compared to surrounding water at 2%. Two characteristic spikes also appear around the 3.5 µm wavelength corresponding to C-H bond stretching within the oil layer. Five different oils were tested with very different viscosities and compositions, displaying almost identical IR spectra dominated by the C-H stretching features. These data, represented by solid, dashed and dotted lines are largely superimposed over each other.

Monolayers consist of much less material than an oil slick and therefore these spikes are much reduced in intensity, although they can be detected under laboratory conditions showing a reflection intensity difference of around 0.5% under ideal conditions (Mendelson, Brauner, & Gericke 1995).

Absorption bands corresponding to CH_2 stretching bands provide the strongest signal/noise ratio (Figure 4.12), and for this reason are the most studied (Sinnamon 1999). For hexadecanol and octadecanol they occur for the C-H symmetric stretching at 3.51µm and for the CH_2 anti-symmetric stretching at 3.43µm. The CH_3 bonds on the tail of the carbon chain are slightly different with an absorption wavelength of 3.47 µm for symmetric and 3.37 µm and 3.38 µm for asymmetric stretching (Sigma Aldrich 2008). The other significant absorption peak at 7 µm is caused by CH_2 'scissoring' .

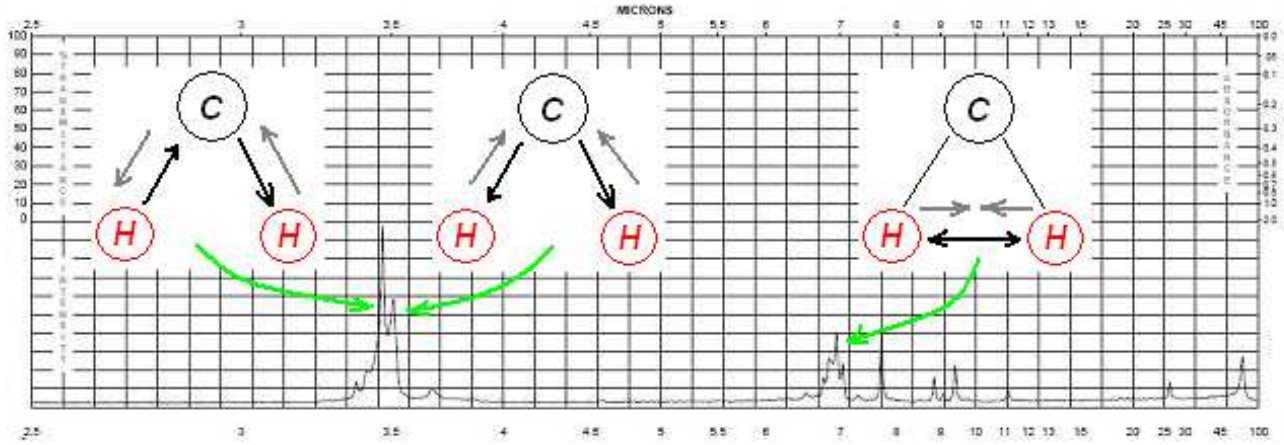

(a)

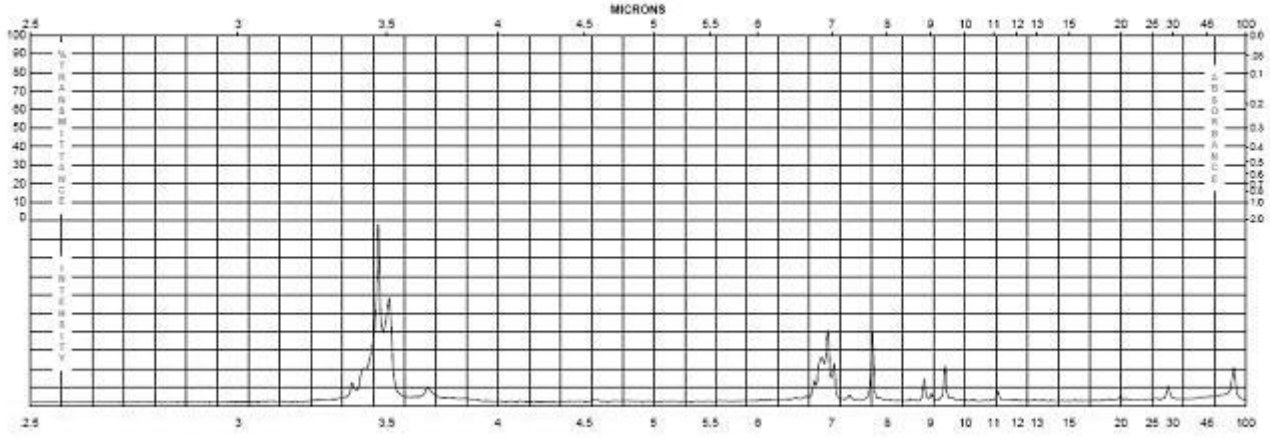

(b)

Figure 4.12 FT-IR absorption spectra of (a) hexadecanol and (b) octadecanol. Source; Sigma Aldrich (2008).

The very low thickness of the layer of these compounds makes it very difficult to detect these spectral features. Moreover, the presence of a monolayer on water surfaces can alter the phase and intensity of reflected IR radiation. Due to the refractive index of monolayers being higher than that of air, it would be expected that a 180° phase change would occur on the air/monolayer surface reflection, and this is true of horizontally polarized rays. The reflection of vertically polarized radiation undergoes no phase unless the angle of incidence is larger than the Brewster angle (Dluhy 1998). The horizontal reflection intensity is, however larger than the vertical for angles larger than 20˚ as shown in Figure 4.3.

Mendelson *et al* (1995) carried out accurate measurements using infrared reflection absorption spectra (IRRAS) on the CH_2 bands at incident angles of 30° and 60°for various surface pressures. The results, shown in Figure 4.13 show an increase in absorbance with increasing monolayer pressure, and a much higher signal/noise ratio at 30°.

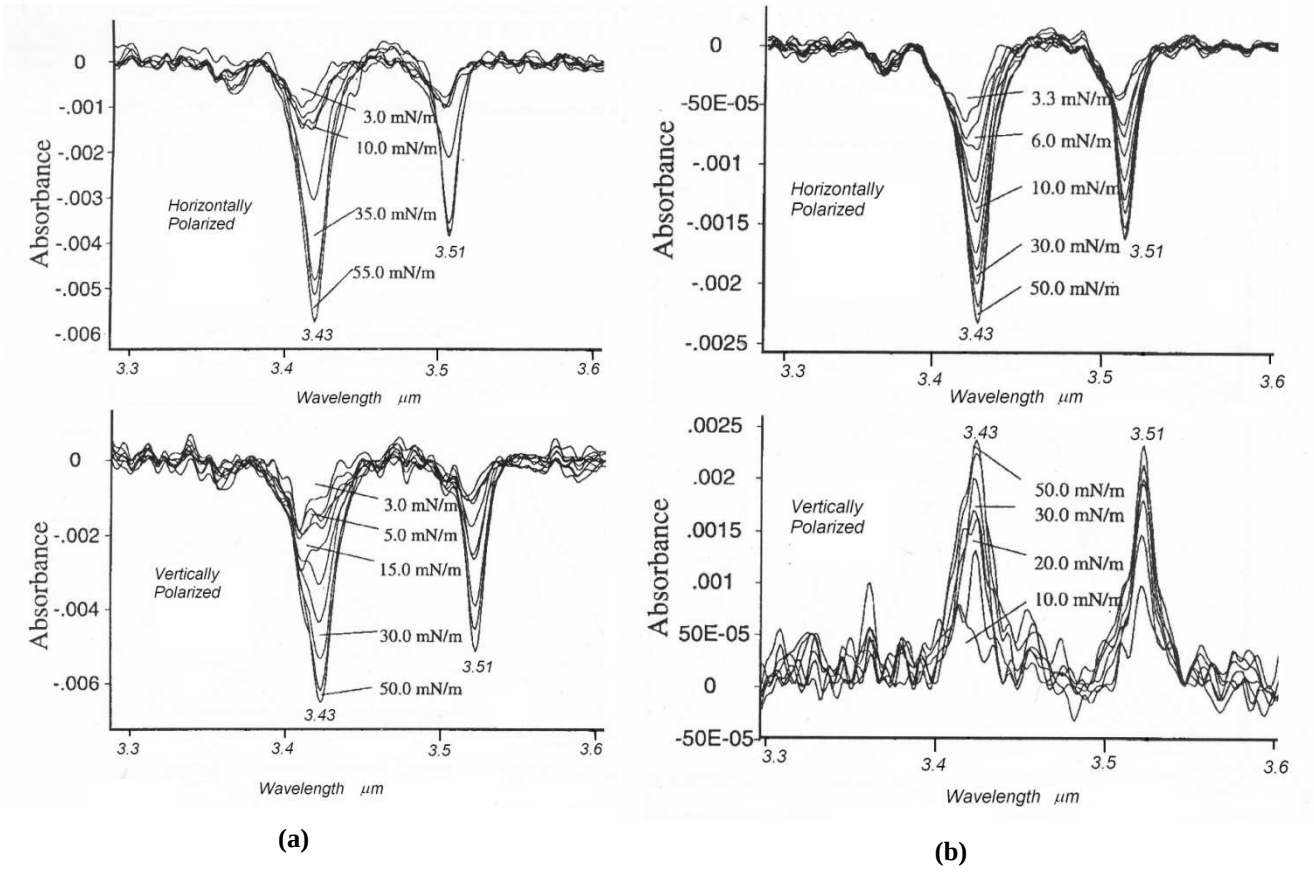

(a) **(b)**

Figure 4.13 IRRAS of methylene C-H stretching bands at (a) 30º and (b) 60°. Source; Mendelson *et al.* (1995).

The appearance of a positive absorbance values (compared to the expected negative absorbance values) in the vertically polarized 60° angle of incidence (Figure 4.13b) can be explained by using Fresnel reflection coefficients, with typical monolayer complex refractive index parameters of n=1.5 + i0.1 substituted. A theoretical graph drawn by Dluhy (1998) (Figure 4.14) shows the asymmetric vibration (the largest absorption band) at 3.43 μm for incident radiation for the two directions of polarization. The horizontally polarized ray has a maximum reflection absorbance at normal incidence (0º) at 0.0045 and this approaches zero at 90º. The vertically polarized ray begins at a similar reflection absorbance at normal incidence and is discontinuous at the Brewster angle (Section 4.2.1):

$$\Phi_B = \tan^{-1}\left(\frac{n_3}{n_1}\right) = 54.73^{o} \qquad (4.17)$$

where n_3 is the refractive index of water and $n_1$is the refractive index of air=1. It then decreases exponentially with increasing angles of incidence. The increase in magnitude of the vertical absorption around the Brewster angle is due to the use of the ratio of relative reflectivity, with the reflectivity of clear water approaching zero. The discontinuity in reflection absorption is due to a phase inversion, which occurs at the air water surface reflection at the Brewster angle and continues for larger angles.

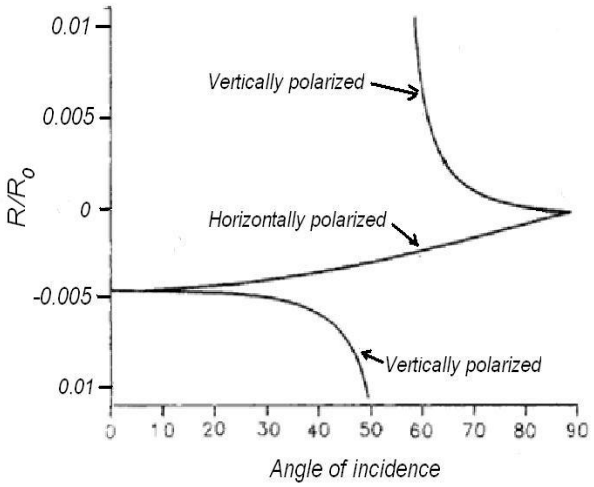

Figure 4.14 Theoretical reflection absorption amplitude for the asymmetric CH_2 peak at angles of incidence for both vertically and horizontally polarized IR radiation. Adapted from Dluhy (1998).

The measured absorption values in the work of Mendelson *et al*. are nonetheless very low. At the peak of the absorption, using maximum surface pressure of monolayer at around 40 mN m^{-1}, the absorbance is only a 0.45% difference in reflection magnitude. The experimental conditions also need to be controlled with any changes in water vapour or wind between sample measurements and background measurements affecting the signal adversely (Mendelson, Brauner, & Gericke 1995).

4.5 Experimental Infrared detection results

4.5.1 IR imaging

Surface temperature measurements of hexadecanol and octadecanol covered water surface consistently show an increase of temperature due to the evaporation reducing effects. An increase of 0.15 ºC was found using laboratory interferometer measurements by Barnes & Feher (1980) with octadecanol. An increase of ~0.3 ^{0}C was measured for a hexadecanol slick using an aircraft-borne IR thermometer by Grossman (1969) when compared to background clear water on a large storage.

Infrared thermometer measurements can be useful in measuring this increase, as the effective optical depth of IR radiation in the region measured by IR thermometers (8-14μ) is 25 μm (Saylor, Smith, & Flack 2000) and therefore this is the depth that is averaged in determining surface temperature. Thus, infrared thermometers measure the temperature as close as possible to the surface. This reading depth is particularly important as there is often a temperature gradient across the skin which is much larger than any other part of the storage.

Materials and Methods

An IR Inframetrics Model 600 (FLIR, USA) imaging radiometer was used to compare images of the surface of a reference clear water trough and a sampling trough. It was not found to give accurate absolute temperature values, but was perfectly adequate for comparisons of small temperature differences of several degrees.

The samples were contained in clear polypropylene food containers of size 16 × 11 × 6 cm high. New containers were used for each measurement and were rinsed with tap water before use to prevent contamination from manufacturing residues.
The radiometer has a specified temperature range of 20–40 °C with a peak sensitivity of 8-12 μm. Using Wien's displacement law, the temperature range corresponds to a wavelength range of 4.3-11.4 μm. Since the temperature of the water is towards the lower end of the temperature range, the peak sensitivity should correspond well with the peak of the radiation emitted.

Images were recorded using a computer equipped with a PCI video capture card (Lifeview, Taiwan), which could show real time and frame grab bitmap images of around 1Mbyte.

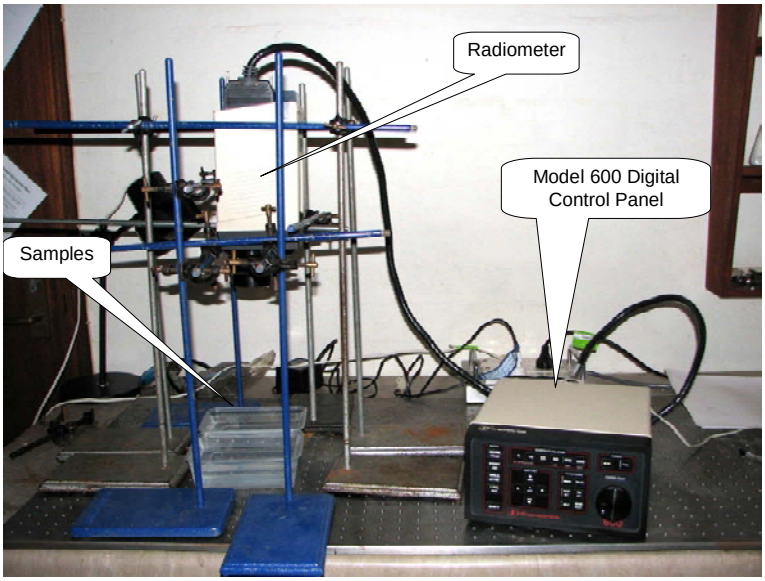

Figure 4.15 Setup for imaging radiometer. The camera was focussed on the two troughs, so that they filled the view.

The radiometer was positioned at various angles above sample water surfaces. Figure 4.15 shows the initial vertical configuration, which was used so that a reference water surface and a film surface could be observed simultaneously, at a distance of 0.40 m. Both troughs were filled with tap water to the level of a ridge just below the top making the depth of water 5.0 cm. One trough was left as a reference while the other was covered with samples of surface active layers. The samples were prepared by dropping several crystals of hexadecanol and octadecanol or adding a single drop of Aquatain to the individual troughs. The samples of monolayers are the same as previously used, and the Aquatain was a sample from a 20 litre drum (Ultimate Products Australia Pty. Ltd) that was thoroughly shaken. Both the reference and sample troughs were allowed to thermally equilibrate for one day before images were taken. Typical laboratory conditions were 40% humidity and temperature 20-25 °C.

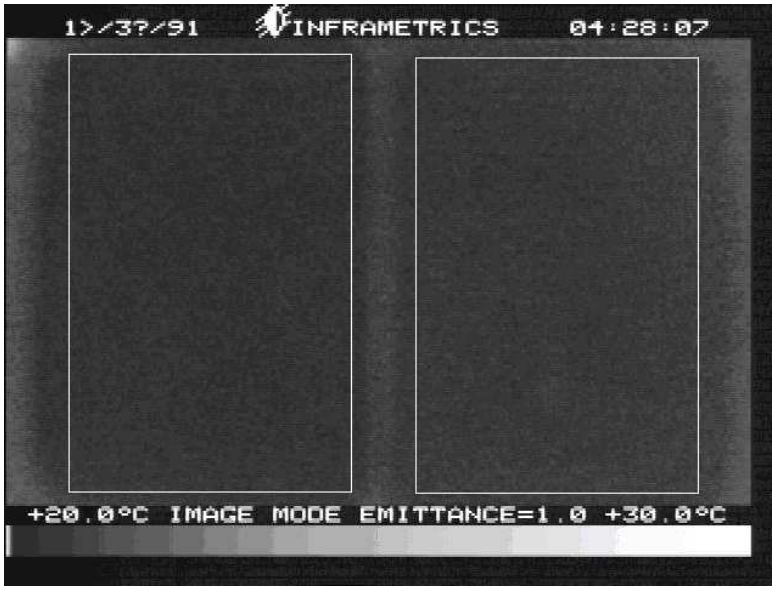

Figure 4.16(a) Image of clear water trough (left), and hexadecanol covered trough (right) with area of pixel averaging drawn(white rectangle) 1 day after the addition of monolayer to the surface. The coolness of both surfaces can be seen by comparing the intensity with the surrounding tabletop.

Results and Discussion

Unfortunately the resolution of the radiometer was too low to discern any spatial variation in surface temperature across each sample (Figure 4.16) as discerned in Saylor's work (2000). However it still could be used to obtain a comparison of surface temperature between samples. This was carried out using the pixel averaging function of Adobe Photoshop in analysing sample images. The pixels can be chosen in a defined area to average all the residing pixels. An average number between 0 (black) and 255 (white) is given to represent the intensity, which can be related to temperature using the intensity bar along the bottom.

The area chosen each time was just smaller than the size of the trough. This number was then compared to the 10 °C difference in the intensity bar positioned on the lower part of the image to convert intensity differences to temperature differences.

The pixel averaging function was then used on the bottom bar to convert intensity to °C. The light end of the bar averaged 197 bits, while the pixels in the darkest part were 27 bits. These extremes correspond to a temperature difference of 10 °C so 1 bit on the intensity scale would correspond to 0.0588 °C for this image. The uncertainty, calculated using standard deviation in all these measurements was $\sigma = \pm 4$ bits. The number of pixels averaged for each of the surfaces was around 15 000. Differences in temperature were recorded after 2 days using samples of hexadecanol, octadecanol and Aquatain (thickness 1.1 μm), with the results plotted in the table below. To remove any bias in the intensity measurements of the camera, the sample was placed both on the left of the reference water, and then on the right. Three measurements were averaged for each position, and the average is shown.

Table 4.2 Measured pixel intensity difference between reference water and (monolayer) film

Film	*ΔT Surface* Sample on Left	*ΔT Surface* Sample on Right	Average pixel increase	Temperature increase °C
Hexadecanol	4.1	7.9	6.0	0.35
Octadecanol	6.7	4.5	5.6	0.33
Aquatain @1.1 μm	-0.7	3.8	1.6	0.094
Addition of temperature changes	10.1	16.2		

Conclusion

A camera bias was found by adding the total pixel brightness for all three measurements. This is shown on the last row of Table 4.2. The test samples are brighter on the right hand side of the reference compared to the left, so both were averaged.

The surface of hexadecanol was measured as being very similar to octadecanol after one day, with the surface of Aquatain being the coolest. This indicates the hexadecanol and octadecanol produced higher evaporation reduction, of a larger magnitude than Aquatain under these conditions. The evaporation reduction for octadecanol however should be higher than hexadecanol, since the evaporation resistance is higher (Chapter1). Geoff Barnes (Pers. Comm. 2009) suggested this is most probably due to impurities in the octadecanol. With a thickness of 1.1 μm, the Aquatain had the poorest evaporation reduction. This was surprising and suggests that further testing should be carried out to determine the thickness which would roughly equal hexadecanol, and also to check whether the emissivity of the various surfaces affects these results (Section 4.5.2).

These results may replicate to some degree the temperature changes produced on water storages, measured with a radiometer, as both disperse the cooling effect of cold thermals, with little change to the bulk temperature. The water storage by its large size, and these troughs, by heat conduction through the thin polypropylene walls.

4.5.2 IR thermometer with insulated trough

Introduction

The previous experiment showed detectable differences for surface active films by measuring the surface temperature. It also raised several questions that needed answering. These include the surprising low evaporation reduction of Aquatain when compared to hexadecanol and octadecanol. The use of single troughs meant that much of the evidence of evaporation reduction was lost by the low heat insulating qualities of the trough walls. The resulting heat flux through the walls acts to reduce surface temperature differences. This experiment uses a more practical IR thermometer and

reduces the wall heat flux using insulated troughs. The evaporative cooling differences may be cumulative and lead to a larger more easily detectable differences in surface temperature.

Materials and Methods

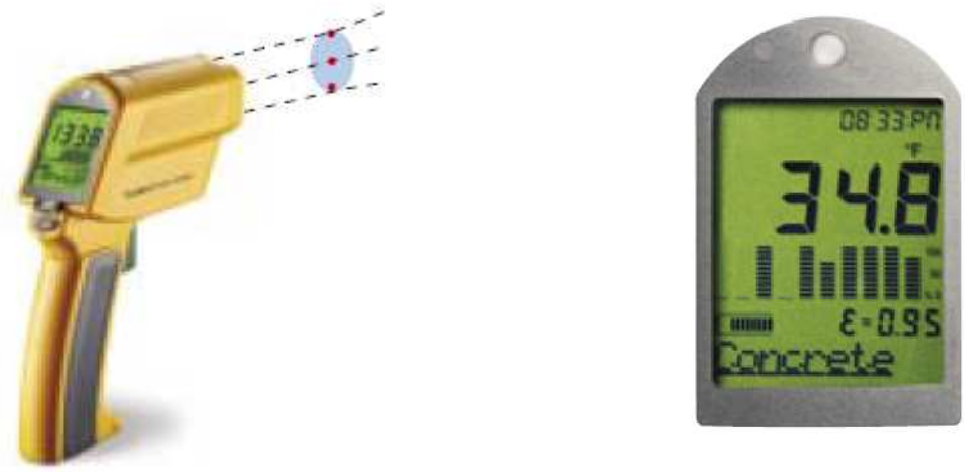

Figure 4.17 Fluke 474 IR thermometer, with display.

Surface temperature measurements were taken with a Fluke 474 IR thermometer (Fluke corporation, WA USA) shown in Figure 4.17. It measures radiation in the 8-14 μm wavelength by averaging readings between the three He- Ne laser sighting beams. The resolution is 0.1 °C, with an accuracy of 1.0 °C in the temperature range used. The emissivity was adjustable in steps of 1%, and was set to 0.96.

Initial measurements checking emissivity changes that may occur with addition of surface active layers

Tests of immediate changes to emissivity for hexadecanol and octadecanol were carried out using the Fluke 474 IR thermometer attached to the computer graphing software. When several crystals were added to the edge of each trough no change was detected. Therefore no alteration of emissivity settings needs to be carried out in comparing the temperature of clear water compared to these monolayers.

The same tests were carried out using Aquatain, and a change in emissivity was measureable. To a trough of clear water, 20 drops of Aquatain was added creating a surface active layer 22.6 μm thick. Since the effective optical depth in the region of the thermometer is around 12 μm (Figure 4.26) the radiation should be emitted only by the Aquatain.

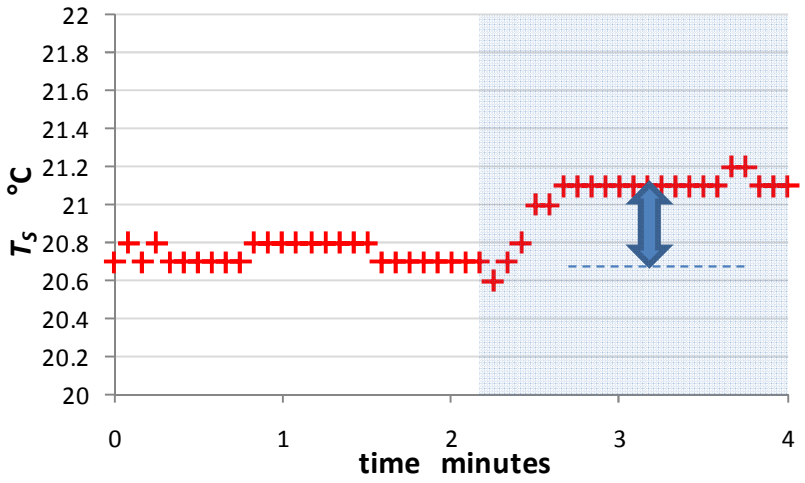

Figure 4.18 Surface temperature measured using the IR thermometer with the addition of 20 drops (shaded area) of Aquatain to clear water showing a rise of 0.4 ºC.

The Aquatain was cooled to 5 ºC below room temperature, so that any initial temperature changes due to the temperature difference of the dropper bottle and room temperature would act to lower surface temperature. The results shown in Figure 4.18 are representative of several runs, showing an initial cooling, followed by a rise of 0.4 ºC. This would indicate the emissivity of Aquatain is lower than water, and the reflectivity is higher. This was found to be true in experiments described in Section 4.7; determining silicone oils have reflectivity values higher than water. The use of 1, 2 or 5 drops rather than 20 would tend to reduce this measured temperature increase. If there is a measurable increase in emissivity with the addition of Aquatain, then a comparison of the warming effects of monolayers and Aquatain compared to reference clear water would overestimate the evaporation-reducing effects of Aquatain. These changes to emissivity for Aquatain were kept in mind in subsequent experiments when comparing IR surface temperature with water.

Five polypropylene food containers were positioned beside each other on a bench top and filled to an internal ridge with water. Another two containers were placed under the sample containers so that there were two insulating air spaces in the sample containers. This created a much better insulation than previously used. Other than this the same setup procedure was used, only an extra trough containing for a different thickness of Aquatain with 3 drops (3.4 µm) was also prepared. A bulk temperature measurement was also made by placing, a mercury thermometer on the floor of the troughs. The results are shown in Table 4.3.

Table 4.3 Difference of surface temperature between a water surface and covered surfaces averaged over several days.

Film	*ΔT Surface* °C ±0.2	*ΔT Bulk* measured near floor °C ±0.3
Hexadecanol	+0.9	+1.1
Octadecanol	+0.6	+1.3
Aquatain 1.1 µm	+0.3	+1.3

Aquatain 3.4 μm	+1.1	+1.4

Results and Discussion

The IR surface temperatures compared to reference water (Table 4.3), generally increased over the results of using the uninsulated troughs. This is not surprising as the bulk water under the covered surfaces were allowed to assume a temperature fairly independent of the surroundings, with the surface possesses a temperature with respect to this temperature. The increase in bulk temperature is shown in the right hand column, measured with a mercury glass thermometer, with the bulb resting on the floor of the trough.

Conclusion

Using insulated troughs it would be expected that the temperature increase would be proportional to the evaporation reducing ability of the film. When the heat flux through the walls of the troughs is minimized, the surface temperature changes that occur with coverage are increased due to warming of the bulk water. The octadecanol again showed a lower *ΔT Surface* than hexadecanol, consistent with the previous experiment. However the bulk temperature difference would tend to indicate a higher evaporation reduction. Aquatain showing a thickness related effect for the two thicknesses tested. The website advertising Aquatain (www.aquatain.com.au 2009) advises a dosage of 0.2 μm every 10 days. According to these results the dosing rate should probably be higher. An evaporation reduction equivalent thickness of 2.8 μm is obtained by using a ratio to determine the thickness that would correspond to the *ΔT Surface* for hexadecanol. This estimated equivalent thickness does not however account for the increase in emissivity detected in initial preparations in this experiment.

4.5.3 Influence of depth on Surface temperature

Introduction:

Experiments described in Sections 4.5.1 and 4.5.2 used shallow troughs of depth 5.0 cm. In the field, water storages will have a much greater average depth, and it is important to determine whether depth affects the natural lowering of surface temperature below air temperature, ΔT_{AS}. While it is impractical to carry out the experiments on full size water storages due mainly to solar heating interference, a replica of the surface of water storages was made in the form of PVC tubes of various water depths.

Materials and Methods

100 mm diameter PVC tubes were chosen for this experiment as they are more sturdy than polypropylene food containers. PVC tubes also offer a much better thermal resistance than metals or a thin layer of polypropylene. PVC pipes provide an ideal way of obtaining a standard surface

area and are very convenient to work with as they are commonly available, have proven tolerance to wet environments and are economical to purchase. The size of 100 mm was chosen as larger pipes had much thicker walls, which made the cost and difficulty in cutting/gluing increase substantially. The lengths of pipe used were 2.0 cm, 10 cm, 20 cm and 30 cm, to which were glued end caps on the lower end (with no increase in internal depth). They were then positioned vertically beside each other on a shelf in an enclosed area. They were filled to the brim with water in laboratory conditions which averaged 35% humidity and a temperature of 22 °C for 1 day. The surface temperature of each was measured using a Fluke 574 IR thermometer. No direct wind was present, however there was a circulating fan positioned nearby. Measurements were taken several times over a period of 3 hours with a measured variation of 6%. The average results are shown in Figure 4.19.

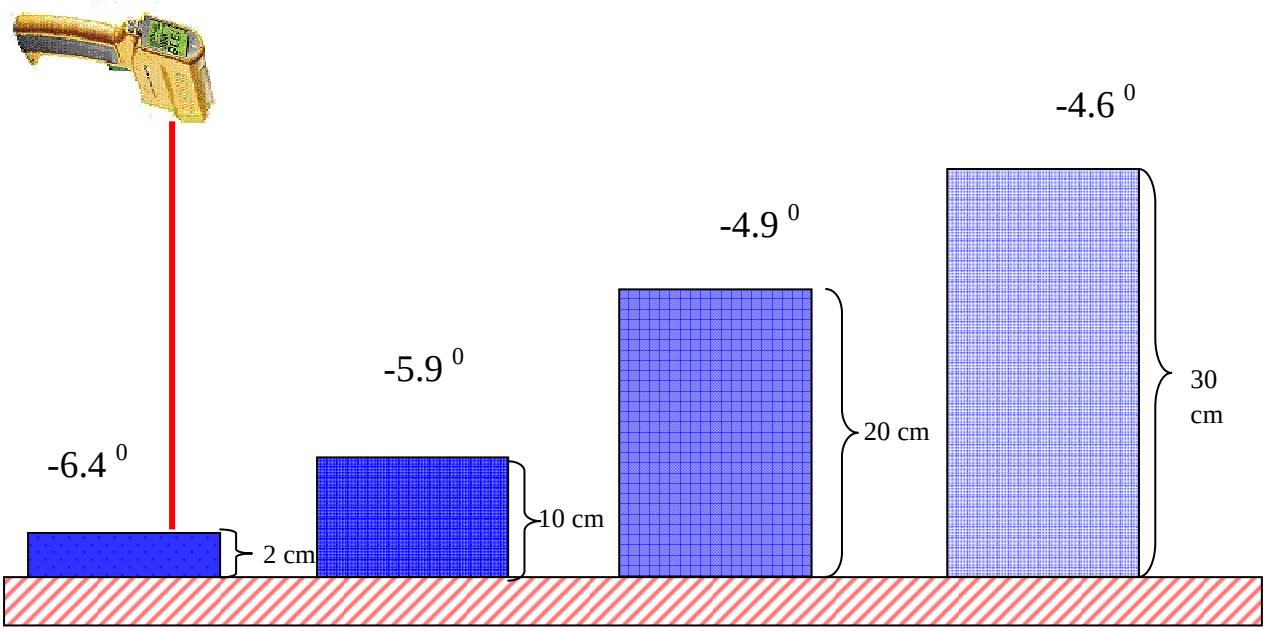

Figure 4.19 T_{AS} of troughs with varying height. T_a=22 ^{0}C and 35% relative humidity.

Results and Discussion

The results show convincingly that the surface temperature is affected quite strongly by the bulk temperature which is in turn affected by heat conduction through the walls. The 2.0 cm high trough surface decreased below air temperature by 6.4 °C, up to 4.6 °C below for the 30 cm trough as depicted in Figure 4.19. The four tubes would possess the same latent heat flux loss at the surface, reducing the surface temperature, and some diminishing of this value due to sensible heating at the surface. The difference occurs due to the restoring heat flux available through the walls and floor of the trough and this flux is reflected in the surface temperature.

Based on these simple results it would seem impossible to calculate the surface temperature to a degree of accuracy needed to detect the presence of a monolayer, by the alteration in evaporative cooling. Surface temperature measurements of around ~0.3 °C (Chapter 3) difference would be difficult to detect in these tubes and impossible if the depth of the tube was unknown.

If the results of this simple demonstration are extrapolated to the size of a large water storage, the difficulty in theoretically estimating the surface temperature in a large water storage can be appreciated. Even with identical surface conditions, subskin processes within the storage can alter the surface temperature. Add to this the hydrodynamic movements of convection cycles within the water storage, wind variations, sun and cloud radiant energy, and deposits and withdrawals of water and it becomes very complicated. Even a microprocessor with sensors floating on the surface linked to weather stations would not be able to discern if the surface temperature is different from the value for a clear water surface of ~0.3 °C indicating a monolayer. The Centre for Water Research and the University of WA (The Centre For Water Research 2006) designed a program they called DYRESM which can determine the temperature profile taking into account many factors such as deposits, withdrawals, rainfall, solar radiation, wind speed, air temperature and humidity, shape and depth of storage. Monitoring all these factors within water storages would be inconvenient if not impossible on many storages. Detection methods must therefore rely on differences in temperature rather than absolute temperature.

4.5.4 Relationship between T_{AW} and % humidity

The mass of water evaporation from an extended wet surface can be predicted using the Dalton equation (Equation **1.1**)

$$m_e = f(U)(e_{SWT} - e) \tag{4.18}$$

The wind speed function *f(U)* is constant for a particular wind speed, and the mass of evaporated water is obviously proportional to the latent heat flux. If the surface temperature remains fairly constant then it might be expected that

$$(e_{SWT} - e) \propto (e) \tag{4.19}$$

Then the lowering of surface temperature:

$$T_{AS} \propto \%\ \text{humidity} \tag{4.20}$$

Where T_{AS} is the temperature difference between air and the water surface and % humidity is the relative humidity of the air.

An experiment was set up to test for differences in T_{AS} values between clear water and hexadecanol surface at thermal equilibrium for constant (low) wind speed. Another goal of this experiment was to determine whether T_{AS} is proportional to % humidity when measuring evaporative cooling of the surface below air temperature T_a.

Materials and Methods

A PVC end cap was used as a trough and filled to the top with water. It was placed in the climate chamber described in Section 3.4.3, where the temperature could be stabilized and humidity altered. The surface temperature was measured with the Fluke 474 IR thermometer for a range of humidity conditions, leaving at least 2 hours for the trough to achieve thermal equilibrium. The procedure was repeated for a hexadecanol monolayer covered surface. This was done to determine the natural

lowering of the surface below the air/chamber temperature of 23 °C at various values of humidity. No direct wind was present in the chamber, though a circulating fan was left running near the ceiling of the chamber.

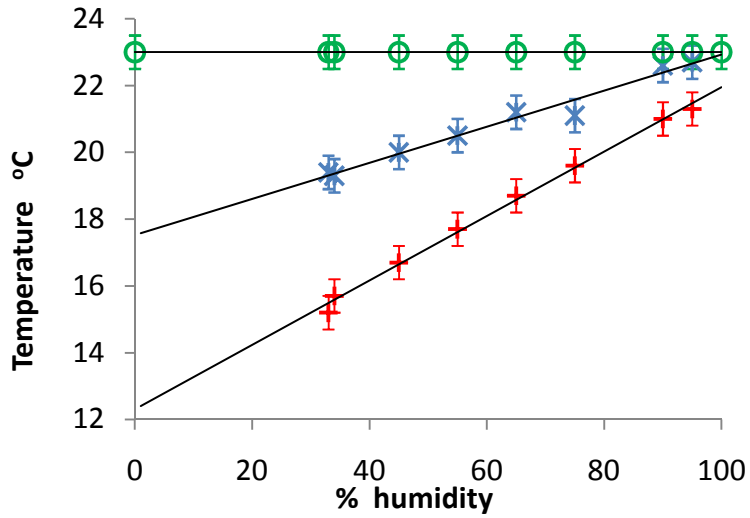

Figure 4.20 Surface temperature of water(+) and hexadecanol (*)cooling in relation to air temperature (○). Error bars are ±1 s.d. of measurements.

Results and Discussion

The values of T_{AS} for hexadecanol were roughly half that for the clear water (Figure 4.20). The relationship between surface temperature and air humidity shows a linear trend as predicted by Equation 4.20.

The graph also shows that the monolayer surface reaches air temperature at 100% humidity, whereas the water surface seems to be heading for 22 ^{0}C, a degree below air temperature. The setting of emissivity on the IR thermometer is an obvious cause; however this would have also affected the monolayer.

One possible explanation is that water the humidity was not as high as read on the humidity sensor and some evaporation was still occurring at the value of 100%. This would tend to lower the water temperature data series more than the monolayer.

4.5.5 Using underwater jet as a method of determining ΔT_S with IR measurements

One idea that has been suggested in literature (Ewing & McAlister 1960) and by John Saylor (Pers. Comm 2009) is to sample temperature at depth by pushing water to the surface using an underwater jet. Radiometers have the disadvantage that they can only measure the surface temperature, and cannot view to any depth. This can be remedied by using an underwater water jet to push water to the surface and measure the temperature of subsurface water pushed to the surface. When the jet is switched off, the radiometer will be measuring surface temperature. When the jet is started the radiometer will be measuring sub surface water temperature. The time it takes for the cold surface layer to be restored is about 5 seconds (Saylor, Smith, & Flack 2000) (see Section 3.2)so the jet needs to create a noticeable slightly raised area at the surface to ensure bulk temperatures are being

measured. This method was successfully employed by Ewing and McAlister (1960) using an underwater jet at a depth of 15 cm.

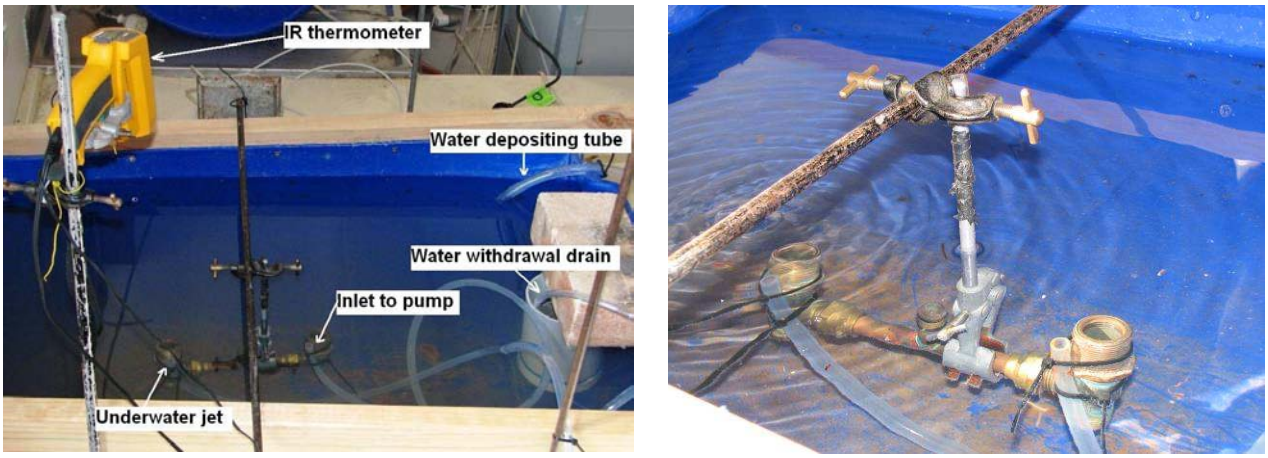

(a) **(b)**

Figure 4.21 (a) IR thermometer clamped on a retort stand aimed at the surface of the underwater jet. The PVC pipe on the right side of the trough was added to keep the surface clean. It had a siphon tube leading to a sink and had a water level below that of the trough. (b) Close up of plastic tubes of underwater jet running. The ripples can be seen moving away along the surface.

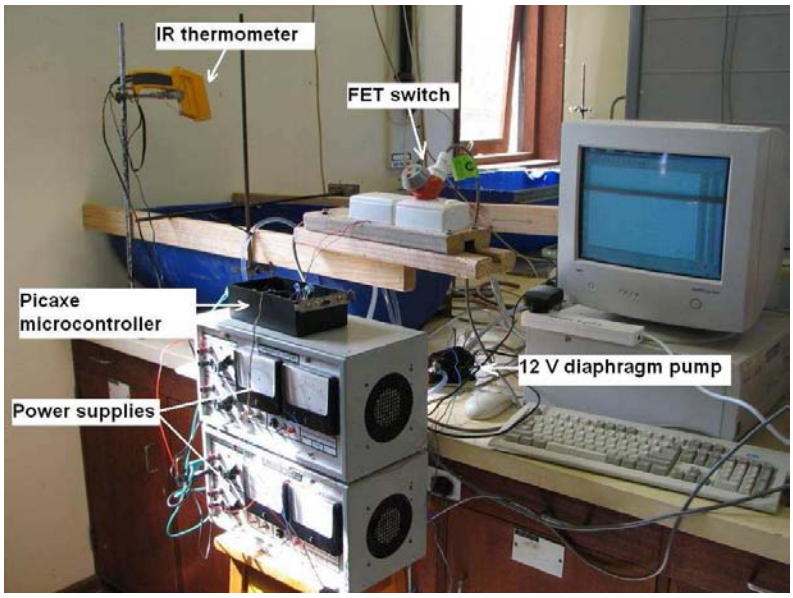

Figure 4.22 Setup for measuring surface deviation temperature.

Materials and Methods

The Fluke 474 IR thermometer was clamped on a retort stand pointing at the surface of an underwater jet positioned in a 200 litre barrel cut in half vertically, as shown in Figure 4.22. The jet was powered by a 12 V diaphragm pump, with an inlet at the same depth as the jet, 5 cm. This depth for the inlet is well below the skin and subskin layers. The output of the jet was strong enough

to form a region of slightly higher than the surrounding water as shown in Figure 4.21(b). The output of the pump needed to achieve this was around 6 litres min^{-1}. The jet timing was controlled a Picaxe, which could automatically switch the pump's 240 V power supply providing the 12 V. power supply through a solid state relay CX240D5 (Crydom,USA). Switching the 240 V to the power supply may seem unusual, as it would seem easier to switch the 12 V output to the pump. However the 12 V DC output was insufficient to reliably power this particular solid state relay, which has specification of a working voltage of 12- 280 V.

The Picaxe was programmed to control a repeated pump sequence of 2 minutes off, then 2 minutes on. Measurements were begun by initially filling the trough with hot water, around 30 °C, and turning the IR thermometer recording software on to log every 3 seconds, then leaving the trough to cool, usually overnight. A recording of the temperature of the surface of the trough, above the jet is shown in Figure 4.23. Generally the initial heating of the trough using hot tap water and gradual cooling of the trough can be observed. The pump switching on can be seen by the small rises in temperature as the bulk water is pushed to the surface, and when it is switched off, a quick cooling is seen as the surface temperature re-establishes.

The difference in temperature between the pump on, and pump off, is the surface deviation temperature ΔT_S. T_{AW} was also simultaneously logged using a thermocouple type K probe connected to the IR thermometer to determine air temperature.

Results and Discussion

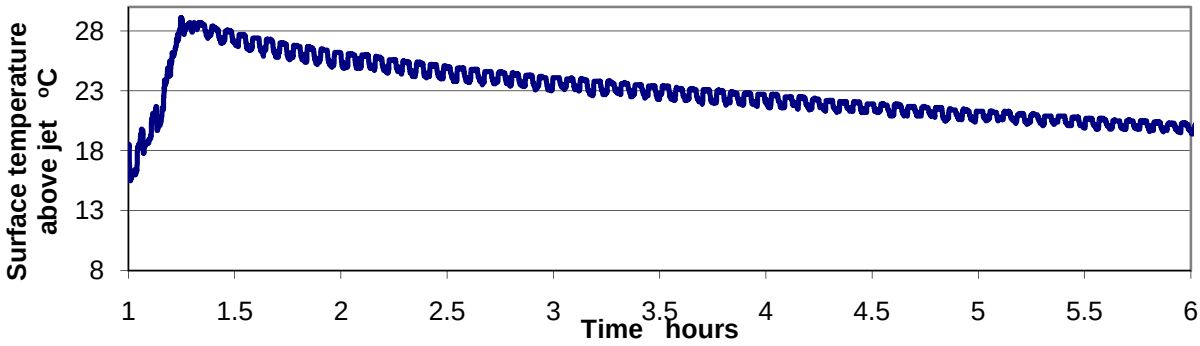

Figure 4.23 Temperature of trough surface above jet as the pump is switched on and off. Initial heating was gained by adding hot water, and then a natural cooling.

The temperature logged by the IR thermometer is shown in Figure 4.23. For several hours hot water was running into the trough and being drained to a sink. This heated the trough water to around 28 ºC. The 2 minute cycling of the pump is particularly noticeable with the high water temperature, as the jet warms the surface when switched on. It reduces as the water temperature decreases over several hours.

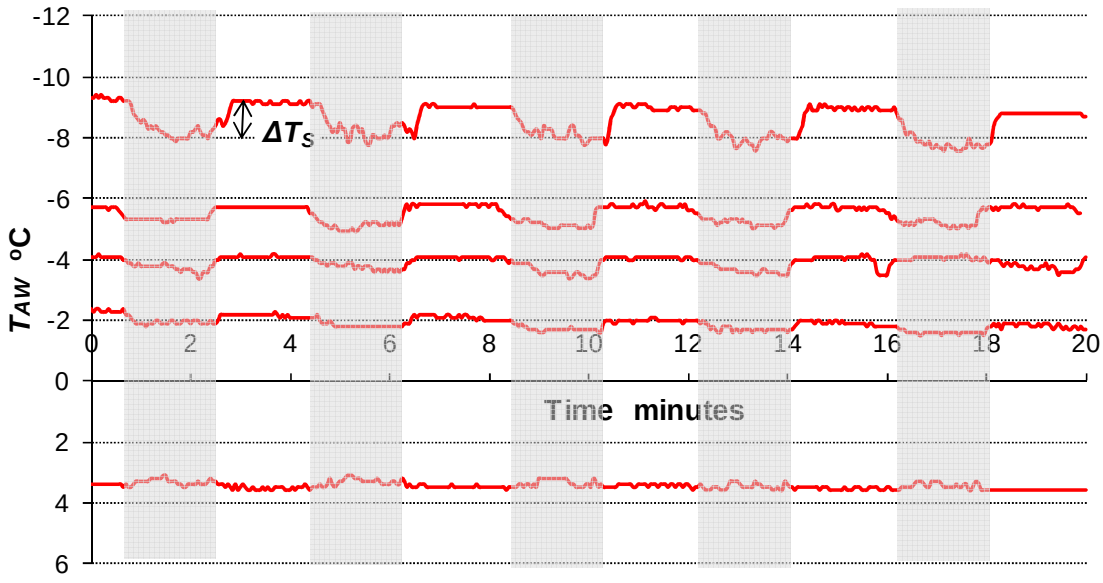

Figure 4.24 Expansion sections of Figure 4.23. ΔT_S can be determined by the difference in temperature difference that occurs between areas of pump on (light areas) and pump off (shaded areas).

Figure 4.24 shows sections of 20 minutes, cut out of Figure 4.23 and positioned over each other with the height governed by the T_{AW} value in. The lengths of Figure 4.23 which showed a high water temperature (negative T_{AW}) are still high on Figure 4.24, due to the y axis being plotted in reverse order.

The value of ΔT_S can easily be found from these 20 minute intervals, as the fluctuations that occur in temperature as the pump is switched on or off. Each data series was a small part of the cooling curve of the trough water beginning with negative T_{AW} values and moving to positive values. When the pump was on, the T_{AW} was being measured, by subtracting the measured value from the air temperature simultaneously being measured by the IR thermometer.

Once the trough had cooled the next day ice was added to to gain a larger positive T_{AW}. However apart from a slight peak when the pump started, because of the warmer water in the pipes, the magnitude of ΔT_S was too small to be measured. This is probably due to latent cooling being opposed to the warming sensible heating of the ambient air. This is in contrast to the negative T_{AW} for warm water, when the heat fluxes for these three processes combined to cool the skin. Gladyshev (2002) cites Ewing and McAlister (1960) who measured the ΔTs in a similar way on a sea surface, with the jet much lower, at a depth of 30 cm. Their results are shown in Figure 4.25.

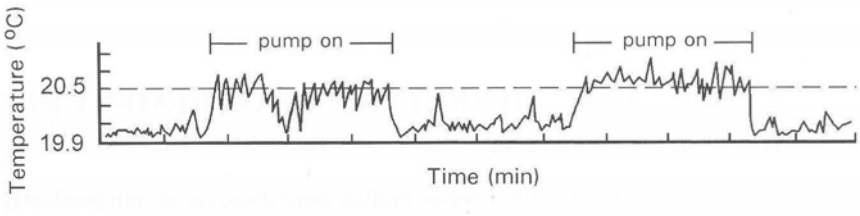

Figure 4.25 Ewing and McAlister (1960) similar measurements using an underwater jet at a depth of 15 cm with an air temperature of 18.4°, therefore a T_{AW} = -2.1°

For these results T_{AW} was around -3 °C when the measurements were taken. This is surprising as T_{AW} is usually positive as the air is usually warmer than the water, and no mention of other values

was made. It seems that this method is capable of showing the subsurface temperature, and therefore determining ΔT_S, however results show a more distinct change of temperature with negative T_{AW}.

An alternative approach to measuring the subsurface temperature would be to place a sufficiently large sheet of metal of known emissivity such as aluminium on the surface. It would assume water temperature, and since there is no evaporation under the metal, it would show subsurface temperatures remotely from above. Thus ΔT_S could be determined by comparing water temperature to metal temperature. This method was attempted using aluminium foil that was shaped like a boat with a flat bottom. An obstacle encountered was setting the emissivity of the IR thermometer. The emissivity of water is around 0.96, while aluminium foil has a value of 0.05 at 5 μm (Kaye & Laby 1973) and it was not possible to set the emissivity of the instrument to this value.

Another possible method of determining ΔT_S remotely makes use of the inherent variations in the absorption properties of water according to wavelength. The absorption of IR radiation in the 1-10 μm region is shown in Figure 4.26. It can be seen that the penetration depth varies widely in this narrow region. The radiation from a shallow depth wavelength could be compared to the radiation from a deeper depth, to determine if the amount of radiation is different, indicating a higher or lower temperature deeper into the water. This may be possible with multiband measurements (Section 4.7).

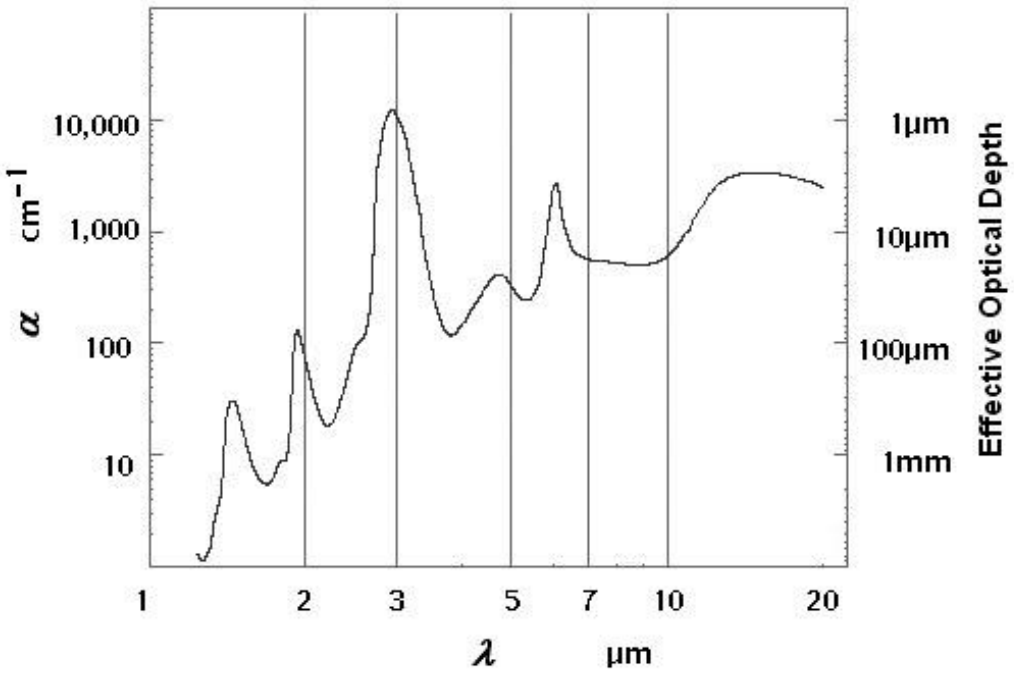

Figure 4.26 Close up of Figure 3.2 in the IR region showing the absorption coefficient *α*, and effective optical depth, in the wavelength region 1-20 μm**. Adopted fro**m **Wieliczka, Weng, & Querry (1989).**

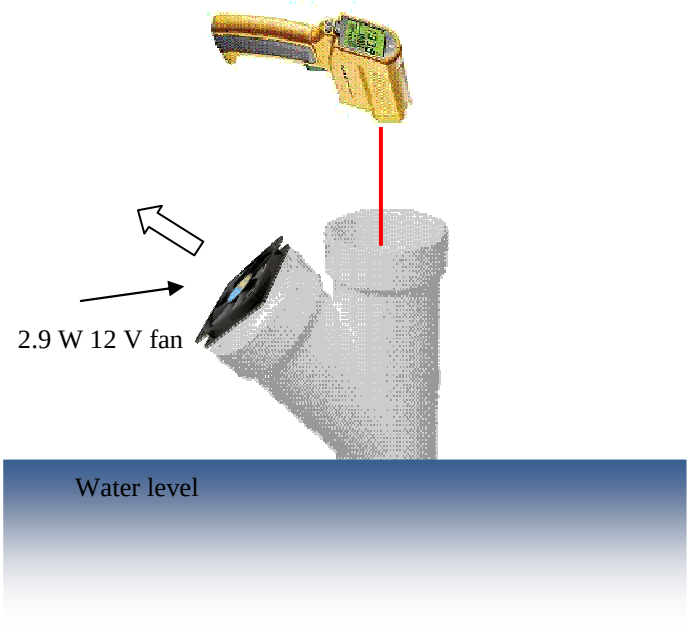

Figure 4.27 Setup for measuring surface temperature for an enclosed surface.

4.5.6 IR surface measurements

Wind causes an increase in the evaporation rate, as predicted by Dalton's Equation. This increase would act to cool the surface, which may be measureable using an IR thermometer. A water surface should cool to a greater degree than hexadecanol as the evaporation rate would increase by a larger amount, as shown in (Section 3.4.1), and this difference may be useful as a detection method.

Materials and Methods

A 100 mm diameter PVC Y tube Y tube with a 12 V 2.9 W (Sunon MD1208PTS1, Taiwan) fan of casing size 80 mm, in the lower arm was held in a larger trough so that an area of surface could be analyzed under various wind speeds.
The 574 Fluke IR thermometer was clamped at a height of 40 cm above the water surface directly above the open top inlet arm, and directed downwards into the centre of the vertical arm of the Y tube, observing the water surface.

By using an IR thermometer the surface temperature for each of these wind speeds can be measured. The fan was only run for short periods, since running times over 5 minutes produced unwanted cooling of the outside container. As the IR thermometer only measures surface temperature, when used in isolation it cannot determine ΔT_S as the subsurface temperature is not known. However, since the value of ΔT_S is affected by wind speed, and the subsurface temperature is fairly constant over short intervals of time, the temperature differences due to changes in wind speed may give a reasonable estimate of the changes in ΔT_S, and show differences between water and monolayer.

Three fan speeds were used as measured with the Lutron LM8000 anemometer at the inlet arm with the fan initially switched on after one minute, then alternatively off and on each two minutes. The

initial voltage supplied to the fan was 5 V, then 10 V, then 15 V. The water run was performed first, so that a few hexadecanol crystals could be added immediately and the run repeated immediately with the monolayer under identical ambient temperature conditions.
A computer interface program called “IRGraph v2.3.16”, supplied with the thermometer, was adjusted to measure temperature every five seconds.

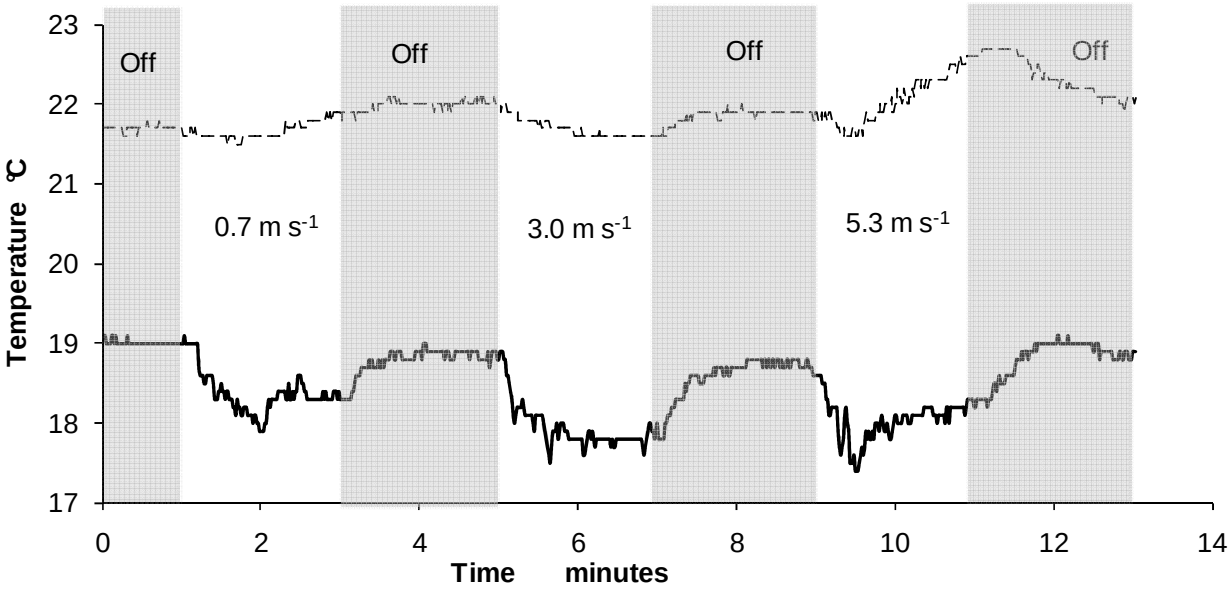

Figure 4.28 Remote IR measurement surface temperature under various wind speeds. Dark series; water surface. Light dashed series; hexadecanol. Conditions; air temp 24 ºC with 35% humidity.

Results and Discussion

The fan sequences for water and monolayer are shown in Figure 4.28. It is evident that the monolayer surface is warmer generally, as expected due to the lowering of evaporation. All conditions were the same since the monolayer data was obtained only 5-10 minutes after the water sample. A much smaller reduction of temperature was obtained with low and medium fan speeds for monolayer. This is important, as it shows the surface temperature of a monolayer is much less affected by an increase in wind speed, suggesting that evaporation reduction would increase with wind speed. The increase in temperature drop of water with increasing wind is similar to those obtained in Section 3.4.8. At wind speeds of 5.3 m s^{-1} an increase of temperature occurs as the turbulence of the surface is probably breaking down and mixing the cool skin with deeper water, leading to a measured higher temperature.

Another unexpected feature are the larger temperature fluctuations for the water data, presumably arising as the surface is less viscous and alters changes temperature more quickly due to more active thermals (Saylor, Smith, & Flack 2001). In general the results show that for about 1 minute after the fan is switched on, the temperature of the water surface cools around 1º C, or more than twice the cooling of monolayer. After this time thermals act to warm the surface and the difference is less predictable.

4.5.7 Conclusion

The detection of monolayers using IR measurement of evaporative cooling that occurs on an enclosed surface appears to show results and this will be further explored in Chapter 6. Wind does appear to be an important factor in creating a surface temperature difference between covered and uncovered surfaces. Efforts to enlarge these temperature differences are presented in Chapter 6,

4.6 Multiband observations

An extensive amount of work has gone into attempting to model and predict the temperature difference across the skin layer (Emery *et al.* 2001) so that the subsurface temperature may be determined remotely. There is a possibility of viewing through the skin using radiometers of larger wavelength, since larger wavelengths have a larger effective optical depth. This may be effective in determining the temperature gradients that occur at the surface, so that sub skin temperatures can be ascertained. For instance Donlon (2002) has used a microwave radiometer operating at a wavelength of λ= 37 mm (6-10 GHz), which averages the surface thickness of 1 mm.

The availability of low-cost spectroradiometers offers an opportunity to revisit the wavelength-dependent measurement of reflectance from monolayers compared to that of clear water. A two channel broad band radiometer was first built and used by McAlister and McLeish (1970) in 1970 measuring the wavelengths of 3.7 and 4.8 μm. They claimed some success with aerial results within 10% of heat flux sub surface/surface values. The radiometer however lacked sensitivity and only two points were produced, on which to base the temperature gradient.

McKeown *et al* (1995) used a 41 channel radiometer that operated in the region 2-5 μm. This particular region was chosen because wavelengths larger than 5 μm show little difference in effective optical depths, while wavelengths smaller than 2 μm penetrate too deeply to map the skin temperature gradient. A sharp variation in effective optical depth provided a temperature depth comparison with minimal changing parameters (such as emissivity and water vapour absorbance) caused by a change of wavelength. For this reason the two regions chosen were both sides of the 3 μm absorption peak shown in Figure 4.26. The possible “sounding widows” were in the wavelength regions:

- 2.2 to 2.74 μm with a minimum at 2.2 μm. This provided a window of effective optical depth of 0.54 mm. A declining Planck radiance below 2.44 μm caused spectral noise to dominate the results which makes this minimum unusable.

- 3.33 to 4.17 μm, with a minimum at 3.8 μm. This provided a window of effective optical depth of 0.084 mm. A radiance variation was measured depending on the skin temperature gradient. With a cool skin, it would be expected that the radiance spectrum would invert Figure 4.29 as the lower the absorption coefficient, the deeper the signal source, and the warmer the region. This was noticed and by measuring the radiance every 0.025 μm, a temperature gradient was obtained which correlated well with thermistor results.

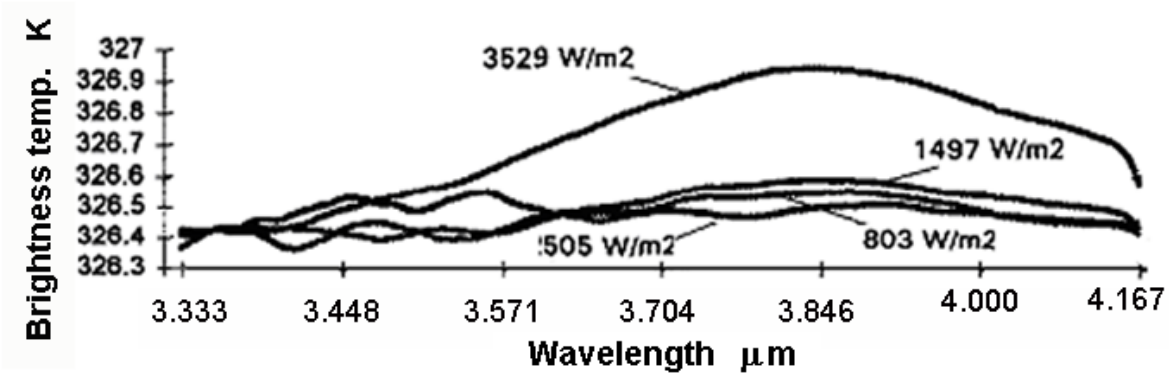

Figure 4.29 Spectral change with decreasing radiance. Adapted from McKeown *et al.* (1995).

This experiment however was performed under controlled conditions, with warm water, initially at 57 °C to increase the radiation which improved the signal to noise ratio. The water was allowed to cool for 60 minutes while continuous measurements were being taken. The volume of the tank was 2 litres and this was positioned out of the sun, so that glint would not interfere with results. The heat flux at 57 °C was 3500 Wm^{-2} and at room temperature 60 minutes layer; 100 Wm^{-2}.

The unobtainable condition used in this technique would be the use of warm water, which raises the signal to noise ratio for the detector. The proximity to the surface in these experiments were also important to minimize radiation from the atmosphere and at some wavelengths; absorption by CO_2, ozone and water vapour. Results shown in Figure 4.29 show the variation in brightness at 3.8 μm, however also shows the large difference that warm water- hence large temperature gradient- plays in obtaining reasonable signal above noise. Therefore although it is a useful technique for laboratory conditions (McKeown *et al.* 1995), there is too many conditions for its successful use in field conditions.

A possibility for applications in the field is to compare IR radiation level from the surface with microwave radiation at an averaging depth of 1 mm. Because of the large difference in wavelength, the calibration would need to be carried out individually for both wavelengths, it would be fairly expensive, and it would possibly be necessary to make measurements at night to eliminate gleam and the solar heating profile.

4.7 Experimental detection using multiband wavelength methods

Detection of hexadecanol, octadecanol and Aquatain were attempted with a wideband spectrometer using clear water to calibrate the instrument, and then taking measurements of the samples. Any differences would show as differences from unity. It would be expected that any increases would be increases based on the reflectivity *R* of water (~2%).

Materials and methods (Vis-NIR reflectance)

The relative reflectivity of hexadecanol, octadecanol and a film of Aquatain surfaces were measured, compared to water. A FieldSpec Pro spectroradiometer (ASD, USA), with a 0.35-2.5μm spectral range, 10 nm spectral resolution and a 25º field of view, was orientated to view the reflection of an incandescent desk lamp as depicted in Figure 4.30.

The spectroradiometer comprised a 512 element, low dark current NMOS photo diode array designed to operate at room temperature. This was combined with two IR spectrometers which use a single element InGaAs detector, thermoelectrically cooled to provide additional coverage for the wavelengths form 1.0-1.75 and 1.75-2.5μm ranges. The integral operating software contains a clibration procedure, where the output from the three internal spectrometers is matched to give a continuous spectral response curve.

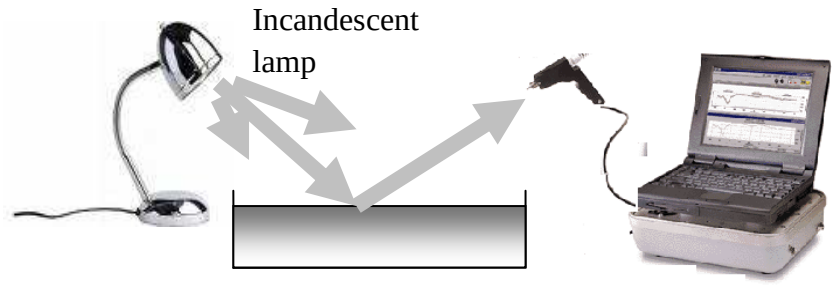

Figure 4.30 Experimental arrangement for comparing the clear water reflection with film reflection intensities over wavelengths 0.35-2.5 μm.

The wavelength-dependent reflectivity of the monolayer relative to clean water, Relative R(λ) was calculated using:

$$Relative\ R(\lambda) = \frac{I_M(\lambda) - dc(\lambda)}{I_W(\lambda) - dc(\lambda)} \qquad (4.21)$$

where $I_M(\lambda)$ and $I_W(\lambda)$ were the intensities of the intercepted radiation measured by the sensor for the monolayer and clean water respectively and $dc(\lambda)$ is the dark current as self-measured by the instrument during the standard instrument calibration protocol. The wavelength-dependent reflectitity was measured for angles of incident (and detection) set at 10º, 45º and 70º. Each set of measurement involved the collection and averaging of 5 spectra.

The water containers used were polypropylene food containers of dimension that the sampling surface area measured 10.95 × 16.48 cm (180.5 cm^2) with a water depth of 5.0 cm. New troughs were used for each sample, which were rinsed prior to use to prevent any cross contamination.

By way of comparison, reflectance spectra were acquired for hexadecanol and octadecanol, each applied by dropping a few crystals onto the surface to produce a full pressure monolayer. The samples of both hexadecanol and octadecanol were obtained from university stores, and were originally purchased from The British Drug Houses Ltd (BDH). No statement of purity could be obtained.

A set of reflectivity spectra for a film of Aquatain was also acquired. An eyedropper was used to add Aquatain to the water surface. The density of Aquatain was determined using a standard laboratory density bottle, and found to be 903.5 kgm^{-3}. An accurate balance was used to measure the mass of 50 drops of Aquatain and from this the drop volume was found to be 49 ± 1.3 drops per ml, or 2.04 $\times 10^{-8}$ m^3. Based on this calculation the thickness of surface film gained by adding one drop would therefore be 1.13 μm. In 2007 the Aquatain web site suggested application rate given was 6 litres/hectare of water surface area with subsequent top ups. This was later changed in 2008,

and reduced to 2 litres/hectare every 10 days (www.aquatain.com 2008). These figures correspond to a desired thickness of around 0.2-0.6 μm. For this work thicknesses based on simple drop-wise addition of monolayers, that is corresponding to 1 drop (1.13 μm), 2 drops (2.26 μm) 5 drops (5.65 μm).

With each application of monolayer or Aquatain to the surface of initially clean water, the surface was carefully observed to ensure the surface layer was uniformly spread, with no crystal or film residue evident within the field of view of the spectroradiometer.

Results and Discussion (Vis-NIR reflectance)

The reflected spectra for hexadecanol and octadecanol was measured for the angles of 10 °, 45° and 70°. Two samples, a 10° and 70° reflectivity are shown in Figure 4.31. Each graph includes a baseline reflectance spectra of clear water taken after each monolayer spectra. This latter spectra should be a horizontal line of unity reflectance and it is evident that the measurements are close to the noise limit of the spectrometer given the apparent deviation in this baseline spectra from the expected unity value. With exception of the 1.8-2.5 μm region, the uncertainly appears close to 1%; in the 1.8-2.5 μm region this fluctuation appears to be considerably larger at around 5%.

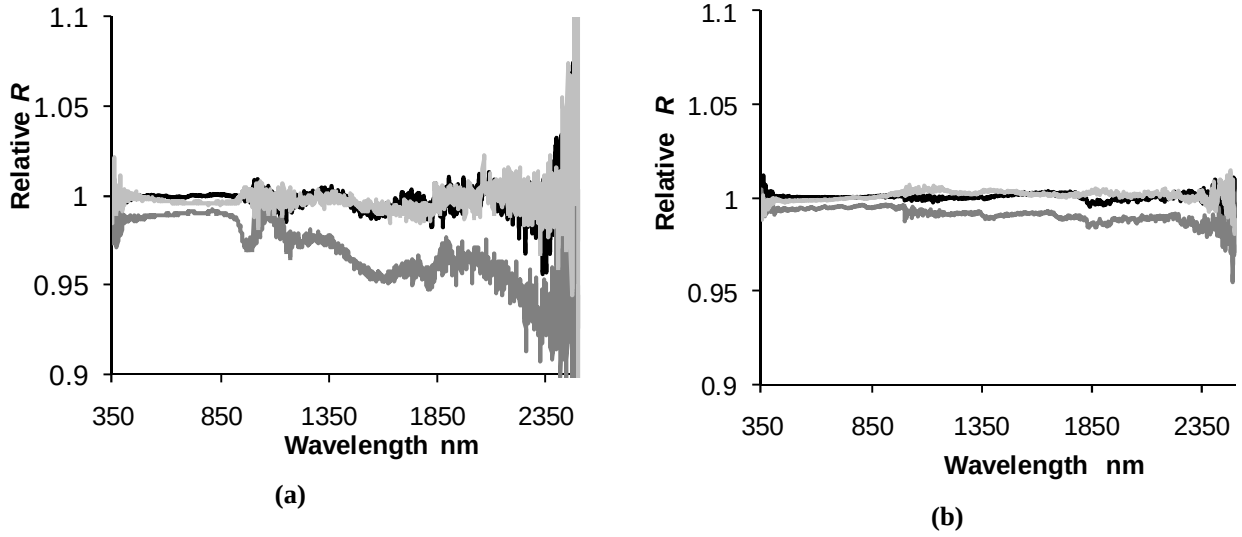

Figure 4.31 (a)Relative reflectivity spectra of hexadecanol(dark grey) octadecanol(light grey) and water baseline (black) (expected to be unity) for angles of incidence of 10º (a) and 70° (b).

Whilst there were small deviations from unity reflectivity for the hexadecanol and octadecanol, there were no significant spectral reflectivity features that could be discerned when compared to the fluctuations in the baseline water spectra. It was noticed that while the average of spectra was being carried out, each spectra was flashed onto the computer screen. Each of these spectra varied by at least 5%, indicating these measurements are on the limit of resolution of the spectrometer. The fact that hexadecanol showed a low reflectivity in these two images is only a random fluctuation as it showed a higher reflectivity than the baseline water and hexadecanol for the 45° run, and also other spectra. So no absorption features, as shown in Figure 4.12 could be identified and also no thin film interference was observable.

These results are inconclusive insofar as identifying any expected spectral features associated with harmonics of the absorption features described in Section 4.4.2. Moreover no consistent change could be measured with the monolayers, using these methods. The differences from unity were generally less than 1%.

The results for the much thicker layer of Aquatain, however showed unambiguous thin film interference patterns when tested using the same procedure, only this time testing three thicknesses of the silicone oil. The same angles were used as for monolayers, are 10º (Figure 4.32), 45º (Figure 4.33) and 70º (Figure 4.34).

Unlike any of the monolayer reflectance spectra, here the hallmarks of a thin film interference pattern show very clearly for the 1.13 μm film thickness at all three angles. The almost sinusoidal reflectance spectra, with peaks of increasing wavelength separation are indicative of harmonics associated with constructive and destructive interference. As the film thickness and therefore opacity increases to 5.65 μm, the reflection from the lower surface creating the interference is lost and reflectivity only occurs from the top surface, leaving a relatively constant value which increases with wavelength. The elevated reflectivity values spanning 1.5-2 compares well with the value of 1.7 measured for a silicone oil by Gainer (1969) when using incident sunlight.

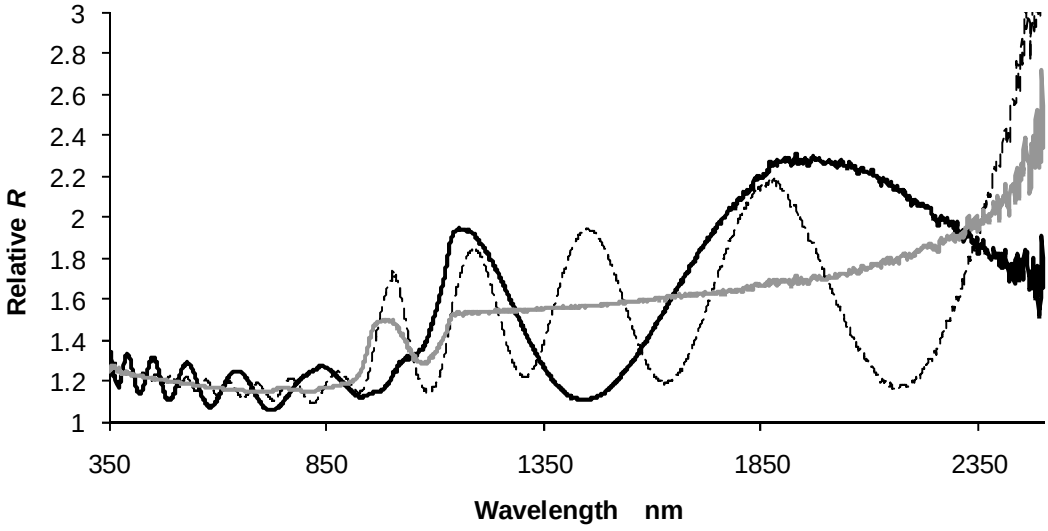

Figure 4.32: Reflectivity spectra of Aquatain films at 10º. Thick black line= 1.13 μm thickness, Dashed line = 2.26 μm thickness; thick grey line = 5.65 μm thickness.

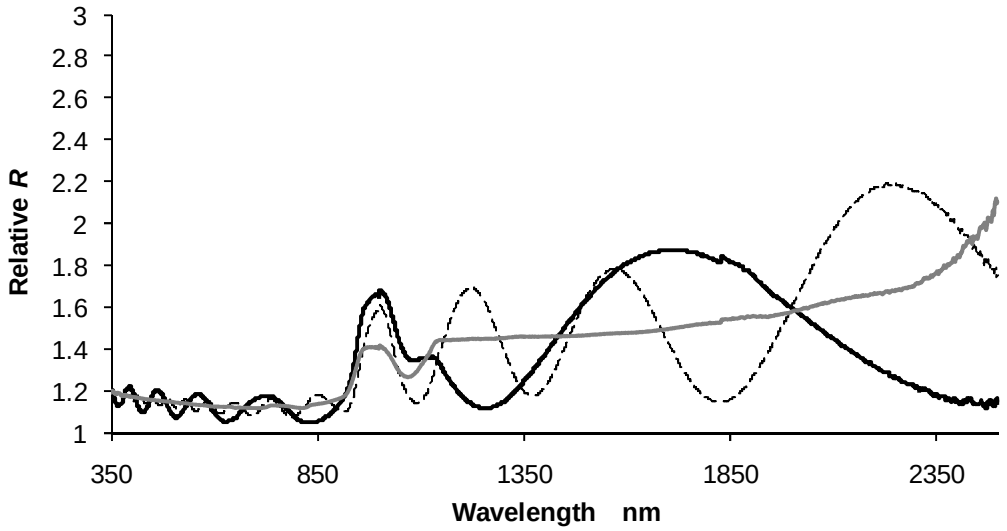

Figure 4.33 Reflectance spectra of Aquatain films at 45°. Thick black line= 1.13 μm thickness, Dashed line = 2.26 μm thickness; thick grey line = 5.65 μm thickness.

.

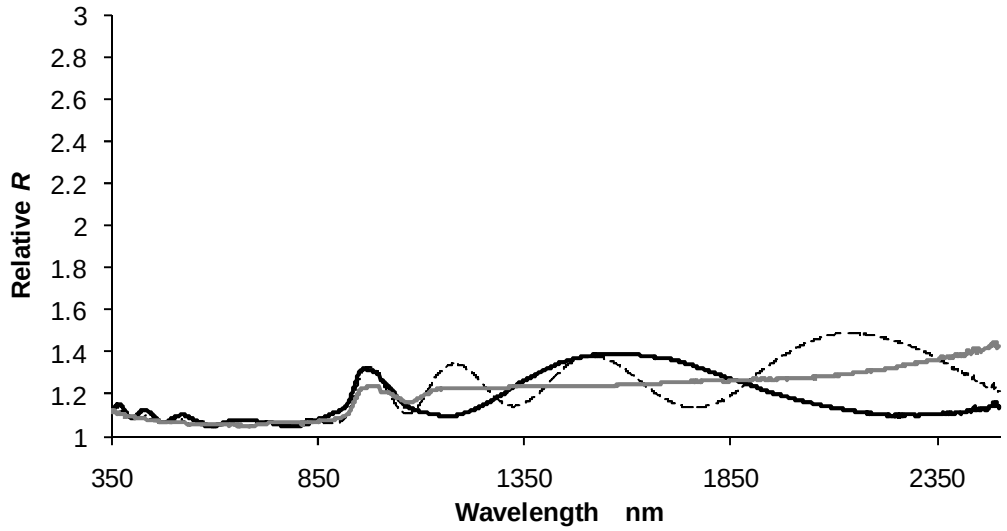

Figure 4.34 Reflectance spectra of Aquatain films at 70°. Thick black line= 1.13 μm thickness, Dashed line = 2.26 μm thickness; thick grey line = 5.65 μm thickness.

Similar behaviour occurs for all three angles, with a generally decreasing reflectivity value for increasing incident angles.

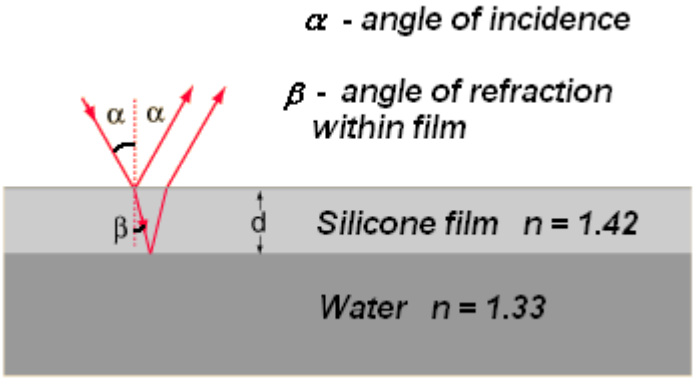

Figure 4.35 Refraction angle notation through the thin film.

The thin film interference spectra produced by the film can be analysed to accurately verify the film thickness. Since there is a phase change as rays enter a material of higher refractive index, the reflection off the top of the silicone oil undergoes a phase change of 180° for the more highly reflected horizontal polarization. The interfering ray that reflects off the oil-water interface undergoes no phase change. Using the diagram shown in Figure 4.35 (Nave 2009):

$$2nd\cos\beta = (m-\frac{1}{2})\lambda \quad \textit{for constructive interference, creating a maximum}$$
$$2nd\cos\beta = m\lambda \quad \textit{for destructive interference, creating a minimum} \tag{4.22}$$

where n is the refractive index of the film- measured to be 1.419 (Chapter1), d is the thickness of the film, m is an integer (1,2,3,…) representing the number of wavelengths making up the path length on the reflection from the lower surface of the film, α is the initial angle of incidence, and β is the refracted angle of incidence on traversing the film.

By way of example using the 1.13 µm series, for each angle the transmitted light reflected from the water surface will undergo refraction, which will change the length of the path travelled through the film slightly. Snell's law can be used to calculate the refraction angle.

Table 4.4 Incident and refracted angles

Angle α	Refracted angle β
10	7.0
45	29.9
70	41.5

By observing the 1.13 µm plot on the 45^0 graph, the maximum on the right side would then correspond to the order of 1.5, and they increase for each maxima moving to the left. The 0.5 order would be a wavelength around 4 times the thickness, as there is a π phase change on reflection at the surface, so the reflected wave would only need a distance of λ/2 for constructive interference. This would make the film about ¼ the wavelength for order of 0.5. To add weight to this choice of

maxima, a few choices were tried and the graph of 1/m against λ also shows a straight line, as it should, only for this choice.

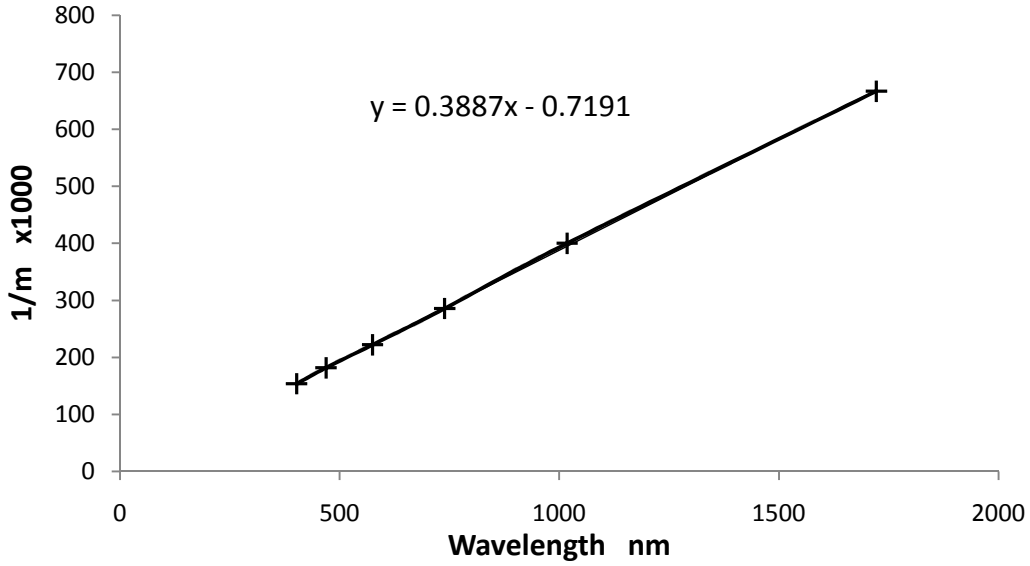

Figure 4.36 Determination of the thickness of the thin film using the interference pattern of Figure 4.33. Angle of incidence = 45°.

The condition for constructive interference, shown in Equation 4.22 can be rearranged as shown:

$$\frac{1}{m-\frac{1}{2}} = \frac{1}{2nd\cos\theta}\lambda \qquad (4.23)$$

to show that a graph of *1/m* plotted against λ will yield $(2ndcos\theta)^{-1}$ as the gradient, from which the thickness *d* can be calculated.

On rearranging:

$$d = \frac{1}{2n(gradient)\cos\theta} = \frac{1}{2\times 1.419(0.000388)\times\cos 29.9} = 1.05\mu m$$

This is slightly below the thickness estimated using the earlier drip volume method (1.13 μm).

In a similar way the thickness for the 10° angle was calculated to be 1.05 μm and 70^0, 1.12 μm. All these estimations are smaller than the physically calculated value. Marple & Vanderslice (1960) suggest that around 0.3 μm of the hydrophilic end may be immersed in water, reducing the thickness obtained by optical means, and this may explain the systematic difference.

Whilst Aquatain has proven an interesting point of comparison for the use of optical reflectance measurements to calculate film properties such as thickness, it remains true that over the wavelength range 0.35-2.5 μm there is insufficient sensitivity to detect changes in reflection characteristics caused by monolayers.

4.8 Fluorescent observations

A combination of monolayer and water-soluble fluorescent dye has been tested by Barger and Garrett (1976) to assist search and rescue efforts at sea using airborne remote sensing devices in addition to visual observation. They tested several water soluble fluorescent dyes, finding uranine to be the most suitable, as it spread out in association with the monolayer. Their aim was to develop a portable package that could be used in times of emergency.

The fluorescent behaviour of various oil slicks was studied by Hengstermann & Reuter (1990) using fluorescent LIDAR (Light detection and ranging) techniques. A 10 MW excimer pulse laser was used, with pulses of 12 ns at a wavelength of 308 nm. This particular wavelength would allow depth penetration of a few metres (check Figure 3.2). At a flight height of 245 m the laser had a footprint of 2.5 m wide. The signal was received with a Perkin-Elmer model 650-40 spectrofluorometer telescope with detection wavelengths of 344-685 nm. The results (Figure 4.37(a) and (b)) show quite a large increase in fluorescence as shown by the clear water run (a) compared to crude oil, fish oil and olive oil. The olive oil is similar to hexadecanol and octadecanol as it contains over 50% oleic acid, a monounsaturated C_{18} acid.

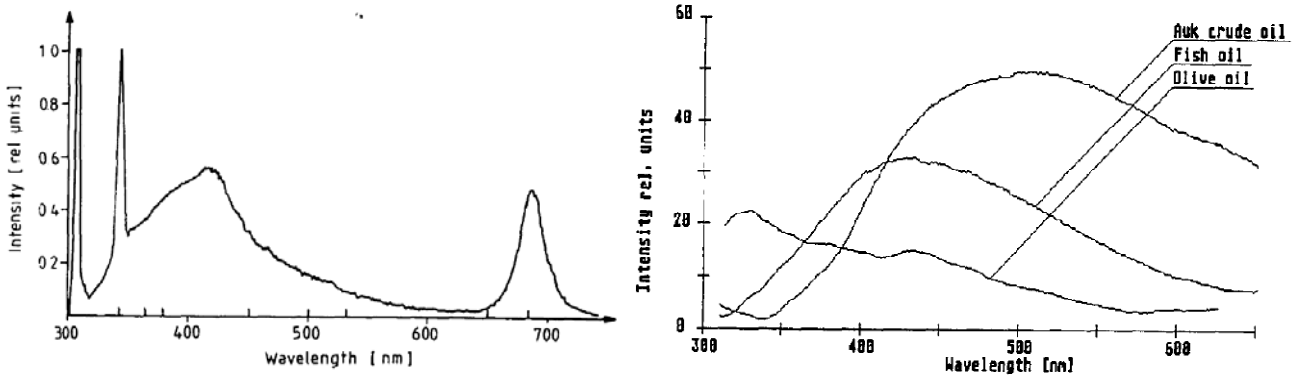

Figure 4.37 (a) Emission spectrum of clear water taken from the German Bight, using an excitation wavelength of 308 nm. The peaks at 308 and 344 nm are due to elastic scattering and water Raman scattering, respectively. The broad band centred at 420 nm is due to dissolved organic matter, that centred at 685 nm is due to chlorophylla.(b) Fluorescence produced with the addition of oils. Adapted from Hengstermann & Reuter (1990).

4.9 Experimental detection using Fluoroscopy

Detection of monolayers may be possible using inherent fluorescent activity with short visible wavelengths or UV radiation, as displayed by oleic acid in Section 4.8 or by combining the monolayer material with a fluorophore.

Material and Methods

An ISS Chronos BH spectrofluorometer was used to examine samples containing hexadecanol and octadecanol by dissolving a small quantity of each into a concentrated solution using ethanol with an excitation wavelength of 379 nm. Also dispersions of Aquatain shaken in water with an excitation wavelength of 360 nm were tested.

These solutions should maximise the degree of fluorescence observable providing more material to observe, improved from the thin film situation, where there is a much lower density of possible fluorophores. This should provide a fluorescence signal several orders of magnitude larger than would be expected for films.

Results and Discussion

The fluorescent emission from hexadecanol and octadecanol excited at 379 nm were quite low as shown in Figure 4.38(a) and (b). The hexadecanol did fluoresce slightly at around 350 nm. The intensity magnitude on the y-axis corresponds to a photon count at these wavelengths and is taken under the same conditions so the absolute values can be compared. Below approximately 800,000, photons are striking the photo detector at a low enough frequency that there is essentially no chance of two photons striking at the same time, and hence the photon count is directly proportional to the amount of substance present.

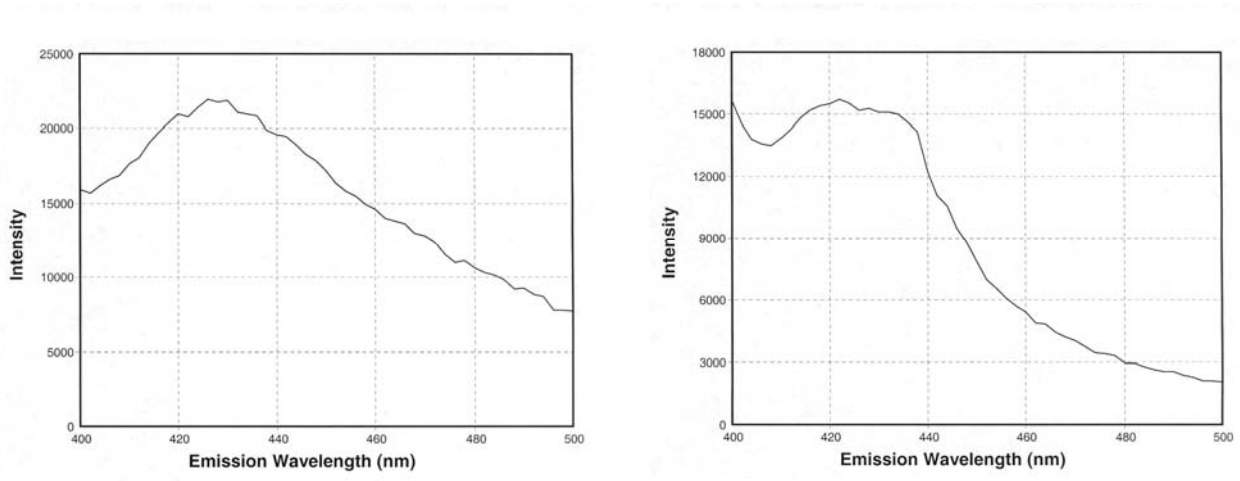

(a) **(b)**

Figure 4.38 (a) Fluorescence signal of (a) hexadecanol and (b) octadecanol in ethanol. Excitation wavelength for both was 379 nm.

By comparison, weaker fluorescence was observed for Aquatain excited at 360 nm as shown in Figure 4.39. The increasing emission intensity corresponds to an increase in concentration of Aquatain in water. It was noticed it formed an emulsion when shaken with water.

The low fluorescence of Aquatain excited at 360 nm was improved with the addition of a lipid fluorescent probe called Prodan (Figure 4.39(b)). A fluorescent probe is a fluorophore designed to localize within a specific region of a specimen or to respond to a specific stimulus. Prodan is a phospholipid membrane surface dye which will fluoresce only within a hydrophobic environment.

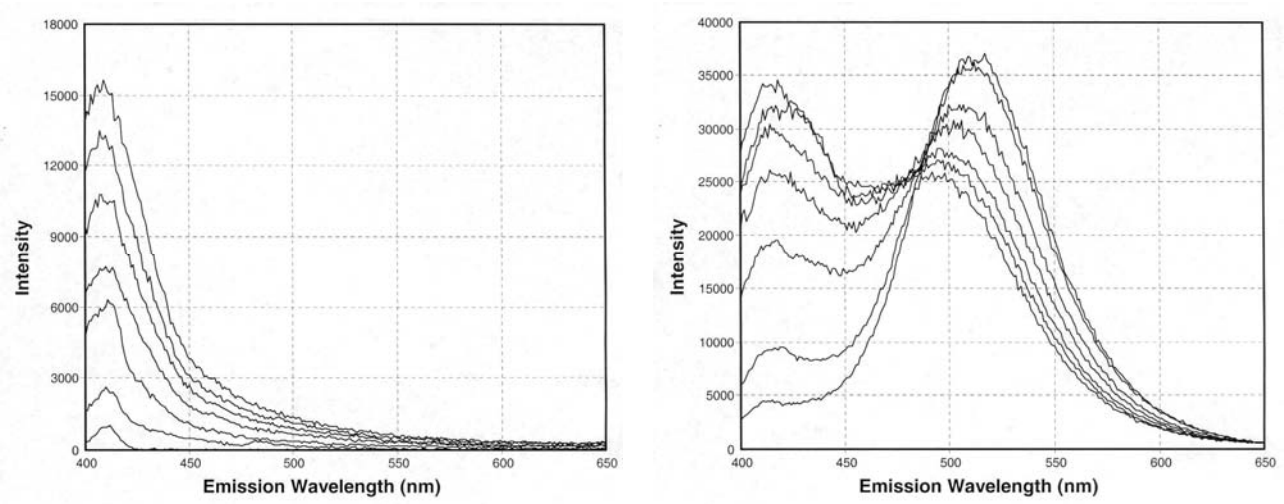

(a) **(b)**

Figure 4.39(a) Fluorescence signal of Aquatain dispersion in water using an excitation wavelength of 360 nm. The lowest line corresponds to pure water, followed by 1% 4%, 8%, 12%, 16% and 20% Aquatain v/v.

(b) Fluorescence signal of Aquatain dispersion in water in the presence of Prodan. Excitation wavelength 360 nm. The lowest line corresponds to a solution of Prodan in water, followed by 1% 4%, 8%, 12%, 16% and 20% Aquatain v/v.

The emission wavelengths are much more intense with two peaks being evident at 420 nm and 514 nm. Prodan in solution gives only the peak at 514 nm. As the concentration of Aquatain increases the left peak at 420 nm increases, with the 514 nm peak decreasing. Absolute values are difficult to use, however if a ratio of the intensity of the 420 nm peak is divided by the intensity of the 514 nm peak, a determination of concentration of Aquatain may be possible in the field. This ratio will then be independent of intensity of lighting conditions.

The use of sunlight as a source of light in detection of fluorophores seems unlikely, as the following answer from a personal communication with Dr. Mathias Lösche (2008) explains, "… I am absolutely positive that fluorescent dyes are totally unsuited for observation in sunlight. The emission from a monomolecular layer simply cannot be seen by the naked eye, i.e. the difference between covered and uncovered surface will be much too low to follow. So, I wouldn't say it's doubtful - it's rather out of the question."

Taking this response into account an artificial light source would be needed and a point testing system would be used, rather than a remote imaging system covering the whole water storage.

The amount of fluorescing amphiphile dye is less than 2% (Barnes & Gentle 2005), and this is could be mixed with the film material before application. The signal fluorescence could then be found by illuminating a portion of the surface and measuring the fluorescence.

4.10 Conclusion

It was found that emissivity changes due to monolayers are not large enough to be detectable under field conditions. Thicker films such as Aquatain, however do show measurable differences both under laboratory, and field conditions.

IR measurements of surface temperature show that the evaporation rate, and therefore evaporative cooling is indeed proportional to the humidity deficit (e_{SWT}-e) as predicted by Dalton's equation.

An attempt to measure the subsurface water temperature using an underwater jet, only produced results when the air temperature was below the water temperature- so that sensible heat processes and latent heat processes both act to cool the surface and produce a noticeable difference between surface temperature and subsurface temperature. When they are acting in opposite directions, when T_{AW} is positive and their effects on the surface cannot be separated to determine the evaporative cooling.

Aerial IR measurements are not as successful at detecting monolayer as might be expected. This has been shown by (Jarvis 1962) to be due to the insulation of the surface caused by impairment of the convective heat flux operating to cool the surface, in opposition to the expected warming due to evaporation reduction.

Fluorescent measurements showed that both hexadecanol and octadecanol produced very little fluorescent activity, unlike oleic acid which is responsible for the slightly luminous glow in olive oil. Addition of the fluorophore Prodan to Aquatain produced interesting results, however due to the cost and difficulties in eliminating solar radiation, as well as the effect of any added fluorophores creating holes in the monolayer cover made any further investigation inadvisable.

The reduction in IR surface temperature measurement with the addition of wind created larger temperature differences between a clear surface and monolayer surface and these will be investigated further in the next chapter.

Chapter 5. The influence of external air flow on evaporation and its potential for detection of monolayers

There is generally agreement between researchers experienced in monolayer field trials that combating the destructive effects of wind whilst harnessing the spreading ability of wind is key to effective deployment of monolayers (McArthur 1962; Tiblin, Florey, & Garstka 1962; Vines 1962). Thus, understanding the processes whereby wind interacts with monolayers should help in developing suitable management practices which can take advantage of the useful aspects of wind, while minimizing the deleterious effects. Wind affects monolayer surfaces and water surfaces differently. For instance the magnitude of the critical wind speed for wave production is higher for a monolayer surface. Also the wind generated wave amplitude is reduced by monolayers, as shown by the higher decay constant in Chapter 2. Some of these differences may lead to potentially useful detection methods, considering the relative ease in producing artificial wind over testing areas on water storages.

Wind affects monolayers in three ways:

- **producing waves** which increase surface area and disturb the packing of molecules in the monolayer
- causing downwind **surface drift** affecting coverage
- increasing the evaporation rate by reducing the thickness of the **vapour diffusion layer**

These three effects will be examined in detail so that some potentially useful differences between a monolayer surface and clear water surface may be examined in the experimental section.

5.1 The production and maintenance of waves by wind

Background theory

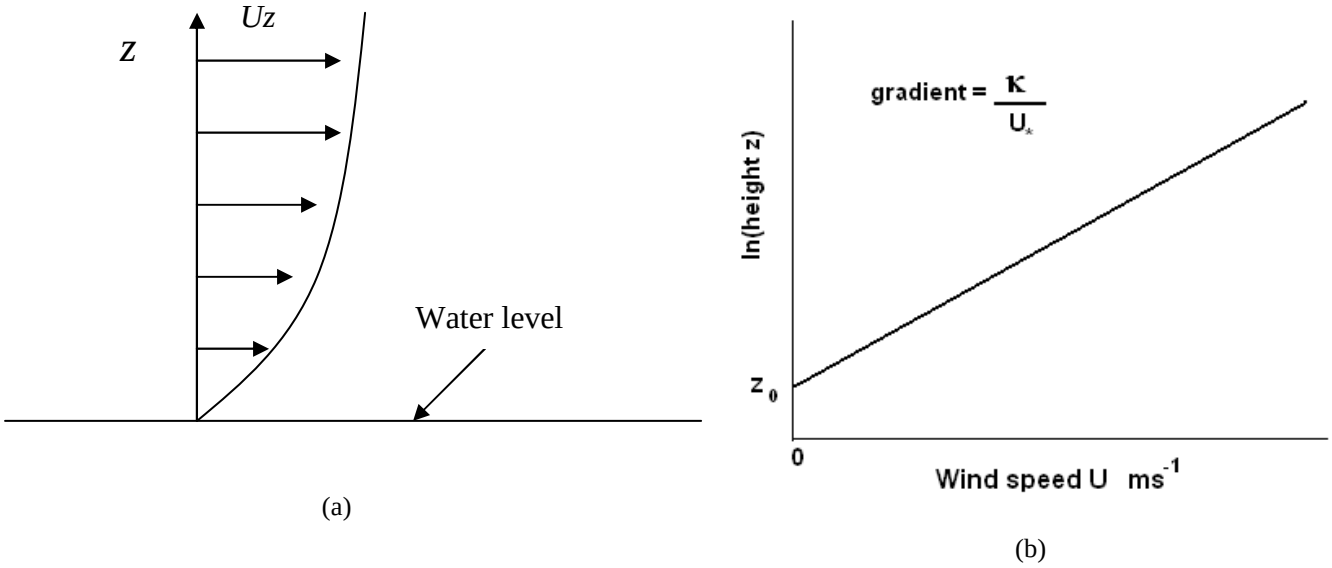

(a) (b)

Figure 5.1 (a) Logarithmic profile proposed by Ruggles (1970). (b) Graphing wind speed as a function of height is often used to determine the frictional velocity *U and roughness length z_0 from experimental measurements.**

In routine meteorological observations, the horizontal wind speed (U_z) above the surface of a body of water at height *z* is measured at a single height of z = 10 m above the surface (Massel 1996:26). There is a reduction of wind speed near the surface due to friction, with the shape of the vertical wind speed profile just above the water surface given by a semi-empirical logarithmic relationship called the "Law of the Wall" initially suggested by Von Karman (1930). It is now commonly called a ***logarithmic wind profile***, given by:

$$U(z) = \frac{U_*}{\kappa} \ln\left(\frac{z}{z_0}\right) \qquad (5.1)$$

where: *U(z)* is the average wind speed at height *z* above the surface, κ is Von Kármon's constant = 0.42 (Takeda 1963), z_0 is the surface roughness length in metres and U_* is the frictional velocity.

The constants U_* and z_0 can be found by taking measurements of wind speed at various heights above the surface and using a rearrangement of Equation 5.1.

$$\ln z = \frac{\kappa}{U_*} U(z) + \ln z_0 \qquad (5.2)$$

A line of best fit (Figure 5.1(b)) reveals the ***friction velocity*** U_* from the gradient, and ***roughness length*** z_0 from the *y* intercept (Ruggles 1970).

The horizontal force wind applied to the surface, called ***wind stress*** is measured by the force applied to a square metre of surface. It unfortunately uses the same symbol as torque τ, so care needs to be taken not to confuse the two. The definition of wind stress τ is:

$$\tau = \eta \frac{dU}{dz} \qquad \text{N m}^{-2} \qquad (5.3)$$

where η is the air viscosity. At the surface (Takeda 1963)

$$\tau_0 = \rho_a U_*^2 \qquad (5.4)$$

where ρ_a is the air density. Thus the stress can be calculated from the frictional velocity. There are several techniques of calculating the wind stress, such as the "set-up", wind profile and retraction methods. The set-up method measures the angle of alteration of the normally horizontal surface when reacting to the force of the wind on water in a wind tunnel. Using this method Fitzgerald (1963) found a lowering of wind stress with the addition of surfactant (Figure 5.2(a)). He found these correlated well with the wind profile method using U_* (outlined in Section 5.1) (Figure 5.2(b)). The retraction method is discussed in Figure 5.16. All of these methods show a reduction in τ as a result of the addition of surfactant.

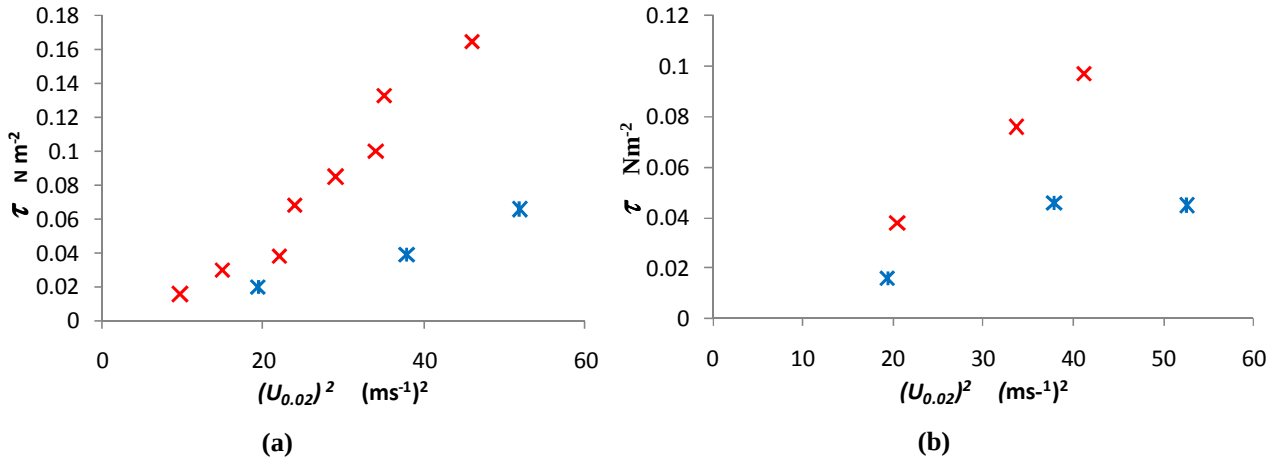

Figure 5.2 Fitzgerald's results (1963) for surface stress using (a) Set-up and (b) Wind profile methods. Clear watersurface; ×, hexadecanol; ✱.

The frictional velocity and wind speed at a height can be related, and this is called the coefficient of drag C_{dz}, where C_d is the variable and subscript z is the height of wind speed that is being compared to the friction velocity. The wind drag is often given in terms of C_{dz} rather than using absolute units (e.g. (Wu 1982)).

The coefficient of drag is a dimensionless ratio defined as $C_{dz} = \frac{U_*^2}{U_z^2}$ and can be found experimentally from the values determined using fitted wind profile (Deaken, Sheppard, & Webb 1956). C_{d10} varies in value from $0.3\times 10^{-3} - 5 \times 10^{-3}$. An approximation often used when relating U_{10} or U_∞ to the friction velocity U_* is that $U_\infty \sim 20U_*$ (Gottifredi & Jameson (2006:391; Ruggles 1970).

The drag of small gravity waves may be the major, if not the only, cause of wind stress at sea according to Francis (1954). These small waves move at a lower wave velocity than the larger gravity waves (Section 2.3.6) increasing the difference in velocity between wind and wave speeds *(U-v)*. They also have a steeper form and a more angular crest than large waves and there are more of them, particularly as the number increases with wind speed. Francis comments that earlier work completed by Van Dorn (1953) with larger waves showed a very similar drag coefficient to a

smaller scale experiment he was conducting, without the large waves, indicating that larger waves may have much less drag. Wu (1988) agrees that large dominant waves have no effect on stress in the field, however he also comments that dominant waves in laboratory wind tunnels do have a direct effect on wind stress.

5.1.1 Effect of monolayers on the roughness length z_0

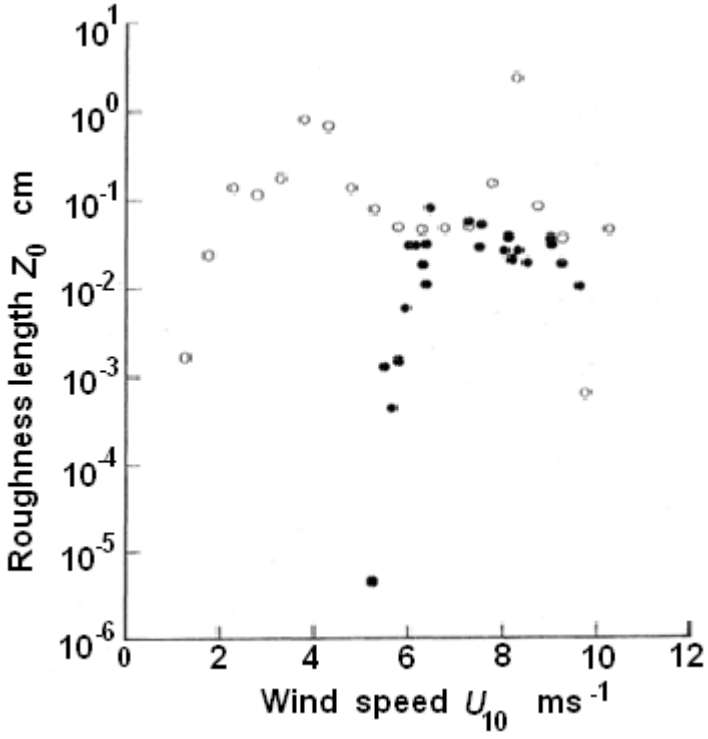

Figure 5.3 Roughness length at sea for clear surface and surface covered with octadecanol. Source; (Wu 1971).

Experiments conducted by Barger and Garrett (1970) show conclusively that addition of a monolayer such as octadecanol affects the wind structure above large gravity waves at sea. They measured the wind speed at heights of 1, 2, 3, 5, 8, and 10 m and used a fitted wind profile as described in Section 5.1 for each wind speed. Wu's (1971) interpretation of the data from Barger *et al*. (1970) is shown in Figure 5.3. The octadecanol monolayer data series shows a reduction in roughness length, for low wind speeds. Barger and Garrett (1970) also measured the instantaneous velocity above large gravity waves with interesting results. With a clear surface they found the maximum horizontal wind velocity is usually at the time of the trough in waves. However with the addition of monolayer it occurs at the peak of the waves.

For the smaller wavelength gravity waves, they explain that the capillary wave induced wind field, which is strongly influenced by the water surface, "loses all knowledge of the motions of the sea" (Barger *et al.* 1970). This would tend to indicate a lowered wave- wind coupling, perhaps due to a decrease in the drag coefficient in addition to a changed wind structure.

Figure 5.3 would also give an indication of the ideal wind speed for maximum contrast using backscatter of radar signals (Section 2.5.1). The backscatter is proportional to wave height, which in turn is related to roughness length. Maximum contrast would therefore be produced by a maximum difference in wave height between the data series in Figure 5.3, which occurs in the area of wind speed below 6 m s^{-1}. The ideal wind speed range found by Alpers & Espedal (2004) (Section 2.5.1) was 3-6 m s^{-1}.

5.1.2 Critical wind speed

The minimum wind speed needed to produce waves is known as the critical wind speed. Theoretically the critical wind speed for water is 0.23 m s^{-1}, since this is value for minimum wave speed, as explained in Section 2.3.6. Wind speeds equal or less than this value cannot produce or reinforce waves below this value since the wind needs to be moving faster than the wave (Lamb 1906:569). Field evidence of the minimum wind speed needed to generate waves is usually higher than this as the waves need to be initiated by slight variations in surface stress, and maintained during a lull between air flow.

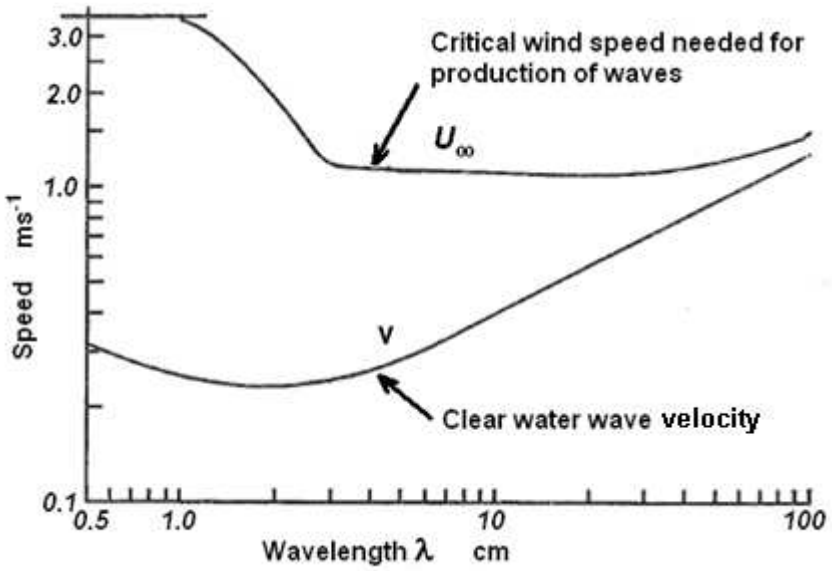

Figure 5.4 Critical wind speed for production of waves for a water surface. Also the critical wind speed needed for production of waves measured away from the surface (U_∞). Adapted from Gottifredi & Jameson (2006).

The minimum value of U_∞ of 1.01 m s^{-1} was measured by Jeffreys (1925:198). Similar results have been obtained for critical wind speed dependence on wavelength by Gottifredi & Jameson (2006), depicted as the curve labelled U_∞ in Figure 5.4. Comparison of the two data series, the critical wind speed and wave velocity show that waves are initiated on the gravity side of the velocity minimum at a much lower wind speed than for capillary waves on the left. This is due to the force on the wave encouraging the wave to increase in size for gravity waves, while there is a conflict for capillary waves, as they need to reduce speed to become larger.

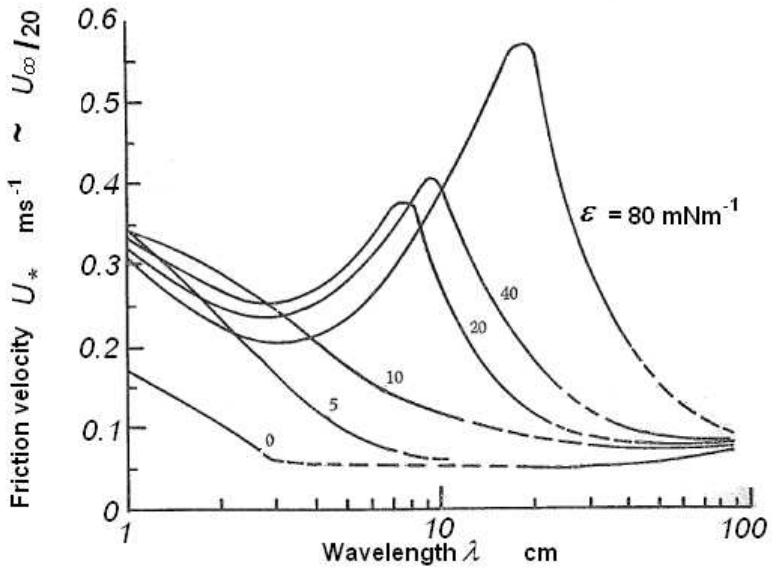

Figure 5.5 Critical wind speed for a range of wavelengths and dilational elasticity values. Source (Gottifredi & Jameson 2006).

The addition of a monolayer such as hexadecanol to the water surface increases the dilational elasticity ε of the surface (Pogorzelski & Kogut 2001) by a value of at least 10 mN m^{-1} (Gottifredi & Jameson 1968). With the addition of a surface film the critical wind speed for wave generation may be increased by a factor of 10 depending on the wave number k and surface dilational elasticity ε as shown by Gottifredi & Jameson (2006) in theoretical calculations of critical wind speeds shown in Figure 5.5. For the shorter wavelengths a very small value of $\varepsilon \approx 5$ mN m^{-1} will double the critical wind speed.

This plot also shows the critical wind speed for pure water (ε = 0 mN m^{-1}) of around 0.2 m s^{-1}. Converting this to actual wind speed (U_∞) by multiplying by 20, produces a value of the critical wind speed as determined by Gade, *et al*.(1998) of 4 m s^{-1} in a wind tunnel. So this is around four times the critical wind speed for water.

Once small waves have been initiated their behaviour depends on the wind speed. The effect of purely tangential force acting in the same direction as existing surface waves in a fluid is to act forwards on the crests of waves and backwards at the trough, changing sign at the nodes. (Lamb 1906:508). This is similar to the circular orbits of the water particles at the surface discussed in Chapter 2 and therefore acts to reinforce their motion. Jeffrey's "sheltering" model (1925) explains the growth of waves in terms of streamlines. He states that with an increasing wind speed, the flow changes from moving steadily throughout the troughs and over the crests to sliding over the crests and impinging on the next wave at some point between the trough and crest.

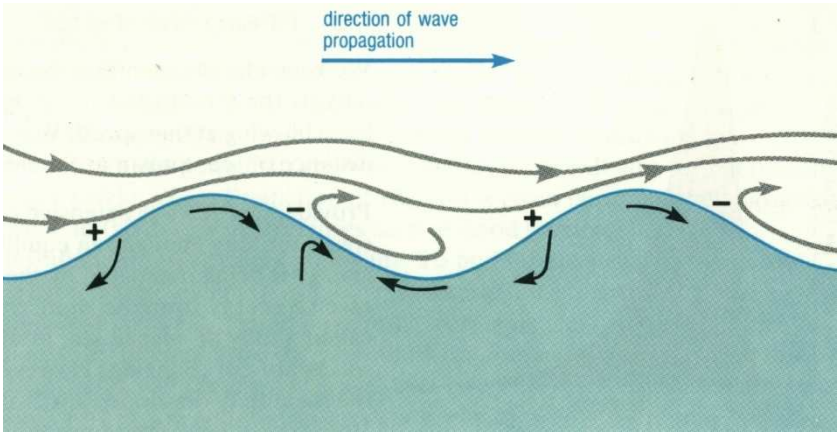

Figure 5.6 Jeffrey's sheltering model. Source; Boss & Jumars (2003) The area of high pressure + on the windward side helps to lift the leading edge of the wave's crest, while the area of low pressure - on the leeward side works to deepen the trough.

With both the wind and waves moving to the right in Figure 5.6, the waves are reinforced. The windward face of the wave experiences an increased air pressure, and the leeward sheltered face of the wave experiences a lowering. In the trough, eddies form reversing the wind direction and decreasing the pressure in front of each wave. The result of this behaviour is to deepen the trough and push the wave along.

As the amplitude of the small gravity waves increases, the wind striking the back face of the wave is deflected upwards to a greater extent (Jeffreys 1925), creating increased turbulence. The addition of monolayer would tend to act against the initial formation and also the process of wave growth described, strongly damping small waves.

5.1.3 Maximum wind velocity endured by monolayers on large storages

Wave damping can be used as an indication of coverage for a range of windy conditions on large storages, when background water can be seen for comparison. McArthur (1962) noticed the damping is visible for hexadecanol for wind speeds ($U_{0.457}$) above 4 m s^{-1} up to 7.4 m s^{-1}. Only poor coverage is possible with U_{∞}= 7 m s^{-1} according to Tiblin *et al.* (1962:184), who goes on to say that for wind speed increases to U_{∞}= 9 m s^{-1} the film would suddenly disappear. They felt that this was probably due to interference of monolayer structure by wave formation and mixing of the hexadecanol in the water by wave action and white capping.

Wave damping can be caused by much lower surface pressure (Section 2.5.6), than the maximum surface pressure possible with the monolayer. So even though the damping may be observed, the surface pressure, and hence evaporation reduction may be substantially lower than what is expected for full pressure. Field trials made in Australia by Tiblin (1962) led to the conclusion that no appreciable evaporation reduction is possible in field conditions above 4 m s^{-1}. Vines(1962:147) noticed that, although winds are known to break up hexadecanol monolayers and sweep them back, under strong winds, a water surface rarely becomes completely uncovered, as shown by the streaky appearance of the wave patterns produced (Vines 1962:147). He also found that the use of solvents causes an increase in the tendency of the film to collapse under windy conditions (Vines 1962:149).

The length of time that strong winds are present and the occurrence of strong winds is not great compared to the evaporation time when they are not present, so the evaporative loss of water due to

monolayer destruction in strong winds in Australia is small compared to everyday evaporative processes (Mansfield 1962:134).

5.1.4 Vapour diffusion layer

A series of experiments performed by Rideal (1924) showed that even under vacuum conditions, the vapour diffusion layer still exists just adjacent to the surface. The effect of this layer on a water surface at temperatures between 20-35 °C is to reflect in excess of 99.5% of vaporised molecules back to the surface reducing the evaporation by at least this amount. Similar experiments on water evaporation led Boer (1968) to postulate that the slow diffusion of water vapour from this layer of water vapour saturation into the air above governs the actual rate of evaporation.

The upper limit on the rate at which molecules can escape from a liquid interface into a perfect vacuum derived from kinetic gas theory is predicted by the Hertz-Knudsen equation:

$$m_e = \sqrt{\frac{M}{2\pi RT}}\, e_{swt} \qquad (5.5)$$

where m_e is the evaporation mass, M is the molecular weight of water, R is the universal gas constant, T the water surface temperature in Kelvin and e_{swt} is the saturated vapour pressure at water surface temperature. This fits Boer's (1968) definition of the maximum rate of evaporation. If the vapour is taken away and kept away, and any molecule is prevented from returning to the surface while maintaining the water at the constant temperature, this rate of vaporization is the maximum rate of evaporation.

Substitution of values for a water surface at 25°C (298 K) in a perfect vacuum into Equation 5.5, results in an evaporation rate of 316 m day^{-1}. This very high evaporation rate however is never observed, since even in a vacuum, as experiments performed by Rideal (1924) showed, the vapour diffusion layer is still present. At 25°C he obtained an evaporation rate of 1.33 m day^{-1}, (0.42% of the evaporation theoretically possible in Equation 5.5). When the atmosphere is also present the evaporation measurement becomes identical to every day measurements such as using evaporation pans. For Sydney, with an average temperature of 20.6 °C (BoM 2010) the annual evaporation is measured at 1330 mm year^{-1} (Table 1.1) or 3.64 mm day^{-1}.(0.27% of that with the vapour diffusion layer) with the addition of air pressure. So both the vapour diffusion layer and air pressure reduce evaporation substantially each contributing around the same evaporation reduction effect.

The vapour diffusion layer, therefore controls the evaporation rate, and any changes to evaporation rate, must therefore affect the vapour diffusion layer. Since the vapour molecules are transferred by diffusion the thickness largely determines the evaporation rate, particularly under windy conditions (Lai 1977). Any changes to the evaporation rate, must therefore be influenced by, or alter the vapour diffusion layer.

Thickness of vapour diffusion layer

Penman (1948) suggested that this evaporation reducing water vapour layer is usually between 1-3 mm thick. Subsequent research suggests it is strongly dependent on wind speed. MacRitchie (1969) suggested that monolayers act, by resisting the effect wind has on the vapour diffusion layer

thickness. The evaporation rate m_e is equal to the rate of this diffusion step and may be described by the equation (MacRitchie 1969)

$$m_e = \frac{D(e - e_0)}{\delta_d} \tag{5.6}$$

where D is diffusion coefficient, δ_d is the effective thickness of diffusion layer, and e_0 and e are concentrations at the two surfaces of the diffusion layer.

The thickness of the diffusion layer has been estimated by (Lai 1977; Makin & Kudryavtsev 2002; Wu 1971) as:

$$\delta_d = d\frac{\eta}{U_*} \tag{5.7}$$

where η is the viscosity of the air, d is a constant which is around 12 (Makin & Kudryavtsev 2002; Wu 1971). Wu's data (Wu 1971) (Figure 5.8) showing a reduction in U_* with a monolayer surface therefore increases the diffusion layer thickness, which in turn decreases the evaporation rate using Equation 5.6.

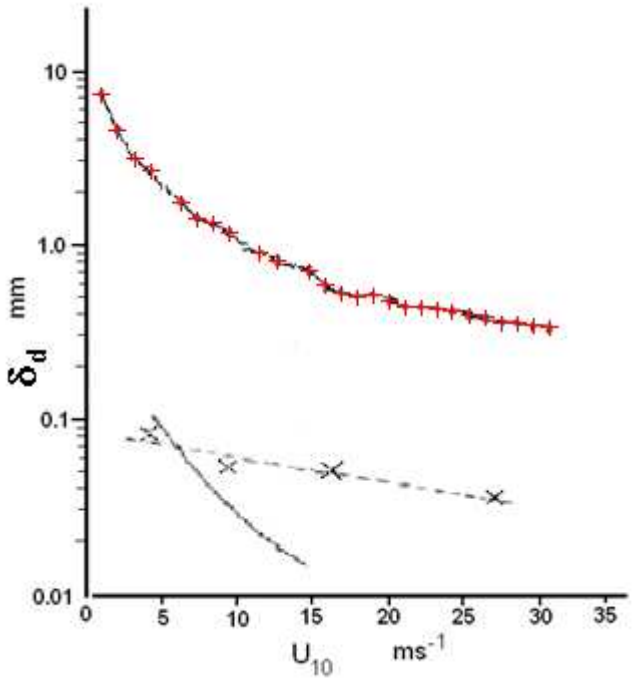

Figure 5.7 Diffusion layer thickness at various windspeeds measured at a height of 10 m. Data adapted from: Wu (1971); +, Mangarella *et al.* (1973); Crosses with dashed line, Schooley (1971); Solid grey line.

A comparison of the experimentally determined thickness of the vapour diffusion layer, as determined by separate researches using different methods is shown in Figure 5.7. Values for sea conditions were collected by Wu (1971) using the wind profile gradient method in Section5.1, and substituting this into Equation 5.7 to obtain δ_d. Magarella *et al.* (1973) used a wind tunnel, while Schooly (1971) used laboratory wind flume evaporation measurements. Although the values vary in magnitude depending on the calculation method, apparatus and conditions, they all show an inversely proportional relationship with wind speed as indicated by Equation 5.7, and as MacRitchie points out (Equation 5.6), this thickness is inversely proportional to the evaporation rate.

5.1.5 Effect of wind on evaporation rates

The evaporation rate of water is proportional to the wind speed according to Dalton's Equation (1.1), however the addition of monolayer to the surface, introduces additional influences which change this rate, such as surface pressure, degree of coverage, temperature and humidity. Tests reporting the evaporation reduction of monolayers over a range of wind speeds are very scarce, as McJannet *et al* (2008) report, probably as it is difficult to ensure coverage under higher wind speeds. They cite the results of Fitzgerald and Vines (1963) which give the following reductions in evaporation due to hexadecanol application at different wind speeds (U).

Table 5.1 Evaporation reduction at increasing wind speed.

Wind speed U m s^{-1}	Evaporation reduction %
2.2	40
$2.2 < U < 4.5$	10-20
6.7 m s^{-1}	~ 0

Langmuir and Langmuir (1927) originally argued that the reduction due to monolayers in the field is mainly due to the combined resistances of the vapour diffusion layer and the resistance to vaporization, with the monolayer simply adding another resistance term to a diffusive evaporation process (O'Brien *et al.* 1976). Accurate characterisation of monolayers using Langmuir troughs in the 1950s and development of desiccant method of measuring evaporation by Archer & La Mer (1955), shows that the energy barrier theory seemed to best explain the differences in evaporation measured with the addition of monolayer under laboratory conditions. In field trials however, the effects of winds need to be accounted for, as they reduce the thickness of the diffusion layer, increase the surface area with the production of waves and cause losses by retraction of coverage. After many experiments Mansfield (1959) states that "Any resistance to vaporization sited within the monolayer is negligible compared to that experienced during diffusion into the atmosphere". Since the diffusion layer is responsible for the major part of evaporation resistance, wind factors which affect the diffusion layer thickness such as wind stress and the action of waves could be considered.

Mansfield (1962) points out that since monolayers reduce the development of waves; the wind near the surface might have a different structure. Researchers such as Barger *et al* (1970) have since shown this to be true and that wind generated waves, in turn alter the wind profile. This often leads to small but significant changes in the transfer coefficients of sensible heat and water vapour (Mansfield 1962).

Wu (1971) conjectured that the retardation of evaporation of monolayers in the field under turbulent wind is partly due to the wave-damping effects of monolayers altering the wind structure. He argues that not only is the roughness length reduced, due to smaller amplitude waves, but also that the friction velocity is reduced, thereby reducing evaporation. Thus the causal link between the presence of monolayers and decreased vapour diffusion is the impact of the monolayer on surface roughness. Within the vapour layer just above the surface, the humidity is 100%, causing the rate of vaporization to virtually equal the rate of condensation. Evaporation occurs when vapour molecules diffuse through this layer along the gradient away from the surface (Wu 1971). So:

$$m_e = -k_w \rho \frac{dq}{dz} \quad (5.8)$$

where m_e is the rate of evaporation, ρ is the density of moist air, k_w is the vapour diffusion coefficient 0.26 x10^{-4} m^2 s^{-1} at 20ºC (Jones 1992), q is the specific humidity (the mass of water per unit mass of moist air) and z is the elevation. The specific humidity is proportional to the vapour pressure divided by the ambient atmospheric pressure p.

$$q \propto \frac{e}{p} \quad (5.9)$$

Substituting this term into Equation 5.8 yields:

$$m_e \propto k_w \frac{\rho}{p} \frac{de}{dz} \quad (5.10)$$

This is a molecular process if the wind is laminar, however in the field there is turbulence which needs to be accounted for: The eddy viscosity k_m within a turbulent boundary layer is proportional to the shear velocity:

$$k_m \propto \frac{U_*^2}{dU/dz} \quad (5.11)$$

where U_* is the friction velocity

If the velocity gradient within a turbulent boundary layer is proportional to the friction velocity then:

$$k_m \propto U_* \quad (5.12)$$

and this can be substituted into Equation 5.8:

$$m_e \propto \frac{k_w}{k_m} \frac{\rho U_*}{P} \frac{de}{dz} \quad (5.13)$$

A variation of Reynolds analogy (Brutsaert 1982), stating that the thermal diffusion layer is proportional to the viscous diffusion layer, can be used at this point to remove both coefficients. Wu (1971) actually states the ratio of thermal diffusion layer thickness to viscous layer thickness for water is 1:2. Since the coefficients are proportional they can be cancelled.

$$m_e \propto \frac{\rho U_*}{p} \frac{de}{dz} \quad (5.14)$$

This relationship is similar to the Dalton equation where the humidity deficit is $\frac{de}{dz}$, and the constants are represented by ρ and p. For a steady turbulent wind passing over a water storage the

parameters ρ, p and $\frac{de}{dz}$ do not vary much, leaving the evaporation rate proportional to the frictional velocity U_*. This is a particularly important result as it means that any change to the frictional velocity due to the addition of monolayer will alter the evaporation rate.

The experimental results of Barger and Garrett (1970) Figure 5.3 have been used by Wu to calculate the frictional velocity He found that there is a difference in frictional velocity in the region of wind velocity of 5-7 m s^{-1} where small waves are being generated. For low values of frictional velocity, below 0.16 m s^{-1}, the wind velocity on a clear surface is nearly twice that of the monolayer covered surface as shown in Figure 5.8(a).

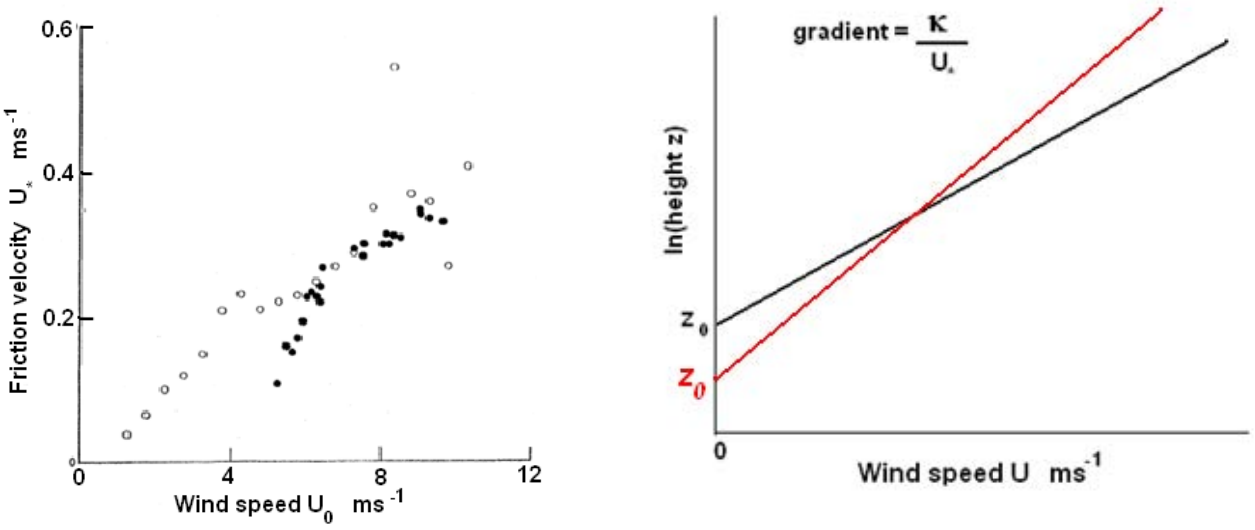

Figure 5.8 (a) Dependence of friction velocity on wind velocity measured at 10 metres height. ○; clear water surface, ●; monolayer surface. Source; (Wu 1971). (b) and the effect this would have on the wind profile, where the original profile for water is shown in black, and the changes by monolayers are shown in red.

He goes on to state, "I conjecture that the retardation of evaporation due to monolayers in the field under turbulent wind may actually be due to the wave-damping effects of these layers" (Wu 1971). So comparable wind speeds measured as part of evaporation reduction experiments for cases of clear water and monolayers may actually have quite different frictional velocities U_*.

Wu (1971) also found a reduction in roughness length z_0. These changes to the wind profile are shown in Figure 5.8(b). By lowering U_* the velocity gradient is altered, leading to lower air speeds above the surface and also a lowering of the roughness length, closer to the surface caused by the wave damping.

Francis (1954) suggests that the wind stress τ_0 is mainly caused by the drag of the slow moving small ripples, and not by the drag of the big waves. He argues it is always assumed that ripples are always present in the same number and sizes, whatever the wind speed; though in fact is a common observation that such ripples appear more frequently and are more prominent in higher winds. He compared stress results taken in the presence of large waves, with those taken in their absence and found little difference.

Surface films affect the capillary waves much more strongly than larger waves, and therefore have a major effect on the wind stress. The smoothness of the damped capillary waves leads to alterations of the air flow velocities, and water flow characteristics as the setup reduces markedly (Fitzgerald 1964).

5.1.6 Surface drift measurement

The speed at which monolayers move across the surface is critical to dispensing rate (McArthur 1962) and to the positioning of dispensers. Monolayer slicks follow the natural drift of the water surface to which the molecules of the slick are anchored (Garrett & Barger 1970).

On small storages and testing troughs it is often measured by observing the speed of floating substances such as talc (Fitzgerald 1964). Wu (1975) argues that a more accurate estimate of drift speed is found by using floats at various depths close to the surface, and extrapolating linearly to the surface as shown in Figure 5.9. Wu conducted measurements on a large tank (22 m long, 1.55 deep and 1.5 m wide) using pitot floats (as shown in Figure 5.9(a)) at various depths. It has been found by other authors such as McArthur (1962) that the larger the float, the slower it moves with drift velocity, so Wu's method of extrapolating to the surface should apply for infinitely small particles.

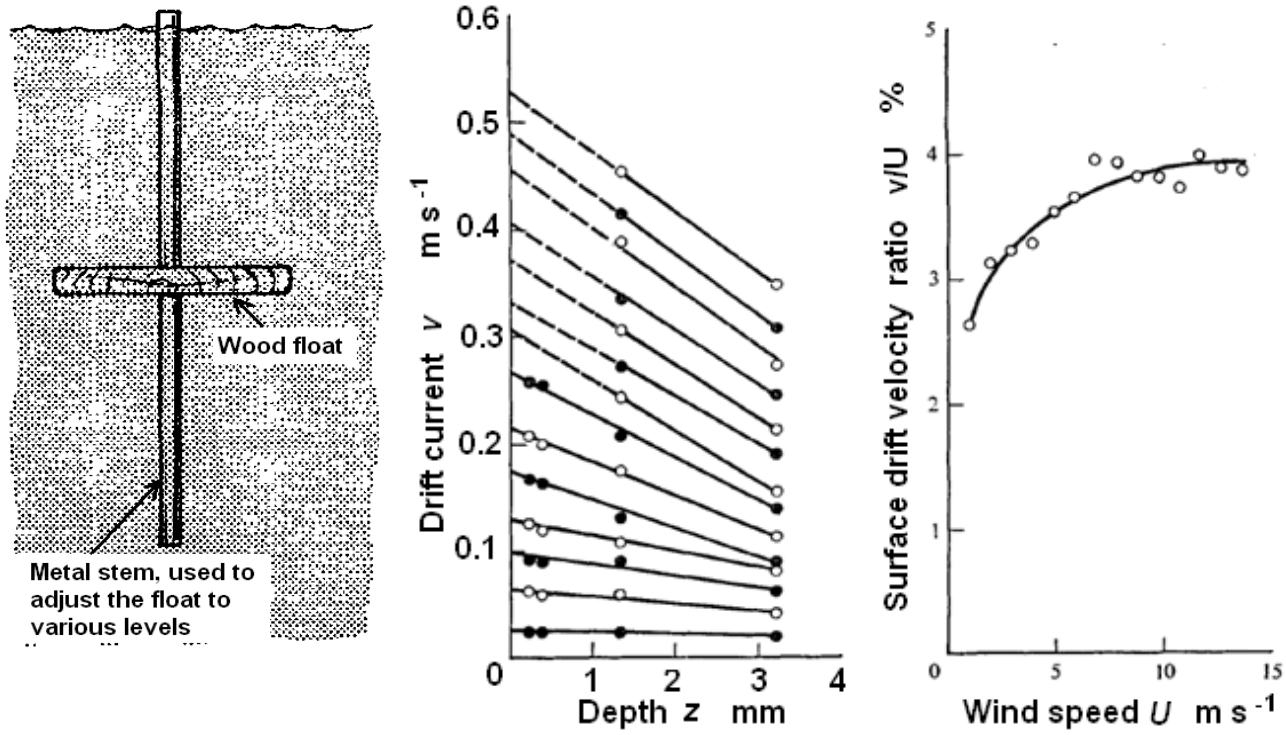

(a) (b) (c)

Figure 5.9 Wu's experimental techniques and results Source; (Wu 1975). (a) The pitot- static tube float which can detect current velocities under the surface (b) Drift current results produced from the pitot floats at near surface depth extrapolated to the surface (c) Results for surface drift velocity percentage using these techniques.

The linearity of the velocity profile near the surface is shown by Wu in Figure 5.9(b), showing that an extrapolation to the surface for the true surface drift velocity is justified. When the ratio of surface wind velocity and wind speed is plotted against wind speed (Wu 1975) (Figure 5.9(c)), a slight dependence of this ratio speed was noticed Results obtained by Keulegan (1951) also show a similar trend, increasing to 3.3%, noting that it increases with depth and decreases with fluid viscosity.

The drift speed of oil slicks at sea due to wind and waves at sea has been measured at between 2.5-4% of wind speed, with a mean value of 3.5% (Spaulding 1999).

A comparison of surface drift between a clear water surface and a detergent covered surface has been completed by Fitzgerald (1964) on a 1.9 m long laboratory channel. These results are shown in Figure 5.10(a). With the decrease in surface stress that occurs with the addition of monolayers, it would be expected that the surface drift velocity would decrease. However it is shown to increase above the clear water speed, reaching a value of 4.5% for a wind speed above 5.5 m s^{-1}. Spillane & Hess (1978) cites Van Dorn (1953) results also showing an increase with the addition of soap to the water. Figure 5.10 also critically shows that virtually full pressure is needed to show the increase. For all other pressures it is slightly below the drift velocity of a clear surface.

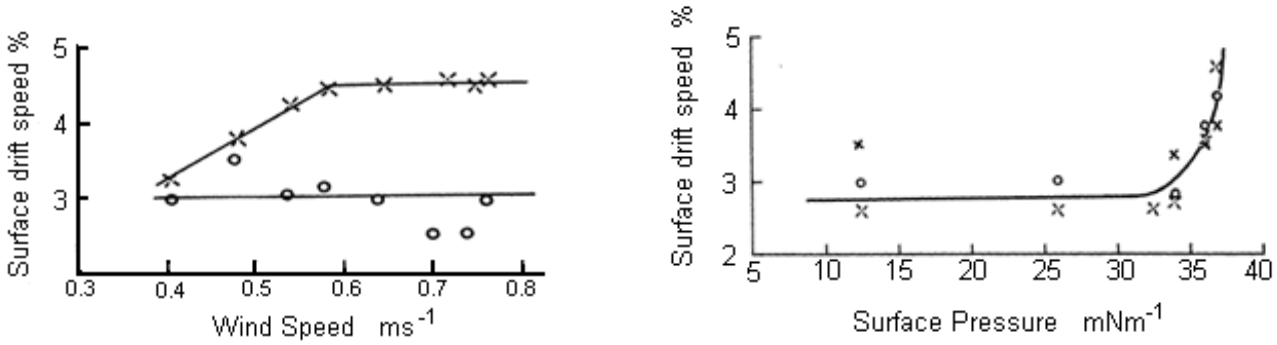

(a) **(b)**

Figure 5.10 (a) Variation of drift velocity with wind speed for; clear water;○; and surfactant; X with a surface pressure of 35-40 mN m^{-1}. (b) Variation of drift speed with surfactant surface pressure at wind speeds of. 0.44m s^{-1}; ×; 0.60 m s^{-1};○, and 0.70m s^{-1}; x. Adapted from Fitzgerald (1964).

Field studies involving hexadecanol showed a drift speed of 3.6% when measurements were made over larger lengths of film covered water (~1.5 km). McArthur (1962) suggest the drift rate is not constant, but shows an increase from an initial 4% early in the drift, and picks up speed to 7% along a downwind length, perhaps indicating that the top layers of water are also being forced downwind. In the work of McArthur (1962), the front of the drifting hexadecanol was used an indicator of drift speed as it was clearly defined against the background water. He observed that solid unspread monolayer material move downwind more slowly than the film front itself. The larger unspread components would be attached to lower layers and move slower in accord with Wu (Wu 1975) data in Figure 5.9. He also noticed that visible solid components in the film that did not spread apart tended to form a tail to the slick, moving slower than that of the leading edge.

A reason for the higher drift speed is given by McArthur (1962). Since monolayers damp small waves, the turbulence produced by these waves is no longer present, and the surface is influenced by a more directional wind. Another way to visualise this is to use Figure 5.6 describing Jeffrey's sheltering model. The waves create turbulence which may oppose the direction of the wind on the surface. The absence of these waves would create less turbulence and more unidirectional wind.

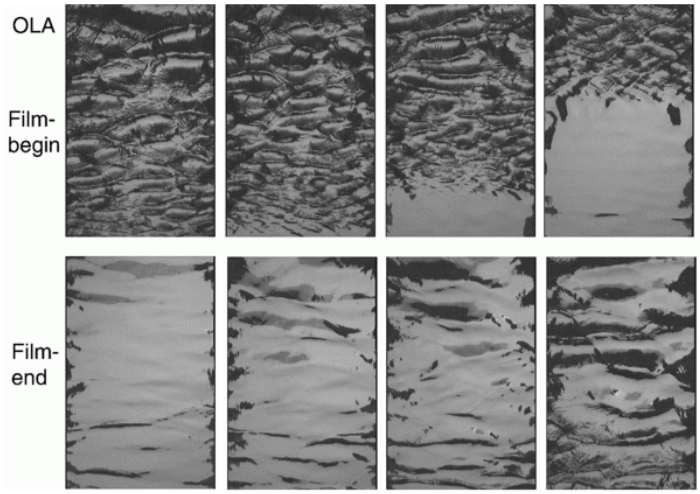

Figure 5.11 Series of photographs showing the progress of an oleic acid monolayers front and back edges upward across the field of view. Source; Gade (2002).

The contrast between the sharp downwind front of the film and the 'tattered', diffuse upwind edge of the film can be seen in Figure 5.11, as photographed by Gade (2002). These are images from a video using a 7.5 m long wind tunnel, spreading an oleic alcohol slick on the surface with a wind speed between 3-9 m s^{-1}. Gade explains the difference is due to different phases of the film, which would be caused by a higher surface pressure on the downwind end. This higher surface pressure would tend to speed up the downwind end of the slick explaining the faster speed of slick, when the downwind edge is measured, as carried out by Fitzgerald (1964).

Vines (1962:147) also measured the retraction rate of hexadecanol films, when bounded downwind by a shoreline. He found the films were compressed and collapse with a speed of 3.3% of the wind speed. This is very close to the drift velocity of clear water. By extrapolating these results plotted on a Wind speed/ Drift plot, the intercepts show that the theoretical maximum wind speed for upwind spreading is 1 m s^{-1} and the rate of spread with no wind would be 0.05 m s^{-1}. On small laboratory troughs the wind resistance is higher than 3 m s^{-1}. Interpretation of measurements made by Mansfield (1959) explains the difference, as will now be explained.

5.1.7 Monolayer retraction

Retraction takes place, when a monolayer, bounded by a downwind boundary is compressed by the wind and collapses. The retraction behaviour for small and large scales show quite different behaviour, making scale modelling ineffective. Hexadecanol on small troughs shows a wind retraction speed above 3 m s^{-1}, whilst on large storage "the retraction rate of an extended film is very nearly equal to its rate of drift on an open surface" (Vines 1962:147). Mansfield (1959) was the first to use film retraction measurements to predict retraction behaviour resulting from wind stress on water storages. A monolayer, such as hexadecanol bounded downwind will produce an elastic pressure gradient (Saylor, Smith, & Flack 2001) that opposes the

wind stress, in much the same way that that a decrease in surface area on a Langmuir trough increases the surface pressure. The difference being that the pressure is being applied along the surface, rather than simply at the end. This pressure gradient along the monolayer cannot be supported indefinitely, as at 40 mN m^{-1} it is in equilibrium with solid hexadecanol, and leads to breakdown of the film.

For instance, if a wind has forced a monoloayer to the downwind bank of a storage and with full surface pressure of hexadecanol $\pi \sim 40$ mN m^{-1}. The film is contracted further by a typical wind stress $\tau = 0.01$ Nm^{-2}, associated with a wind speed of 2 m s^{-1}. The film will oppose this, with a surface pressure gradient equal to the stress

$$\tau = \frac{\pi}{s} = \frac{40 \times 10^{-3}}{s} \tag{5.15}$$

where s is the distance downwind.

Evaluation of s shows that at a distance of 4.0 m downwind, the film can no longer support the pressure gradient, resulting in film retraction, to a length supportable by the monolayer. This provides an excellent method of determining the surface stress, by simply measuring the length of monolayer coverage able to withstand contraction from the downwind end of a trough, and for each wind speed use Equation 5.15 to determine τ. This also explains why downwind bounded monolayers on large water storages show absolutely no drift resistance to wind and move with surface drift speed, while wind resistance is strong (above 3 m s^{-1} for hexadecanol) on laboratory Langmuir troughs.

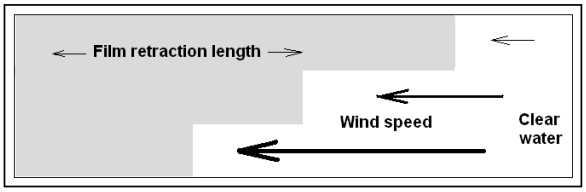

(a)

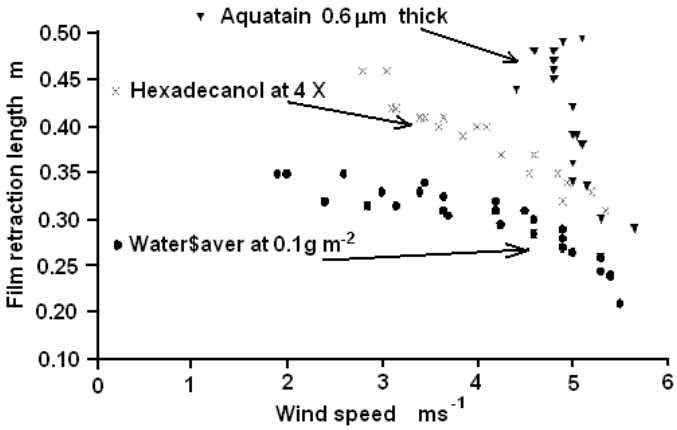

(b)

Figure 5.12 (a)Measurement of contraction of film retraction length with increasing wind speed. (b) Turnbull's data (McMahon *et al.* 2008) for film retraction of Aquatain, Hexadecanol and Water$aver. Adapted from McMahon, *et al.* (2008).

Results obtained from Turnbull (McMahon *et al.* 2008) at USQ, measured film retraction on a Langmuir trough, however the results measured distances from the windward end of the trough rather than the downwind end. This would give a value depending on the length of the trough. If the results are reversed and the measurements are taken from the downward end of the trough for film length, as shown in Figure 5.12(a), then the results in Figure 5.12(b) are obtained. They show the film retraction length decreasing as the wind speed increases. The graph shows that Aquatain is

affected least by wind, then hexadecanol, and most affected is Water$aver. The WaterSaver has the lime particles which would be affected by wind, decreasing its wind resistance. The Aquatain is much thicker, and this is possibly why its resistance is higher. At around 6 m s^{-1} it appears all wind resistance for all three disappears.

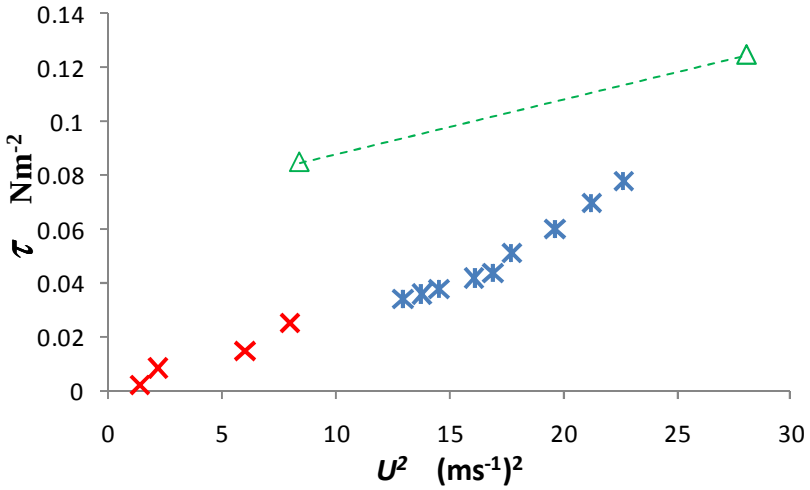

5.13 Figure 5.14 Wind stress of hexadecanol, measured using the film retraction method. Results from Vines ×Fitzgerald; , Vines∗ and Turnbull; Δ.

Turnbull's results were averaged for hexadecanol and a line of best fit was used. The stress of the two endpoints were calculated using Equation 5.15. For comparison the results of Fitzgerald (wind measured at a height of 2 cm) and Vines (wind measured at a height of 5 cm) are shown in Figure 5.14. This graph can be used to determine the maximum wind speed that coverage can be maintained for fetch length on a trough.

This also explains the higher drift rate of monolayers, despite a lower wind stress being exerted on monolayers measured using a wind profile method , and setup methods Fitzgerald (1963). On a large slick the downwind end has a higher surface pressure created by the dilational elasticity of the monolayer. This has the effect of expanding the slick as it is drifting downwind. The experiments conducted observed the downwind edge of the slick as this edge is more pronounced resulting in a higher drift rate being measured.

5.1.8 Maximum Wind Velocity on large storages

Wind on large storages moves the surface downwind, and monolayers do not have any effective drift wind resistance, apart from near the downwind bank. If it is assumed that coverage is maintained by dispensing on the upwind bank, or following a slick downwind, then coverage can be maintained for fairly high wind speeds. On large storages, the wave damping can be used as an indication of coverage for a range of windy conditions (McArthur 1962). Tiblin, Florey & Garstka (1962:184) noticed that for winds over 9 m s^{-1}, the film would suddenly disappear. They felt that this was probably due to interference of monolayer structure by wave formation and mixing of the hexadecanol in the water by wave action and white capping.

Field trials made in Australia by Tiblin (1962) led him to comment that no appreciable evaporation reduction is possible in the field conditions above 4 m s^{-1} . Also that poor coverage was usually

obtained for winds greater than 7 m s^{-1} and any coverage was usually impossible wind velocities of over 8.5 m s^{-1}

Vines noticed that, although winds are known to break up hexadecanol monolayers and sweep them back, under strong winds, a water surface rarely becomes completely uncovered, as shown by the streaky appearance of the wave patterns produced (Vines 1962:147).

The length of time that strong winds are present and the occurrence of strong winds is not great compared to the evaporation time when they are not present, so the loss of water due to monolayer destruction in strong winds in Australia is small compared to everyday evaporative processes (Vines 1962:149).

5.2 Experimental measurements of the effects of wind on evaporation

Wind increases the evaporation rate for both water and monolayers as shown by the change in thickness of the vapour diffusion layer (Section 5.1.5), however the two surface may be affected disproportionately. Methods of detection relying on evaporation rate would obviously be most successful in the wind speed region where the evaporation reduction produced by the monolayer is highest. The literature on the effects of wind on evaporation reduction by hexadecanol is scarce (discussed in Section 5.1.5), as the addition of wind creates difficulties in ensuring full pressure coverage. Unlike tests on large storages, where no wind resistance exists, small troughs show quite a strong wind resistance. For instance Figure 5.12 shows that hexadecanol on a trough of 0.3 m length would maintain coverage for winds of up to 5 m s^{-1}. So a wind speed of this magnitude can be used in this situation without removing monolayer. Evaporation reduction can be measured both by measuring the loss of water, and relative changes in temperature. Both will be tested.

5.2.1 Evaporation reduction of hexadecanol using loss of water

A convenient way to determine evaporation reduction of monolayer is to set up two identical troughs, where the conditions are alike so that the monolayer sample can be referenced to clear water. The evaporation reduction can then be calculated by the water needed to top up the troughs after a period of days.

Figure 5.15 Identical insulated troughs positioned in front of fan.

Materials and methods

Two 1.05 m long PVC tubes, with a wall thickness of 5 mm and 250 mm inside diameter were capped at one end and positioned vertically beside each other. Silver foil-backed, glass wool insulation (Bradford Gold Insulation Anticon 55 R 2.0 W $°C^{-1}$ m^{-2}) was attached to the external walls of the tubes to minimise radial heat conduction out from the tubes. The building rating R is the heat resistance which can be converted to the conductivity *k* by $R = \frac{thickness}{k}$. When the thickness of 20 mm is substituted, this results in a conductivity *k* = 10 mW K^{-1} m^{-1},. Both tubes rested on a 35 mm thick Styrofoam blocks (*k* = 0.033 W^{-1} $°C^{-1}$ m^{-1}, *R* = 1.1 W $°C^{-1}$ m^{-2}). The insulation of the 5 mm thick PVC walls with *k* = 0.15 W $°C^{-1}$ m^{-1} (Kaye & Laby 1973) will add to the insulation slightly.

Holes were drilled near the top of both troughs, and polycarbonate 10 mm outflow tubes were inserted to act as overflow pipes reducing the water level to 25 mm below the top of the troughs. The junctions were sealed with “Selleys” wet area silicone sealant. These allowed the flooding technique to be used to clean both surfaces initially, without the water flowing over the top and into the insulation. Both tubes, with a contained volume of 0.048 m^3, were filled with clean water to the level of the outflow tubes.

An external air flow was introduced by an electric fan (Mark 9 12 Bonaire, 250 W, Australia) which had 4 fan settings. It was placed on a stand at a distance of 0.5 m from the centre of the troughs, at a height to produce maximum wind speed at the top of the troughs. Horizontally this fan produced higher wind speed directly outward, towards the centre of the tubes, however correctly positioned; the fan should be able to provide identical air flow for both troughs. Air speed was checked to be identical for both tubes using a hand-held anemometer (Lutron LM-8000, Electronic Enterprises, Taiwan) held as close to the surface as possible (approximately 2 cm above).

Several hexadecanol crystals were added to the surface of one trough, and several more were added each few days. It was noticed however that no spreading occurred with the additional crystals, indicating a full pressure monolayer already existed. The evaporated water was replaced every day or second day, and each run lasted for between 2-3 weeks. At the end of this time the total evaporation reduction for the monolayer was calculated from the difference in added water. The air temperature was between 14-23 ºC the large range was due in part to the diurnal fluctuation that occurred over several weeks.

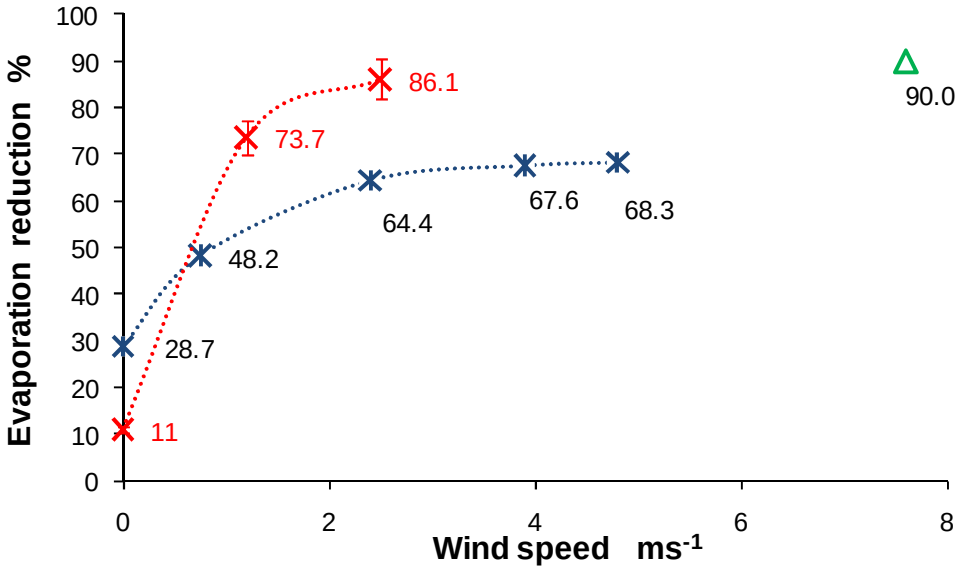

Figure 5.16 Evaporation reduction for a range of wind speeds measured 2-3 cm above the surface. Experimental results; ✕. Also for comparison, the results of other researchers; MacRitchie (1969); ✱ and Ghumman. (1971); Δ.

Results and Discussion

The large evaporation reduction figures, shown in Figure 5.16, confirmed that monolayer remained effective for all the wind speeds attempted. The experimental data show an increase of evaporation reduction with increasing wind speed, tending asymptotically to a maximum value of 88%. As noted in Section 3.4.1, the increase in evaporation reduction appears to be due to the evaporation from the water surface increasing disproportionately compared to monolayer surface, rather than any substantial change in the monolayer evaporation rate. Data from MacRitchie (1969), appears to converge to a maximum at 70%. It is unknown why there is a difference between MacRitchie's data at higher wind speed and the data gained in this work. He used a very similar setup with hexadecanol on a small trough; 9 cm square at a temperature of 20 ºC, with the main difference being to present the entire trough surface to a uniform wind speed of dry air. Ghumman's result (1971) showed a higher value of 90%, and was gained using a small trough of 471 cm^2 at a temperature of 49 ºC.

Humidity was not taken into account in our measurements of evaporation reduction. It was hoped that the long period of measurement of several weeks would both make the measurements more accurate and produce fairly average humidity values. There also seems to be a dependence on temperature, as higher air temperatures seemed to produce higher evaporation reduction. Also measurements performed in winter with the laboratory often below 10 ºC showed a much lower evaporation reduction of 50%. Measurements averaging humidity and temperature would need to be carried out to confirm this.

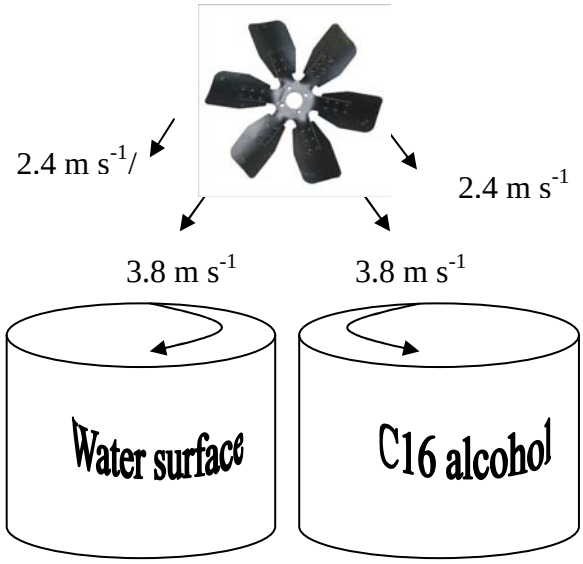

Figure 5.17 Schematic diagram showing the measured velocity difference at the wind source, ultimately resulting in the circular movement of monolayer on the water surface within each tube.

On the central (inside) edge of both tubes the wind speed was measured to be 3.8 m s^{-1} while on the outside it was 2.4 m s^{-1} (Figure 5.17). The difference in wind speed across the surface causes the monolayer to move downwind on the outside side, and upwind on the central side, causing a surface rotation that continuously presented new monolayer on the upwind side. This rotation of the monolayer was clearly evident by observing the rotation of excess floating crystals of the monolayer. The wind speed in this case was far below the maximum 5 m s^{-1} predicted to resist wind in Figure 5.18, however this circular motion may help to preserve monolayer coverage in winds previously thought to cause contraction.

5.2.2 Heating of water storage under wind

The bulk and surface heating that occurs with the addition of a monolayer for a water storage depends on many heat fluxes and is difficult to estimate, although the previous experiment (Section 5.2.1) has given a clear indication that at the very least, the evaporation reduction is significantly modified by monolayers. The lower evaporation rate of a monolayer surface would be expected to decrease the evaporative cooling of the surface, and in turn bulk temperature. The thorough insulation of the walls and floor of the troughs were in order to model the surface of a large storage, where by producing little interaction with the ambient conditions, the bulk is free to assume a temperature in response to the surface interaction with the surrounding climatic conditions. Under a fairly high wind speed, the maximum difference in bulk temperature that occurs with the addition of monolayer can be found which should correspond quite well with similar processes occurring on a large storage.

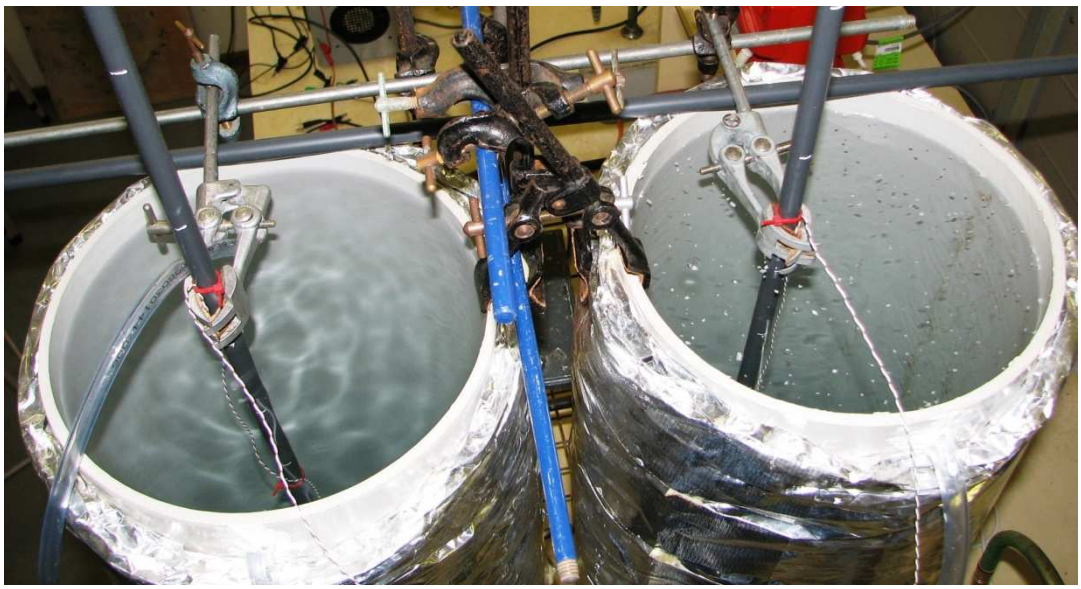

Figure 5.18 Overhead view of thermocouple leads attached to plastic rods, which positioned the junctions at a depth of 0.5 m.

Materials and Methods

A reference clear water surface and a hexadecanol monolayer were compared on the same apparatus described in Section 4.3.1. A full pressure hexadecanol monolayer was created by adding a few hexadecanol crystals to the water and making sure that there were excess crystals available to reinforce the monolayer at all times. The surface temperature was measured using an infrared thermometer, Fluke 474, with associated logging software. In this experiment, the absolute volume temperature was not required, rather the temperature difference between the two volumes of water was recorded using a Type T (copper constantan) thermocouple with the junctions placed in the body of water at a depth of 0.5 m in both the monolayer trough and the reference junction placed at the same depth in the body of the clear water. This was done by attaching each junction to a plastic rod, which was clamped above the water level using a retort clamp.

The junctions were connected to a precision amplifier (LT1050, Linear Technology Corporation, CA. USA), the output of which was digitised using Picaxe, 10-bit, A-D converter (40X1 Microchip Technology Inc., UK.) with the output transmitted every 5 minutes to be logged by a computer. Relative humidity (%) was simultaneously measured using electrical humidity sensors (HIH 4000 Honeywell) positioned near the surface of the water in each of the tubes, and the output digitised and logged using the same configuration as the temperature sensors.

In this way the bulk temperature difference ΔT is the difference between the bulk water under a clear water surface, and the bulk water under a hexadecanol surface:

$$\Delta T_B = T_{\text{B hexadecanol}} - T_{\text{B clear water}} \qquad (5.16)$$

Initially both troughs were left to thermally stabilise for several days in preparation for measurements. At time $t = 0$ the monolayer was added to the sample trough. Both no wind and an

average wind speed of 3.1 m s^{-1} were trialled. For the measurements of wind speed the fan was switched on at t = 0, simultaneous with initiation of logging.

Results and Discussion

The ΔT_B values are represented by thick red lines in Figure 5.19, along with simultaneous measurement of ambient room relative humidity. These measurements were carried out indoors in temperatures 18-24 ˚C. For the condition of no wind the ΔT_B shows a gradual increase from essentially zero to 0.2-0.3 ˚C over a period of ~1 day, from which it appears to retain an equilibrium value. At equilibrium, the evaporative cooling would equal heat gains either by sensible heat transfer at the surface or conduction through the insulated walls and floor.

When the wind speed was increased to 3.1 m s^{-1} the ΔT_B equilibrium value of 2.7 °C took longer to achieve; at around 2 days. Results from Section 3.4.1 show that the evaporation for a water surface increases in response to wind at a higher rate than for a monolayer surface. These results show that evaporation reduction of hexadecanol increases with wind speed, for the speed tested.

Also shown in the data are data series (thin blue line) for the relative humidity. The variation is diurnal with the minimum humidity occurring just before dawn, with minimum temperature. ΔT_B data series show a slight response that is delayed by about ½ day, as would be expected considering the volume of water.

So the evaporation rate of the water surface leads the monolayer in driving the bulk temperature below the laboratory environs. The ΔT_B would seem then, to be a useful indicator of the evaporation rate occurring at the surface, in this case delayed by ½ day.

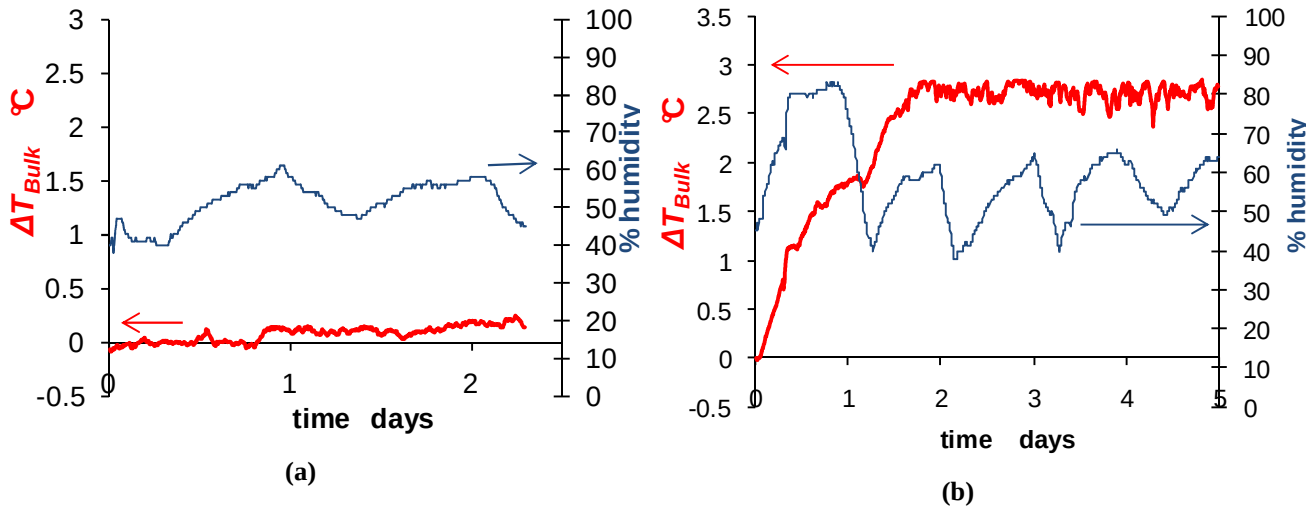

Figure 5.19 Bulk temperature difference (thick red line) between both tubes occurring as a result of no wind (a) and a wind speed of 3.1 m s^{-1}. (b). The simultaneous measuring of relative humidity(thin blue line) is also shown.

This 2.7°C equilibrium water temperature difference is consistent with a value of 2.9 °C obtained a mixture of C_{16} – C_{20} alcohols, on a 240 hectare Pactola reservoir (South Dakota) by Bartholic, Runkles & Stenmark (1967). They also quote Crow (1961) as obtaining an average water increase of 3.0 °C with application of a blend of C_{14}-C_{20} alcohols to a small pond of depth 2.1 m.

This increase in water temperature would cause a higher evaporation rate when the monolayer is removed and perhaps lead to an overestimation of the evaporation reduction. Wolbeer (1963) has suggested, using theoretical considerations that the overestimation could amount to as much as 41% if the monolayer is present 50% of the time. Bartholic, Runkles & Stenmark (1967) use a combination of theoretical and experimental data to obtain a figure of 8-14%, and predict much higher water temperature changes depending on conditions. Any water temperature rise above 3.0 °C would seem unlikely on a large storage due to the difficulties in maintaining coverage at the wind speeds >3.1 m s^{-1} needed, as demonstrated by the results of this experiment. Neither of these methods used to calculate the lowered evaporation reduction accounted for the increased radiation from the surface created by a disproportionately warmer skin temperature (discussed in Part 3 of this experiment). Evidence of some storage temperature rises are provided by Crow (1961) who measured a 3 °C temperature rise near the surface of small dam 2 m deep, and 1.7 °C increase at a depth of 1.5 m.

The increase measured on a large storage was measured by Barththolic, Runkles & Stenmark (1967) over a few months to be around 3 °C at the surface tapering off to no effect at ~ 5 m. This is again in contrast to Wolbeers assumption that assumes the temperature increase is constant at all depths of the storage, down to the hypolimnion (the lower region which does not circulate with the upper layers).

Mansfield suggested that the reduction of evaporation and increase in temperature will give a small compensating increase in the rate of evaporation, but with a monolayer of high resistance to evaporation the net result will be a significant decrease in the amount of water lost through evaporation (Jarvis 1962; Katsaros 1982).

5.2.3 Surface temperature differences under wind

Surface temperatures were measured simultaneously with the bulk temperatures described in Section 5.2.2.

Materials and Methods

Results from Section 4.5.2 show that there is no measurable change in emissivity occurs with the addition of hexadecanol, when using the Fluke 574 IR thermometer. Therefore the measured temperatures can be compared using the emissivity setting of 0.96.

The hand held IR thermometer was directed at a position near the middle of the surface from a height of around 30 cm for both troughs, initially, and over a period of days, while the bulk temperatures was being collected.

Results and Discussion

Initially the difference in surface temperature between a clear surface and hexadecanol surface was measured to be 0.2-0.4 ˚C taken several hours after applying the monolayer to one tube. This is similar to the 0.3 °C measured by Grossman (1969), who compared covered and uncovered areas of a large water storage from the air.

The surface took 2 days to stabilise, notably the same time it took for the bulk to assume thermal equilibrium. The results for various wind speeds are shown in Table 5.2

Table 5.2 Difference of surface temperatures between both tubes using IR thermometer

Wind speed m s^{-1}	Temperature difference of surface after 2 days ˚C
0	0.6 - 1.0
1.6	2.4 - 2.6
3.1	3.6 - 5.0

These results show a larger temperature difference than the bulk temperature. Once the surface has reached a stable temperature, latent and sensible heat fluxes must be equal. The sensible heat flux would originate from equilibrium conduction, radiation, and convection with the air, as well as some heat from the bulk being conducted through the walls. As pointed out in Part 1 of this experiment, the difference is created mainly by the water surface cooling as the wind speed is increased, with the hexadecanol surface cooling less.

5.3 Conclusion

These results show that increasing wind speed over the surface increases the evaporation reduction of hexadecanol with a maximum occurring at around 90%, as long as coverage is maintained. The literature (McJannet *et al.* 2008) showed a decreasing trend for larger storages, which is probably due to a lack of coverage, rather than a property of hexadecanol monolayer. Complete coverage can be assured using a smaller surface where wind stress cannot accumulate along the length of the fetch. A safe fetch distance for a specified wind speed is given by Equation 5.15. Larger fetch distances than that given by this equation may lead to an accumulation of pressure along the surface from wind stress and collapse of the film.

The collapse of the film by wind stress also is the reason why monolayers cannot show any wind drift resistance on large storages, and that dispensing needs to take place upwind to allow the film to drift downwind in a predictable manner.

As further evidence of the increase in evaporation reduction that takes place under windy conditions for monolayers, the both the surface and bulk temperature differences between clear water surface and monolayer covered were also found to increase. The measured temperatures show that the surface temperature (4.3 °C) appears to alter to a larger degree than the bulk temperature (2.7 °C), with the addition of hexadecanol using this model, and that the increased difference that occurs to the bulk, is added to by the surface difference to an even greater difference. This shows great promise in using detection methods on confined samples of water, as measurements using an insulated trough under windy conditions (3.1 m s^{-1}) show a signifciant difference in bulk temperature using thermocouples and surface temperature using an IR thermometer. The next chapter will develop these monolayer indicators into a working detection system.

Chapter 6. Development of a prototype Wind-Assisted Surface Probe (WASP) for detecting the presence of monolayers on water

Monitoring changes that occur with the addition of monolayer that are unrelated to evaporation rate directly, such as surface tension and wave amplitude, risks false indications of coverage as explained in Chapter 2. Evaporation liberates heat from the surface, and so changes to evaporation rate affect the temperature profile in a direct and predictable way, as long as ambient factors such as T_{AW} and air humidity are taken into account. Contact measurements, such as the evaluation of ΔT_S shows some promise, as described in Chapter 3, but would be difficult to measure in the field due to the small magnitude of the changes and the difficulty in positioning temperature sensors at the water surface. Isolation of a region of surface, using a sampling chamber has helped stabilise the surface, and confinement of a volume directly under the surface using an insulated trough, described in Chapter 5, has been shown to accumulate the evaporative cooling, thus increasing the temperature changes caused by monolayer, for both contact profile and remote IR surface measurements. Development of an insulated enclosed trough detection system will be the focus of the work described in this chapter.

6.1 Accumulating cool water in a trough

Measurements of trough temperature using a Y tube apparatus were taken using a thermocouple to compare the temperature inside the trough with that just under the base of the trough outside the Y tube, as shown in Figure 6.1.

At this stage, no insulation was used around the PVC end cap plastic of the trough. Initial tests were carried out to determine whether small troughs such as these would act in the same way as the large troughs in Chapter 5. If cold thermals are trapped, it would be expected that the temperature inside the trough would be cooler than outside. With the fan switched on the trough should cool below the surrounding water temperature at a rate, and by an amount determined by the balance of heat fluxes at the surface, behaving in a predictable way. This would hopefully lead to a measureable trough temperature difference between a clear water surface and hexadecanol surface.

Material and Methods

The lower end of the 100 mm PVC Y tube was capped and the assembly was positioned at the surface so that a shallow trough of around 2.5 cm deep was formed (Figure 6.1). An access hole was drilled in the side of the trough measuring 5 mm wide by 15 mm high just above the edge of the trough to allow the surface to flow freely into and out of the Y tube chamber. The Y tube was positioned so that the water level was at the level of this hole. A thermocouple junction was glued

to the inside floor of the trough, and another reference junction on the underside of the trough using silicone gutter sealant (Selleys) so that the junctions were protruding out of the glue at a distance of 2mm away from the PVC surface. The thermocouple voltage was stored and converted to temperature using the same method as described in Section 3.4.6 with the temperature being measured every 30 seconds.

A 4.5 W 12 V computer exhaust fan (YX2518 Sirocco, Taiwan) with casing size of 120 mm, was used for these experiments.

The setup was left for several hours with no wind, and data logging was switched on for several minutes before switching the fan on. It was run at its recommended voltage of 12 V, which produced a wind speed measured with the hand held anemometer (LM8000 Lutron,Taiwan) at the inlet of 3.2 m s^{-1}. The run was then left until it was considered that thermal equilibrium was again stable, with the fan running (around 40 minutes).

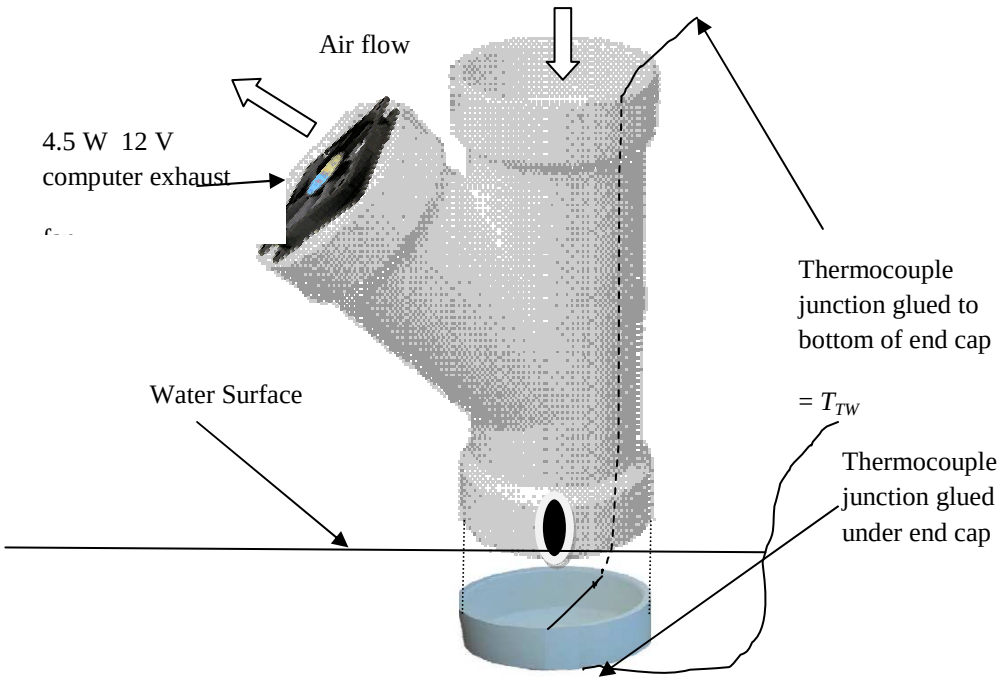

Figure 6.1 Expanded view of sealed end cap glued to the base of the Y tube showing positions of thermocouple junctions inside and outside the end cap. The hole near the base allows the surface to move freely into and out of the trough.

Results

The results displayed influences of humidity and fan speed. Typical results for a low humidity of 32% (Figure 6.2) showed a small raise in trough temperature T_{TW} to -0.2 °C for a full pressure hexadecanol, while the clear water showed a decrease to -1.0 °C. As ambient conditions were identical, as the tests were conducted on the same day, with an hour in between the difference seems to have been created exclusively by the difference in evaporative cooling. The results also show the larger temperature fluctuation of the water, due to higher convective heat flux, this was

discussed in (Section 4.4.1), where Saylor shows that the convection currents are larger and slower due to higher surface viscosity.

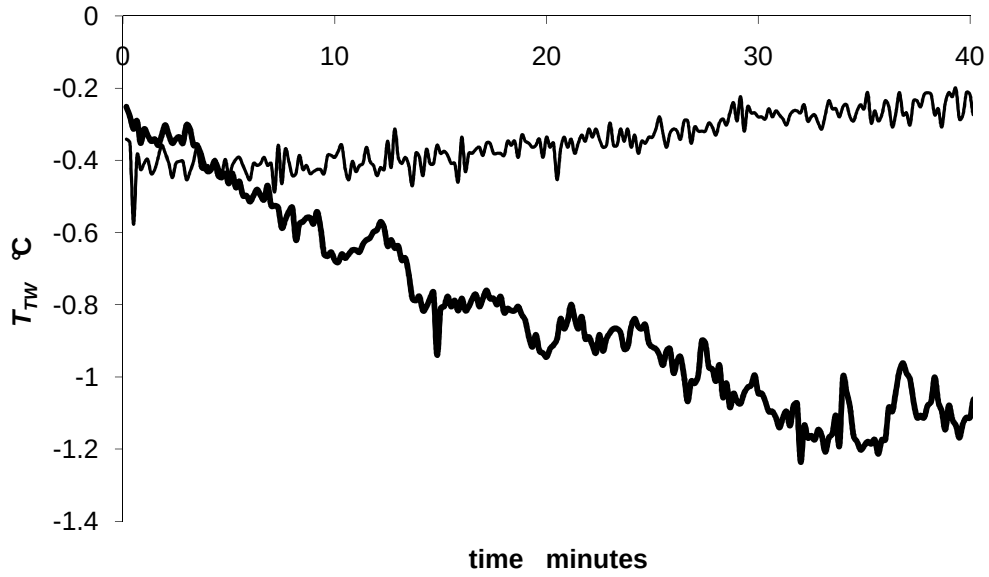

Figure 6.2 Comparison of the temperature difference T_{TW} of the Y tube trough apparatus for conditions of humidity 32% and wind speed at fan 3.2 m s^{-1}. Water surface; dark line. Monolayer; thin line. Notice the smaller temperature fluctuations for the monolayer.

Conclusion

The Y tube trough with artificial wind showed promise in providing a reliable indication of the evaporation rate for the particular surface contained in the trough. This system relies on an accumulation of evaporative cooling rather than the sensitive surface flux balance occurring in open water. It would appear that the accumulation of evaporative cooling enlarges the final T_{TW} differences between clear and covered surfaces and provides a stable sample of water in which the temperature is measured with relative ease at the more thermally stable floor of the trough.

Humidity is an important factor in the rate of evaporation as the Dalton equation predicts the evaporation is proportional to the humidity deficit δe (Segal & Burstein 2010) . The effects of evaporative cooling are trapped by the trough rather than sinking to the depths via thermals.

Humidity was found to be the main factor which affects the value of T_{TW}, which at values above 90%, would make the surfaces indistinguishable. At high humidities in the field however, there is also very little evaporation, and therefore little need for checking monolayer coverage.

Another variable is the temperature difference between air and water T_{AW} acting to influence the sensible heat, either heating or cooling the water in the trough.

The amount of heating or cooling inside the trough would depend on how well the walls and floor are thermally insulated against the surrounding water, the results presented were obtained with a single PVC end cap with average thermally insulating properties. Higher insulation in the trough would produce larger T_{TW} values.

Logging the initial temperature may also prove useful for monolayer coverage determination, as the initial temperature of the hexadecanol-covered surface was usually higher than the clear water.

Each of these influences will be investigated separately so that they can be accounted for in predicting the final T_{TW} both for monolayer and water. A decision can then be automatically made as to the presence of monolayer simply on the basis of the final T_{TW}.

6.2 Development of the Wind Assisted Surface Probe (WASP)

As outlined in Section 6.1, the accumulation of cold water in a trough using an artificially produced turbulent wind has shown promise in monolayer detection. This section is concerned with the optimisation of this method and investigation of all the heat fluxes operating around the trough which may affect final trough temperature so that predictions can be made on the final T_{TW}.

Equipment and methods

The magnitude of the wind speed was increased until observation of the spare hexadecanol crystals floating on the surface showed signs of turbulent motion, suggesting that monolayer integrity was being affected. This occurred at values slightly higher than a tube wind speed of 3.5 m s^{-1}. In each run the fan was allowed to run for 1 hour, by which time the T_{TW} temperature had stabilized.

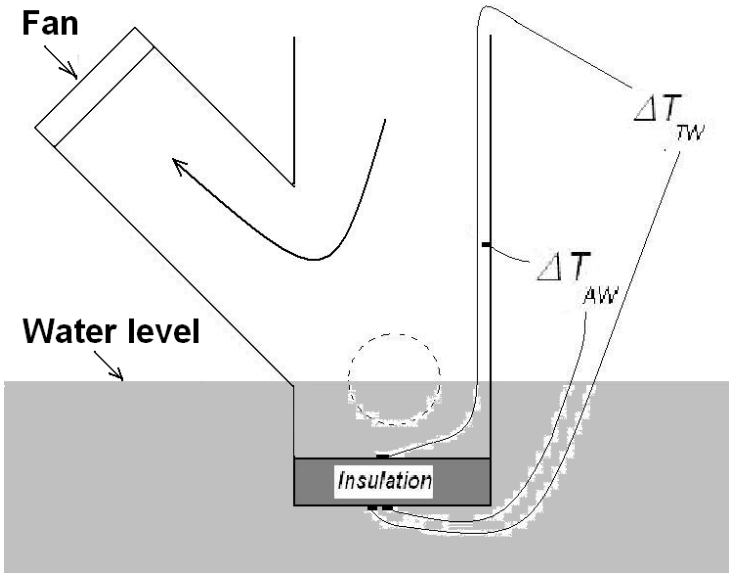

Figure 6.3 Position of junctions for two complete thermocouples: T_{AW} and T_{TW}. The dashed circle at water level is the inlet port which allows movement of the surface outside of testing runs, though has a flap which closes during testing.

6.2.1 Combining thermocouples T_{AW} and T_{TW}

Materials and Methods

The temperature differences T_{AW} and T_{TW} were determined using two thermocouples attached to the inside of the tube as depicted in Figure 6.3. The T_{AW} thermocouple was added to include sensible heat conduction due to the possible wide range of values for T_{AW}.

The amplifier was an LTC 1050 precision zero drift amplifier (Linear Technology, Ca., USA) placed on the output of each thermocouple with wiring as shown in Figure 6.4.

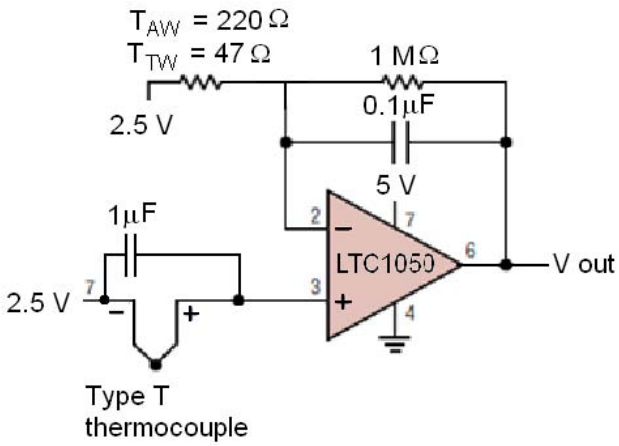

Figure 6.4 Precision amplifier setup, depicting resistors used for gain settings and a balance position of +2.5 V.

The gain used for T_{TW} is:

$$G(T_{TW}) = \frac{1000000}{47} = 21\,280 \qquad (6.1)$$

making 167 counts/°C. The range therefore would be -3 to +3°C

The gain for T_{AW} is:

$$G(T_{AW}) = \frac{1000000}{220} = 4\,545 \qquad (6.2)$$

making 36 counts/°C. The range therefore would be -14 to +14°C

To overcome the oxidation of the junctions, created by the positive voltage at which they were held in the water (2.5 V) polyester resin was used to coat the junctions to electrically insulate them from the water. The fan was switched on for 2 hours and the temperature recordings from both thermocouples were recorded.

The temperature decrease was tested in the climate chamber with various values of humidity. The WASP type tube already outlined was used, with a permanent hole at water level was used.

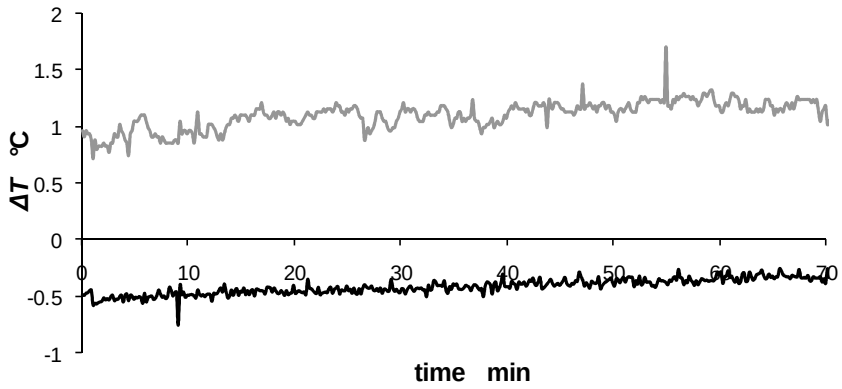

Figure 6.5 A sample run using water at 70% humidity, measuring temperature differences for both thermocouples. Dark line; the trough thermocouple T_{TW}. Grey series; the air water difference $T_{AW.}$

Results and Discussion

A typical example of the data from both T_{AW} and T_{TW} thermocouples is shown in Figure 6.5 with both thermocouples referenced to separate junctions glued to the underside of the trough.

This is a run with high humidity, at 70% with a clear water surface. The dark series of T_{TW} temperature shows a slight temperature increase. The lighter grey line T_{AW} shows a warmer air temperature. At the end of 40-60 minutes the balance of latent heat cooling opposing sensible heat cooling results in a slight warming of the trough.

As expected, the T_{AW} thermocouple fluctuates in temperature more than the T_{TW} thermocouple. To overcome the random fluctuations in thermocouple measurements particularly the T_{AW} value as shown in Figure 6.5, a running average was used in the programming of the Picaxe. The stored values for thermocouples were found by multiplying the previous value by 9, adding it to the current reading and dividing by 10. This worked very effectively at removing random fluctuations, however still allowed for a much quicker temperature variation than was needed for the trough. T_{TW} was used to measure the trough cooling, and T_{AW} was used to monitor the possible effects of air water temperature differences.

6.2.2 Effect of humidity

The T_{TW} was found by placing the Y tube with incorporated fan in the climate chamber described in Section 3.4.3. and measuring the T_{AW} reduction at various humidities.

The trough temperature T_{TW} runs measured for various humidities using water are shown in Figure 6.6, and results for a similar series of runs using a monolayer surface are shown in Figure 6.7.

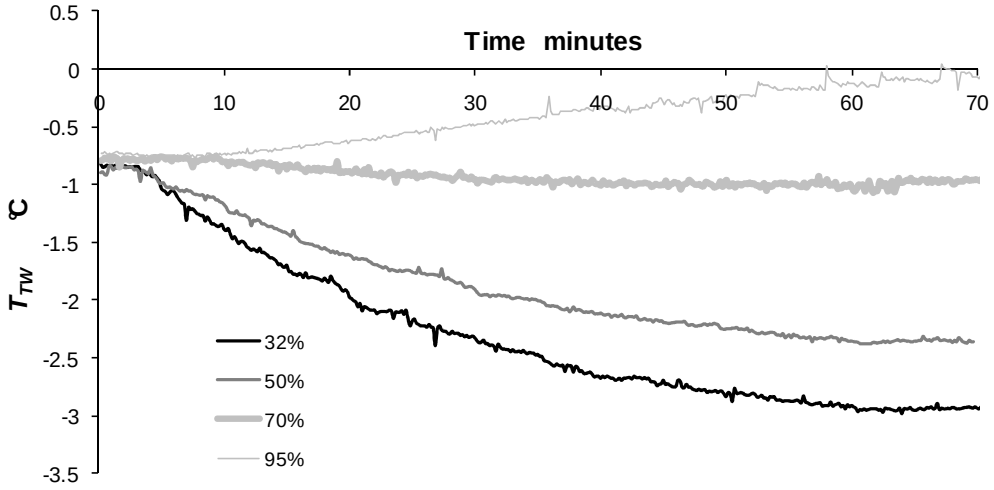

Figure 6.6 Dependence of T_{TW} on humidity for water.

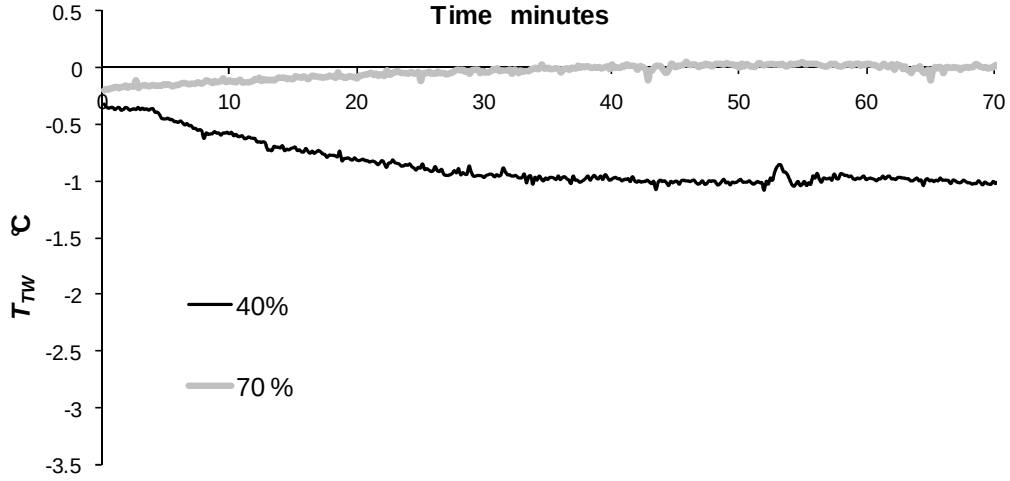

Figure 6.7 Dependence of T_{TW} on humidity for hexadecanol monolayer.

The lower latent heat flux can be seen to be noticeably increasing the trough temperature for all humidities. This is the desired feature showing the difference between water and monolayer. These plots however do not show the T_{AW} temperature which varied between 0-5°C, and was difficult to control in the climate chamber. This may have significantly affected results. The dehumidifier contributed to these difficulties as it heated the air as it was operating. The effect of T_{AW} on the final T_{TW} was then investigated.

6.2.3 Determination of sensible heat flux coefficient

A thick layer of Aquatain was used to effectively stop the evaporation so that the effects of T_{AW} (sensible heat) on the trough temperature T_{TW} could be ascertained. If the air above the trough was

similar to air above the surface outside the tube, it might be expected that T_{AW} would have no influence on the T_{TW}. However, higher wind speed may make it easier for the warm air to penetrate the vapour diffusion layer and allow conduction to the surface and affect the very thin air layers above the surface to allow more sensible heat conduction between air and the water surface.

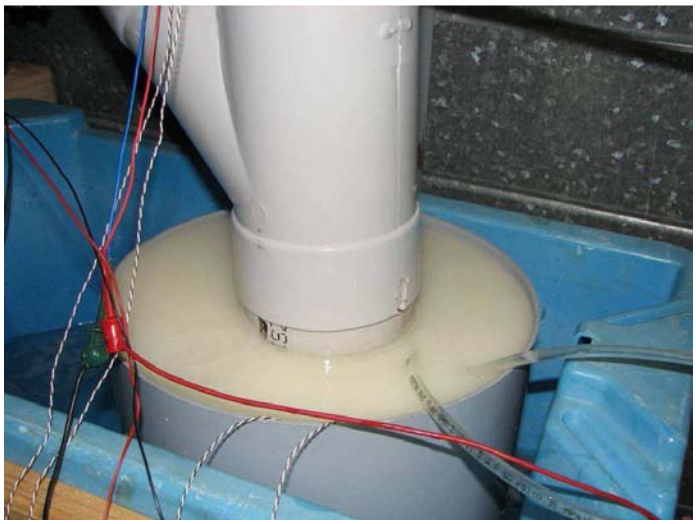

Figure 6.8 Aquatain added to the WASP inner container in the climate chamber.

Materials and Methods

The silicone oil Aquatain was poured into the inner trough surrounding a WASP in the climate chamber to a thickness of around 1 cm It was considered there would be no evaporation under these conditions, since the recommended thickness should be about 1 μm. The Y tube used was an old model, no longer going to be used for testing monolayers. This was important since the silicone oil is "impossible to remove from equipment" (Gainer, Beard, & Thomas 1969).

The Picaxe was programmed to complete an hour cycle, then rest for two hours, and store the T_{AW} and final T_{TW} for each run, lasting three hours. It was left running for several days.

Results and Discussion

The results are shown in Figure 6.9, showing there is a clear proportionality between T_{AW} and final T_{TW}. This shows that sensible heat needs to be taken into account in predicting final values of $T_{TW.}$

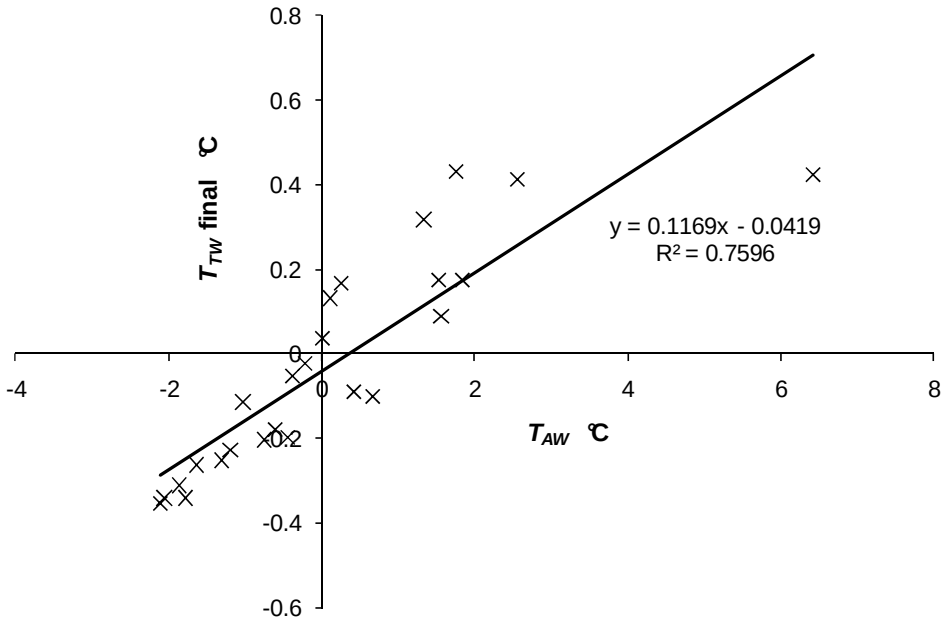

Figure 6.9 Effects of T_{AW} on final T_{TW} in the case of no evaporation.

A linear line of best fit was added to the graph which showed a gradient of 0.16. This value can be used as a coefficient for an air/water heat conduction term in predictions of final $T_{TW.}$

6.2.4 Heat flux into the WASP trough

Heat conducted through the walls of the trough reduces the evaporative cooling, so tests were carried out to determine the contribution of conduction through the trough walls to the trough temperature.

The thermal conductivities of materials important for the WASP are given in the following table:

Table 6.1 Thermal conductivities of materials (Engineering Toolbox 2010; Kaye & Laby 1973)

Material	Thermal conductivity k $WK^{-1}m^{-1}$
Air	0.024
Water- no convection	0.58
PVC – Polyvinyl chloride	0.15
Glass wool- insulation	0.0167
Copper	440

The thermal conductivity of PVC is quite low, less than half that of water, and therefore it is effective in insulating the trough. Attempts were made to insulate the trough more thoroughly to

obtain larger evaporative cooling temperatures. (It is possible to perform this too thoroughly, as the trough needs to return to thermal equilibrium between runs).

Figure 6.10 Measuring the heat flux into the double trough. The magnetic stirrer had just enough magnetic influence at that distance to influence a stirrer placed inside the trough.

Materials and Methods

In order to test the heat flux flowing into the trough, the trough was used without the Y tube. The infrared thermometer was positioned above a trough which was initially cooled with ice to somewhere around 5-10° C.

This was in turn held in a tray of deep water placed on a magnetic stirrer, to agitate the contained water in the trough, so that no temperature profile could be set up in the trough. The temperature was recorded every 15 seconds using the IR thermometer software. The expected outcome would be an increase in temperature as conduction takes place through the walls of the trough.

Four types of insulation were tested, as pictured in Figure 6.11. These are pictured below:

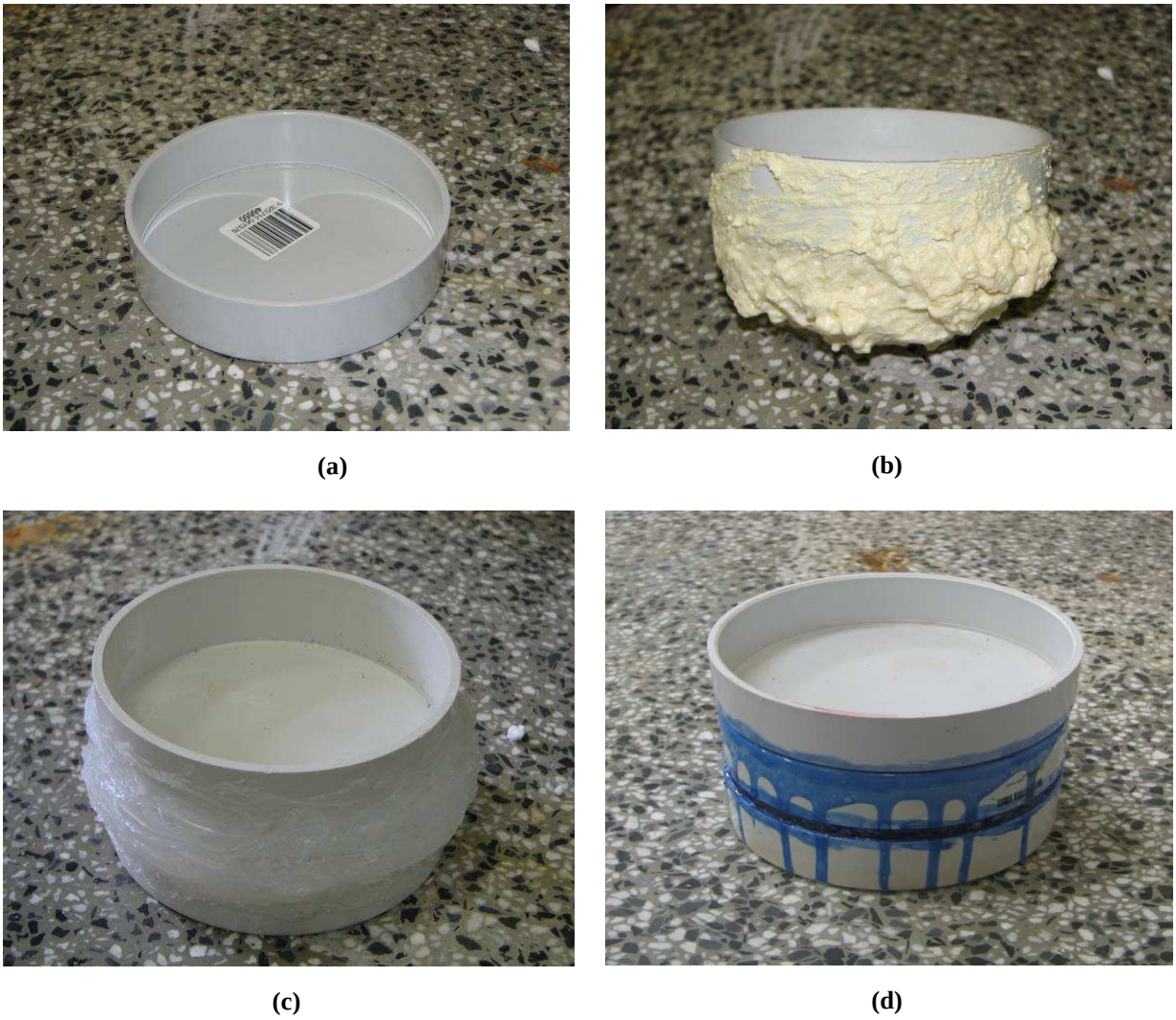

(a) **(b)**

(c) **(d)**

Figure 6.11(a) Single 100 mm PVC end cap (b) Single end cap with expanding foam attached to the bottom (c) Double end cap with joined with silicon sealer (d) Triple end cap. The lower two end caps are joined with a small piece of tube, and this is glued to the top end cap.

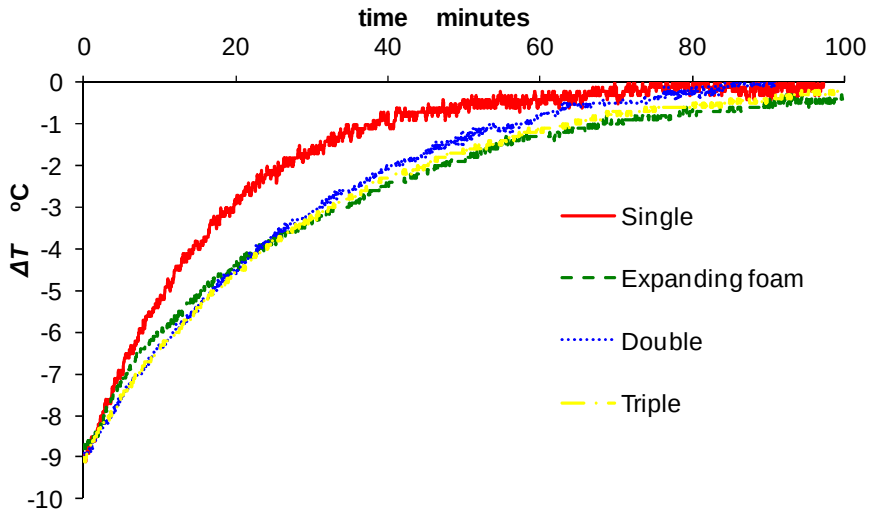

Figure 6.12Thermal equilibrium being restored in various types of end caps.

Results

The results shown in Figure 6.12 indicate that the single cap was the first to reach equilibrium as expected. The double end cap was the next, and the best insulators were the expanding foam and triple end caps. Unexpected problems occurred for the double end cap, which contained water in the air space after several months of immersion under water. Similarly the expanding foam seemed to partially fill with water. This was not totally unexpected as the instructions supplied with the foam advised it was not to be used as a water displacer.

Conclusions

The best insulator should show the least temperature change at an average temperature that the trough is subjected to. This average temperature was chosen as 2°C cooler than the surrounding water. The gradient was measured around this point with the results shown below:

	Single °C min^{-1}	Expanding foam °C min^{-1}	Double °C min^{-1}	Triple °C min^{-1}
Gradient	0.15	0.066	0.092	0.068

This shows the expanding foam trough as being the best thermal insulator. The standard deviation in these gradients for multiple trials carried out separately showed a 30% relative uncertainty. From these trials, the triple end cap was chosen for further work as it showed similar insulation to the expanding foam but stayed impervious to water. The triple end cap also allowed easier attachment of thermocouple reference junctions.

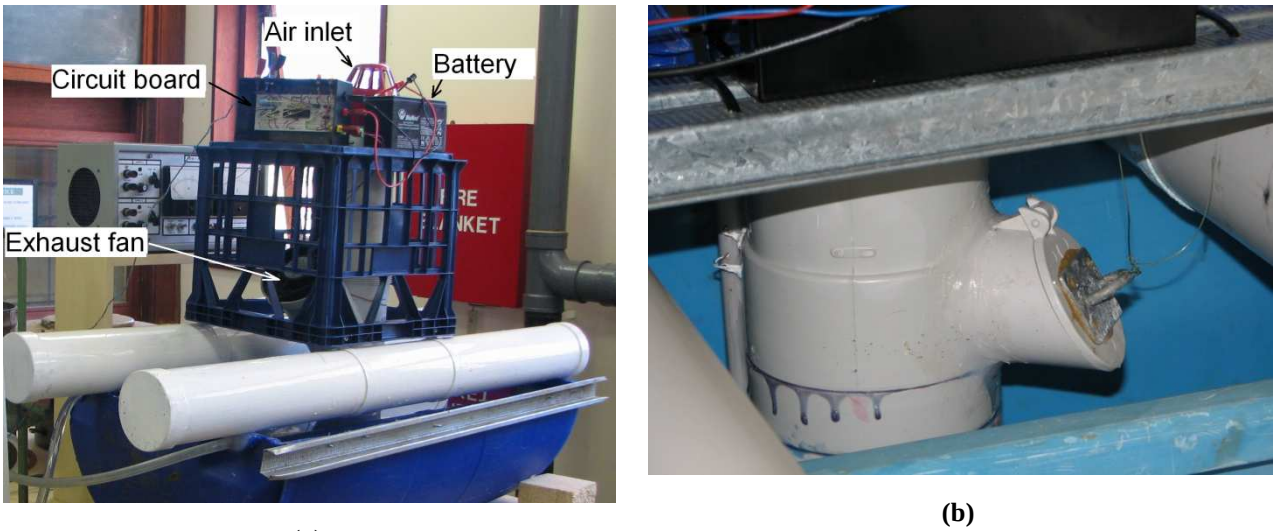

(a) **(b)**

Figure 6.13 (a) WASP using kit board circuit and permanently open water surface entrance hole (b) Closed servo controlled "frog flap" attached just above trough to control surface entrance.

6.3 Construction of WASPs

The assembled version of the WASP is shown in Figure 6.13. The Y tube was clamped to an inverted plastic milk crate, and 100 mm PVC floats were tied underneath. The two thermocouples T_{TW} and T_{AW} were attached. A Honeywell 4000-001 humidity sensor and thermistor were added to the circuit board to sense the condition of air ~40 cm above the water. This circuit board consisted of a project kit type, where the wires were plugged in. The surface entrance consisted of a permanently open small hole, and a 12 Amp hour (Ah) battery was positioned on top.

Trials in a 1.8 m cattle trough under windy conditions showed less evaporative cooling than measurements indoors. It was considered that water was moving through the small hole in the device and in and out of the trough area while measurements were being taken. To prevent this occurring a plumbing “frog flap” was used, as shown in Figure 6.13(b) . A hook was glued to the flap using contact adhesive, and nylon fishing line was attached to a microprocessor-controlled servomotor mechanism tied to a right angle bracket that was clamped higher on the Y tube. It could then be left open in resting periods to allow equilibrium temperatures to be established and closed during measuring periods.

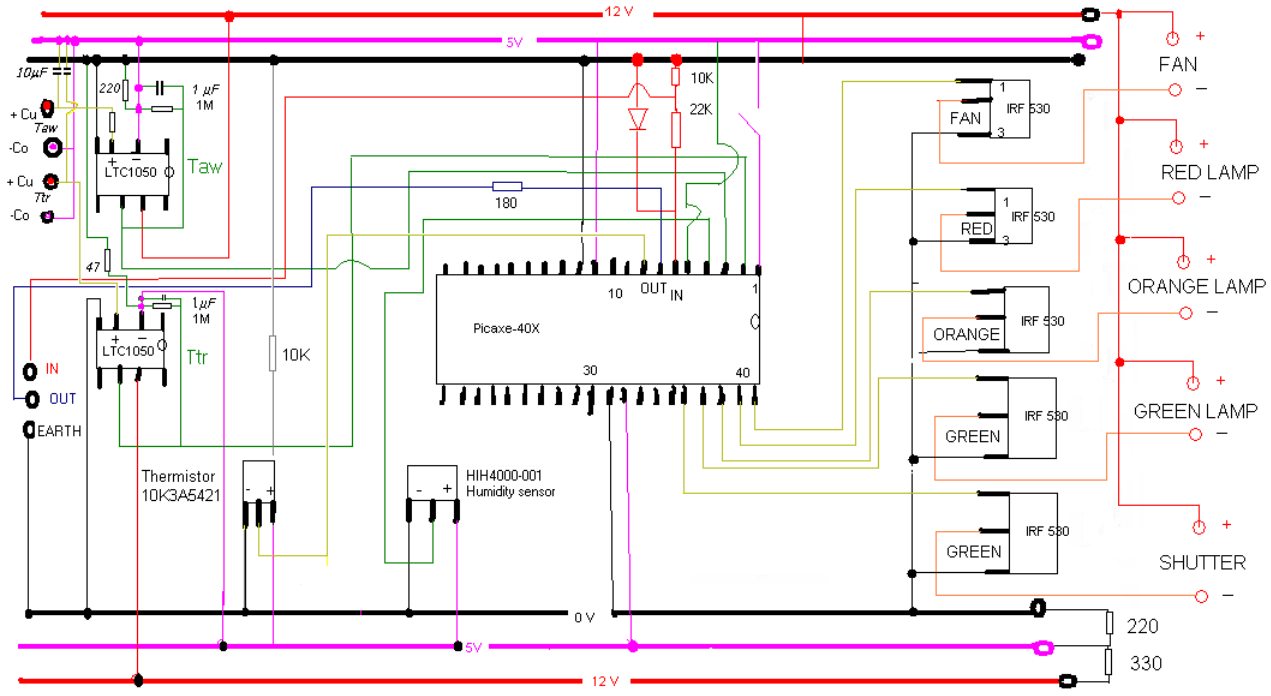

Figure 6.14WASP circuit diagram

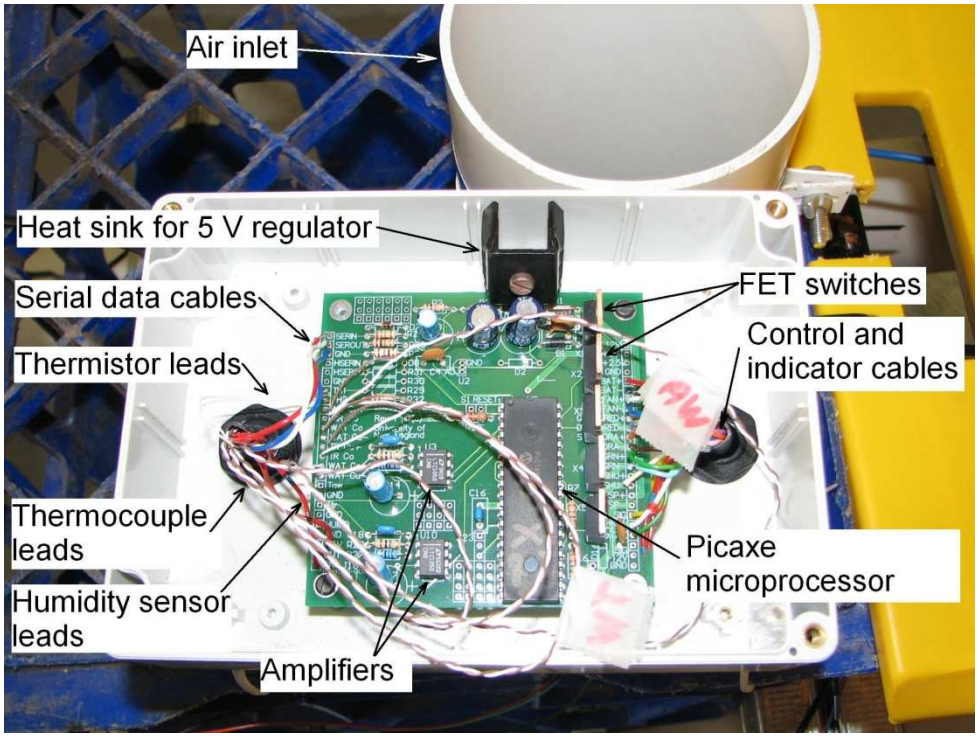

Figure 6.15 Printed circuit board installed.

6.3.1 Circuit development

The WASP circuit diagram is depicted in Figure 6.14 with a photograph of the assembled circuit on a printed circuit board shown in Figure 6.15. The positioning of components on these boards included a segregation of sensitive sensors and serial data cables on the left and controls cables, indicator lights and power on the right.

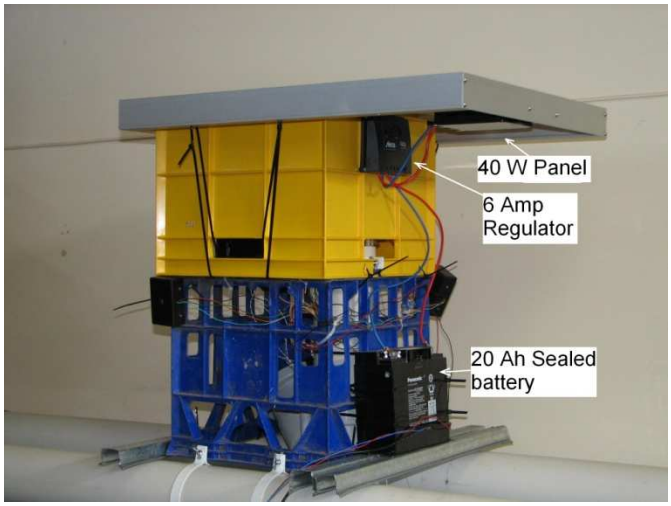

Figure 6.16 Front view showing electrical system.

6.3.2 Electrical supply

The electrical system consisted of a 40 W solar panel (BP solar), attached to a 6 Amp Solsun regulator. This was stored in a 20 Ah Panasonic sealed LC-X1220P battery. The position of each is depicted in

Figure **6.16**. The battery needed to be kept as low as possible to prevent the assembly from being top-heavy. The choice of this configuration allowed enough energy reserves for the running of the system for about 4 sunless days. However rarely is there no sunshine at all for the solar panel, so the battery would last at least a week.

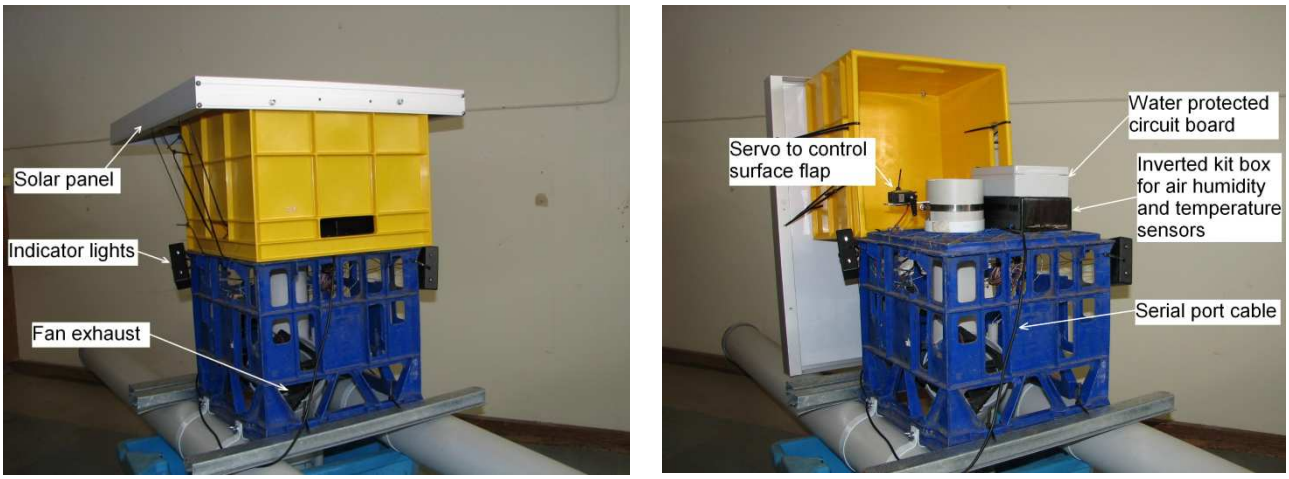

(a) **(b)**

Figure 6.17 (a) Rear view (b) Rear view with pivotting top open.

The final setup of the WASP is shown in Figure 6.17 above. The top yellow waterproof was an inverted plastic toy box, which protected the electronics circuit board, and held the solar panel firmly.

6 V radio-controlled plane servos were used. Being supplied with 12 V makes little difference, only producing faster and more powerful movements. They are particularly easy to program, as the Picaxe has a servo function, and numbers just need to be added to describe the angles needed.

6.3.3 Communications

Decisions on the presence of monolayer, and malfunctions of the WASP can be indicated either using the indicator LEDs shown in Figure 6.17(a) or they serial port cable shown in Figure 6.17(b) . The indicator lights were orange and green. Orange indicated that the monolayer was not at full pressure, while the green indicated all is well and the monolayer coverage is intact. The lights were programmed to keep flashing irrespective of whether tests were being run. A pattern was devised by flashing a different number of times to show the last 5 decisions made. The Picaxe itself can store 1024 bytes in a "scratch pad" which could hold past diagnoses of the coverage and also any malfunctions of the WASP. The data can be accessed using a second serial port allowed for in the printed circuit board. An easier way through is to use the existing serial port and program it to send all stored data, when switched on. Then the data could be accessed by switching the power off and on.

6.3.4 Operational Algorithm

It is very difficult to predict water temperature using remote measurements, for instance from weather stations. However, as the apparatus is floating on the water surface, it is measuring variables that can be difficult to determine, such as air and water temperature and humidity, closely to the water surface. Thus, the water in the sampling chamber is under known and controlled conditions.

The Picaxe program uses data from the T_{TW} and T_{AW} thermocouples, an air humidity sensor and a thermistor to predict the final depression temperature of the trough. A comparison of experimental measurement with theoretical prediction indicates the presence of the monolayer.

Beginning with Dalton's Equation (1.1):

$$m_e = f(U)(e_{SWT} - e) \qquad (6.3)$$

where m_e is the evaporation rate, $f(U)$ is a function of wind speed, e_{SWT} is the saturation humidity at the water surface temperature, and e is ambient air relative humidity.

The saturation humidity pressure can be found from an polynomial curve fitting of empirical data (Nave 2009):

$$V(Pa) = 747.51 + 1.0755T + 4.257T^2 \quad \text{(Pa Celsius)} \qquad (6.4)$$

The sample surface temperature is assumed to have properties close in value to the surrounding water T_W. which is calculated by subtracting T_{AW}, the difference between air and water temperature, from T_a, measured using the thermistor positioned just below the circuit box.

$$T_W = T_a - T_{AW} \tag{6.5}$$

Therefore Dalton's equation becomes:

$$m_e = \frac{Q}{t} = f(U)\left[V(T_a - T_{AW}) - e\right] \tag{6.6}$$

If the wind speed function *f(U)* is replaced with an empirically determined proportional constant $A \times U$, where U is the wind speed, the change in temperature of the trough due to latent processes is proportional to the mass of water evaporated, and therefore is:

$$\Delta T = AU\left[V(T_a - T_{AW}) - e\right] \tag{6.7}$$

where ΔT is the change in temperature, A is an experimentally determined constant.

The theoretical prediction of the trough temperature due to sensible and latent heat processes T_{TW} is then. :

$$T_{TW} = T_W - AU\left[V(T_a - T_{AW}) - e\right] + BT_{AW} + CT_{TWI} \tag{6.8}$$

where B and C are determined empirically, with the value of constant A found by testing surfaces with and without monolayer covering. The variable U is the air flow speed of 3.2 m s^{-1} generated by the fan, T_{TWI} is the initial temperature of the trough measured by T_{TW}.

- The second term (containing A) uses the humidity deficit of the Dalton equation to predict evaporation. The value of A is set midway between the expected latent heat absorbed due to evaporation of water, and that of the monolayer.
- The third term involving B allows for the sensible heating of the trough, which is proportional to T_{AW}, the air water temperature difference.
- The fourth term involving C is added since the initial T_{TW}, measured just as the fan is switched on, is higher for monolayers. This is shown in Section 4.5.2 using insulated troughs.

6.3.5 Evaluation of constants

The coefficient; A, has been estimated from the average of the gradient of final temperatures for water and monolayer shown in Figure 6.18.

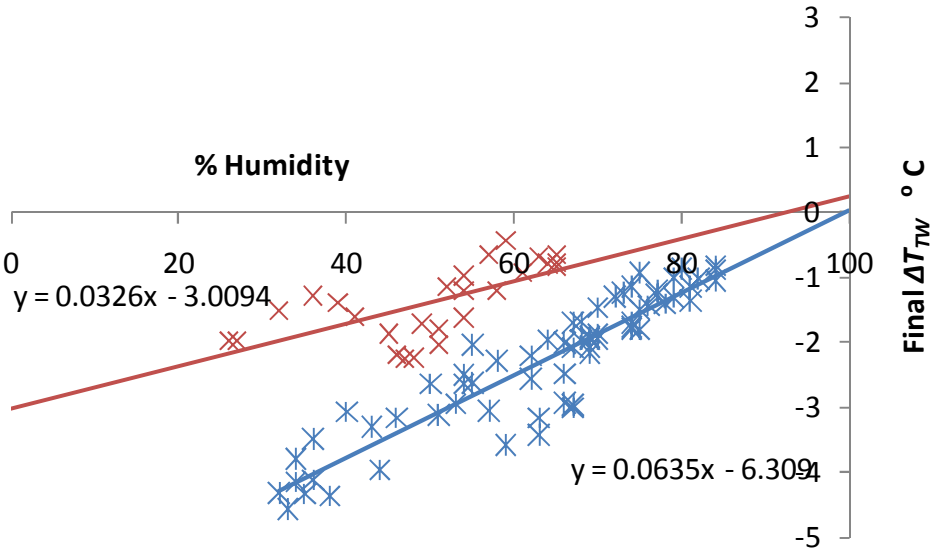

Figure 6.18 Final T_{TW} for hexadecanol (×) and water (∗) relation with air humidity. The large scattering is mainly caused by no allowance being given for the range of temperature and T_{AW} values from which the data was taken. The trendlines would then average the evaporative cooling, for a range of temperature conditions.

The scatter is mainly due to the effect of measurements being taken under different ambient temperature. As temperature increases, the saturated vapour pressure increases, leading to larger evaporative cooling. These are the temperatures being tested however, so a trend line describes the trough cooling that occurs under average temperature conditions. The average of the two gradients is 0.048 °C. This can be converted to °C Pa^{-1}.using the calculation that air at 20 °C has a vapour pressure of 2379.3 Pa (Equation 6.4). 1% of this is 23.79 Pa. So the gradient is 2.02 °C Pa^{-1}. When the result is is divided by the wind speed, $A = 6.25 \times 10^{-4}$ °C m^{-1} s Pa^{-1}.

The constant B representing sensible heat effects was determined in Section 6.2.3 and found to be 0.16

The constant C is part of a term which allows for changes that have occurred before the fan begins. The initial T_{TW} Figure 6.6 and Figure 6.7 show that with no wind – the water temperature tends to start below -0.5 °C, while monolayer begins above -0.5 °C. If the difference from -0.5 °C is added to the Theoretical T_{TW} differences which have occurred before the fan begins can be accounted for. The constant C is an estimation of how much this can be trusted considering the initial T_{TW} seems to fluctuate. An estimation of C = 0.25 biases the final theoretical value a small amount without causing an error if the value is unusual.

With the constants A, B, and C determined for the instrument, the processor can compare the measured temperature of water in the trough, with the theoretical prediction of T_{TW} outlined above. If the water temperature within the trough is lower than the theoretical T_{TW}; the monolayer is not present. If the water temperature in the trough is higher than predicted by the theoretical T_{TW}, the monolayer is present.

6.3.6 Programming the WASP

Three Models of Picaxe were used, with the final 40X2 being used as soon as it became available. The programs could be written in Basic. However there was a limit of 27 variables with a 2 bit value. This also meant that all calculations needed to be positive and between $0\text{-}2^{16}$ (256×256). The Picaxe received all information from the humidity sensor, 2 thermocouples, the exact zero voltage of the amplifier (2.5 V) level, thermistor digitised the signals and calculated an appropriate output with surprising efficiency. So much so that it was also used to "clean" the thermocouples readings which fluctuated to a large extent. The digitised values T_{TW} and T_{AW} from the thermocouples were smoothed using a running average of 10. The previous result read by the thermocouple was remembered and multiplied by 9 to which the new reading was added, and the sum divided by 10. This virtually removed all random fluctuations in the data series for both thermocouples. A running average of 5 was also used for determining the initial T_{AW} and thermistor, and humidity measurements. The running average is slightly below the initial values, however they have less variation. A large proportion of the scatter in this graph due to variations of absolute temperature affecting the evaporation rate.

6.3.7 IR measurements using WASP

The evaporative cooling that occurs within the enclosed insulated trough occurs as a result of changes to the surface temperature. The procedure described in Section 4.5.4 repeated for a fully assembled WASP to more fully understand the temperature profile changes occurring within the trough.

Materials and Methods

The IR thermometer was clamped above the inlet tube of the WASP and pointed at the middle of the surface to measure surface temperature for each hourly cycle, in a similar way to the setup in Section 6.2.1. The differences being the addition of the insulated trough and the enlargement of the measured time, from a few minutes to 60 minutes to allow for the longer time taken temperature stabilization of water in the trough. The setup was photographed (Figure 6.19(a)) with the results shown in Figure 6.19(b).

(a)

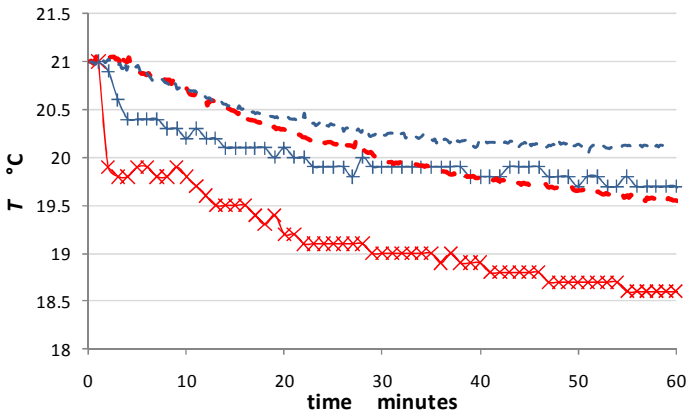

(b)

Figure 6.19 IR(a) Setup for surface measurements within WASP. (b) IR Data for one 60 minute cycle for clear water (×) and hexadecanol (+), taken from circled regions of Figure 6.20.Dashed lines represent thermocouple measured results T_{TW}, with representing clear water (red) and hexadecanol (blue).

Also shown on this graph is the measured thermocouple values as dashed lines for 50% humidity for both clear water (red), and hexadecanol (blue) over one 60 minute cycle. The humidity values for the IR measurements were 49% for the clear water (red) and 46% for the hexadecanol (blue). With similar humidities the results can be compared. To aid the comparison the data was adjusted vertically to initially begin the cycle at exactly 21 °C. From results of surface cooling in Figure 4.28, with no trough, using a wind speed of 3.0 m s^{-1}, the surface of clear water is around 1.0 °C cooler than the subsurface water, and around 0.3 °C for a hexadecanol surface when measured with an IR thermometer. This difference occurs in Figure 6.19, however it can be seen that this surface evaporative cooling occurs in the first 3 minutes. Afterwards the surface cools to an equilibrium temperature quickly, unlike the earlier graph, as the cooled water cannot escape, and accumulates in the trough, cooling the surface further over around 60 minutes before reaching an equilibrium temperature.

The data for a single cycle already discussed was chosen as an average cycle (circles) taken from a diurnal measurement of around 10 cycles for clear water (Figure 6.20(a)) and hexadecanol (Figure 6.20(b)). Also plotted in these figures is the air temperature T_a (green dashed line), as measured with the IR thermometer. These graphs contain several interesting features:.

- The 60 minute cycle appears not to be long enough to attain thermal stabilization
- Both the initial temperature drop, and final temperature appear lower for clear water.
- The difference between the fan off regions and T_a is larger for hexadecanol – possible due to some trapping of cold water at the surface due to inefficient thermals caused by surface viscosity (see Section 4.4.1).
- The water surface temperature is more responsive to changes in air temperature

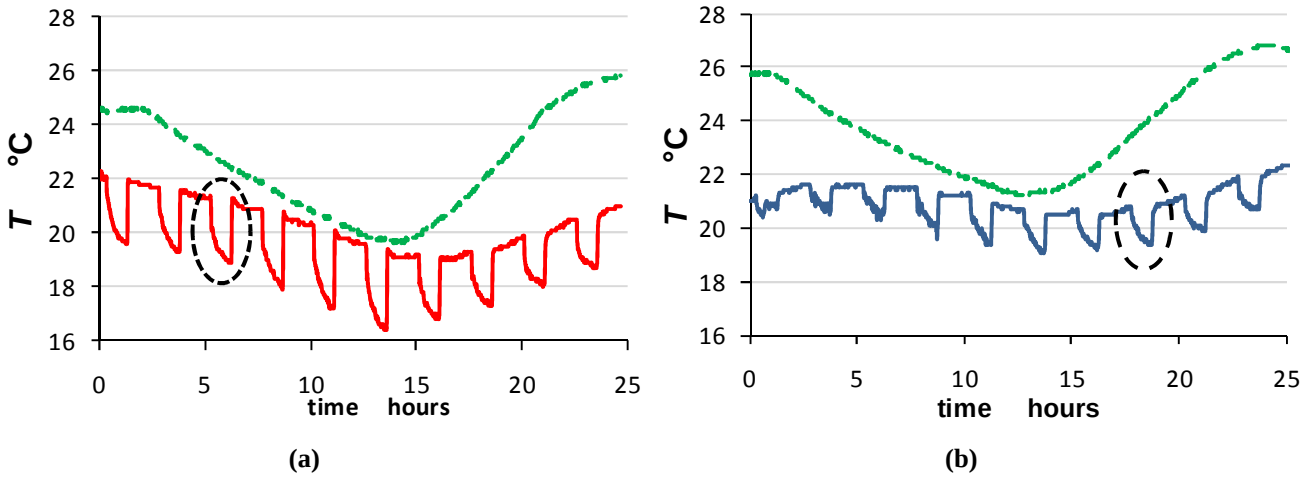

Figure 6.20 IR measurements of surface temperature taken over a day.(a) for water (red solid line) and (b) for a hexadecanol monolayer (blue solid line). The dashed green line is the air temperature T_a. The dashed circles are the data cycle chosen for Figure 6.19(b).

Conclusion

These measurements show that small difference in IR measurements are indeed possible and the use of an IR sensor may improve the diagnosis of coverage more quickly by either being incorporated into thermocouple data, or replacing the thermocouples with an IR sensor. The advantage of IR trough temperature sensing would be that it produces a larger temperature difference between the clear water and hexadecanol samples, since the difference to surface is added to the difference between troughs. A disadvantage is the relatively large 0.1 °C resolution with the IR thermometer used. This is a resolution produced as a result of digitising radiation from absolute zero within the thermometer. A higher resolution may easily be possible by amplifying the voltage in the relevant region 0-40 °C before digitisation is used. It is again only differences that occur with the fan switched on that need be measured. Thermocouple measurements may not be as accurate as usual in relating voltage to temperature as the reference thermocouple may fluctuate slightly affecting the thermocouple resolution, due to temperature fluctuations in the water immediately under the trough. The EAIR-1816-510300 low temperature (0-300 °C) sensor retailed by Pacific Sensor Technologies is currently being investigated and may be useful in a final product.

6.3.8 Accuracy of the WASP

Using thermocouples to measure the evaporative cooling in on an indoor trough, the WASP indicated the correct cover 100 % of the time. However only using full pressure and clean surfaces were tested. Also the room had a humidity which was never above 80%, even when raining outside.

The accuracy of the WASP under field conditions has yet to be determined. When positioned on a trough indoors, it correctly predicted the existence or absence of a full pressure hexadecanol up to the available humidity of 80%. The humidity of the air within the laboratory did not rise above this value, even when raining, and the room was too large to use the humidifier from the climate chamber. Under field conditions there may be partial monolayer pressures and more variations in reference temperatures under the unit. In any case the diagnosis of monolayer coverage is less important in high humidity conditions as there is less evaporation. Some outdoor testing showed the testing chamber to be fairly resistant to environmental factors such as sun, wind, waves and water currents, since it is shaded from the sun and sealed from water influences.

6.4 Conclusions

Measurement of the evaporative cooling change produced by monolayers seems the most practical method for assessing their presence or absence since this directly related to evaporation reduction; the desired characteristic in their use. Use of an artificial wind moving over an insulated trough both increase the differences in temperature caused by the presence of a hexadecanol monolayer on the surface.

Characteristic temperature changes that occur when the fan is switched on may be identified, using either the quicker IR differences measured with an IR sensor directed at the surface, or the slower measurement of T_{TW}. These are measurements which necessarily need to include T_{AW} and % humidity and initial T_{TW} for maximum accuracy in diagnosing the state of the surface.

Hexadecanol was used in this work, however any surface active layer which reduces evaporation is capable of being monitored, as they would cause similar temperature differences, and hence would be capable of being measured with this system. This includes any oil slick with a thickness greater than 3 µm as this appears to be the thickness which matches the effectiveness of hexadecanol (Section 4.5.2). These surface active layers also reduce surface tension, which is crutial for aiding the spread of the layer into and out of the testing chamber.

Chapter 7. Achievements and Summary

The primary aim of this research was to investigate current methods of monolayer detection and explore any techniques which can automatically assess the state of monolayer coverage. It was found that the two existing methods; the oil indicator method and observation of damping were labour intensive and very difficult to automate. So an entirely new detection technique was required, and to this end, monolayer characteristics were examined, using various fields such as spectroscopy, thermodynamics and rheology. The most promising existing methods of monolayer detection; identified through a literature review were investigated experimentally with regard to reliability, and ease of incorporation into an automatic detection system. Many detection methods have deliberately been investigated to cover as many options as possible. Many people gave advice on detection methods, and all of these valued comments were explored, as there was concern, that in focussing on one method, a simpler, more effective method may be overlooked. There was also a deliberate emphasis on obstacles which made some detection methods difficult or unusable, as further work in monolayer research may benefit by knowing the nature of the impediment in the use of these methods.

A literature review is given in Chapter 1 covering the main techniques used for evaporation on water storages. Monolayers are presented as one of these with some history, characteristics and factors governing effectiveness.

These changes that occur to surface tension and wave damping are explained and tested experimentally tested in Chapter 2. The two main existing detection techniques; indicator oils and damping are discussed and tested experimentally, however neither showed any promise for automation. Additionally false indications may occur as other impurities and occurrences may lead to a lowering of surface tension and increased wave damping.

Direct evidence of evaporation is found by measuring surface temperature changes, and this was carried out experimental in Chapter 3. These changes showed particular promise for reliable temperature indicators with the addition of artificial wind, and by using an accumulating trough.

Alterations to interactions with electromagnetic radiation by monolayers are studied in Chapter 4 determining that absorption, Brewster angle and emissivity are too small to be reliably detected in the field. However IR measurement of surface temperature showed consistent differences, particularly with the use of an artificial wind. Equipment for IR multichannel analysis and passive microwave absorption was not available, however may hold some possibilities for detection methods.

The effects of wind on evaporation rates and coverage are discussed in Chapter 5. Results show that wind is shown to increase both surface and bulk temperature differences which occur with the addition of hexadecanol in large laboratory troughs.

The addition of reliable indicators were combined in Chapter 6 to develop an automatic monolayer detector, using temperature differences, which are augmented with the use of artificial wind and an

accumulating trough, in an enclosed chamber using a combination of thermocouples and IR sensors. Since measurements are being conducted under known conditions, the final temperature of the trough T_{TW} gives an assessment of the evaporation occurring which becomes easier to assess under low humidity conditions (<60%) however harder to distinguish under high humidity conditions (>80%). It becomes less important to detect monolayer coverage state under conditions of high humidity, however as there is little evaporation occurring.

Important key outcomes which have been shown to be controversial are repeated here as they are considered crucial to efficient monolayer usage.

- Numerous experiments from various authors (Wu 1971), show the damping of waves produced by monolayers alter the wind structure above the surface. This reduces the friction velocity U_* which increases the vapour diffusion layer thickness leading to a decrease of evaporation. So the damping of waves by monolayers may be responsible for a significant reduction in evaporation.
- While monolayers exhibit wind drift resistance on small troughs, this characteristic is virtually lost on large storages due to an accumulation of surface pressure produced by wind stress, and monolayers follow close to the normal drift speed that occurs for clear water under windy conditions. Therefore allowance needs to be made for surface drift in deciding dispensing methods.
- Evaporation resistance of monolayer actually increases with wind speed, rather than decreases, so long as coverage can be maintained. This was shown to be caused mainly by the dramatic increase in evaporation from an uncovered water surface under windy conditions. \
- Alterations to the evaporation reduction of a surface are caused by changes to the vapour diffusion layer. Whether monolayers function by limiting the supply of water molecules to this layer (energy barrier theory), or changing the turbulence and air structure above; thereby thickening this layer remains to be tested.

Recommendations for further work

The key outcomes need to be checked more thoroughly using experimental methods to better characterise the behaviour of monolayers and the processes that occur around them which contribute to the desired ability to reduce evaporation.

It may be useful to conduct initial tests on the WASP, on a large trough, where flooding of the trough can be used to provide a clean surface with minimal surface active impurities. This flooding provides an opportunity to experiment under controlled conditions of purity and surface tension which are not readily available on most water storages. Improvements to the WASP include reducing the run time from the present 60 minutes to around 5-10 minutes. This would probably involve the use of a higher wind speed, and an IR sensor detecting surface temperature within the trough. Development of feedback link to the dispenser(s) needs to be incorporated. The aim of future development is the deployment of a complete system which would assure storage owners of most efficient monolayer coverage. The WASP could be deployed at strategic positions around storages to feedback to sensors positioned in a grid positioned across the surface. Alternatively a mobile sensing/dispensing system could be useful to always operate upwind on large water storages.

In the initial stages of this work Australia was experiencing record droughts. On submission there are record rainfall and floods. It is hoped that rational management of water storages in conjunction with efficient evaporation reducing techniques such as monolayers may help ameliorate both.

Appendix 1 Group velocity of waves

The speed of energy transfer away from a disturbance is called the group velocity v_g, and describes the velocity at which a pulse, or train of waves moves away from the source. When looking at velocity differences it is important to distinguish between measuring a pulse of waves traversing a distance; group velocity c_g and the speed of an individual wave moving the same distance in a continuous wave pattern; wave velocity c_w. This effect is noticeable in deep water with large ocean waves, where waves of similar wavelength are moving away from a disturbance. If an individual wave is followed, it is seen to advance through the group, gradually dying out as it approaches the front, while a succession of waves moves forward to fill its position in the group.

The group velocity can be derived by adding groups of waves of similar, but slightly different wavelength. The wave equation will have the form

$$y = A\sin(kx - \omega t) + A\sin(k'x - \omega t) = 2A\cos\{\frac{1}{2}(k - k')x - \frac{1}{2}(\omega - \omega')t\}\sin\{\frac{1}{2}(k + k')x - \frac{1}{2}(\omega - \omega')t\}$$

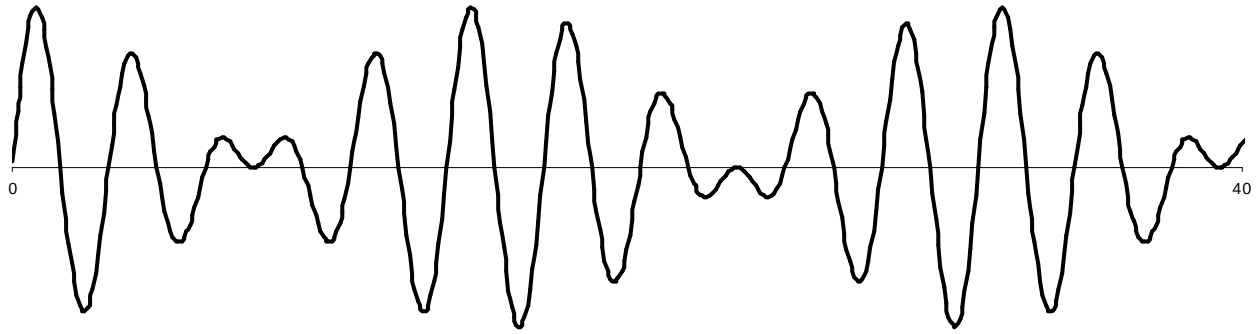

Figure 7.1 Wave groups produced as a product of a sine wave and a larger period cosine wave.

If *k* and *k'* are almost identical, the cosine expression would vary very slowly with x, so that the wave-profile at any instant has the form of curve of sine in which the amplitude alternates gradually between the values *0* and *2a*. The surface will look like a series of groups of waves, separated at equal intervals by bands of nearly smooth water. The surface will therefore present the appearance of a series of groups of waves, separated at equal intervals by bands of relatively smooth water. The motion of each group is then independent of the; presence of the others.

The distance between two successive groups is $\frac{2\pi}{(k - k')}$, and the time taken for the group to move through this distance is $\frac{2\pi}{\omega - \omega'}$, the group velocity $v_g = \frac{(\omega - \omega')}{(k - k')}$ or $v_g = \frac{d\omega}{dk}$. In terms of wavelength $\lambda = \frac{2\pi}{k}$ and $\omega = kc$:

$$v_g = \frac{d(kc)}{dk} = c - \lambda\frac{dc}{d\lambda} \qquad (7.1)$$

where *c* is the wave velocity.

For a gravity wave, $c = \sqrt{\frac{g}{k}\tan kh}$ the group velocity $\frac{d(kc)}{dk} = \frac{1}{2}c\left(1 + \frac{2kh}{\sinh 2kh}\right)$

So the group velocity matches *c* when *h* is very small compared with the wavelength, and decreases to $\frac{c}{2}$ when h is very large. For deep water the group velocity is half the wave velocity.

For a capillary wave, c varies with

$$\frac{1}{\sqrt{\lambda}}, \text{ so } v_g = c - \lambda\frac{dc}{d\lambda} = \frac{3}{2}c \qquad (7.2)$$

So the group velocity moves faster than the wave velocity. The depth term *tankh* is not considered here for capillary waves, since λ is relatively small.

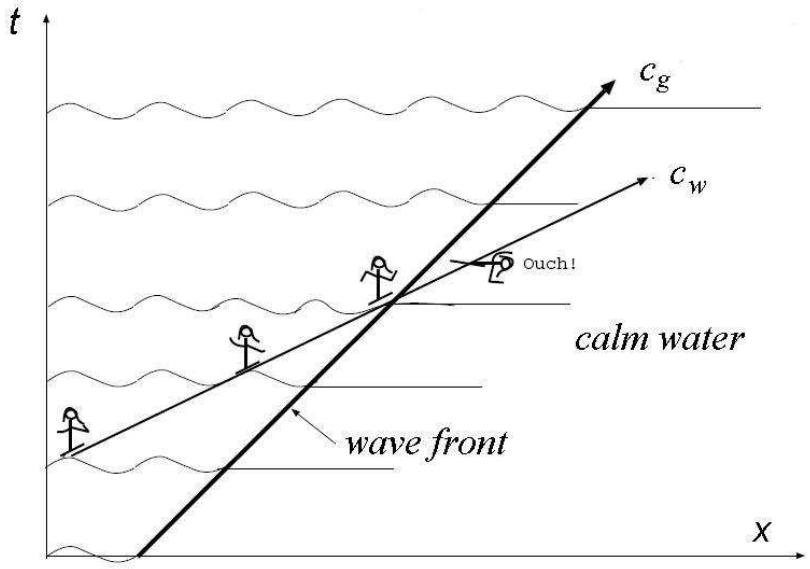

Figure 7.2 Gravity waves move slower than the group wave velocity. v_g=c/2 A surfboard rider would move forward through the wave train and fall onto calm water. Adapted from Ananthakrishnan (2005).

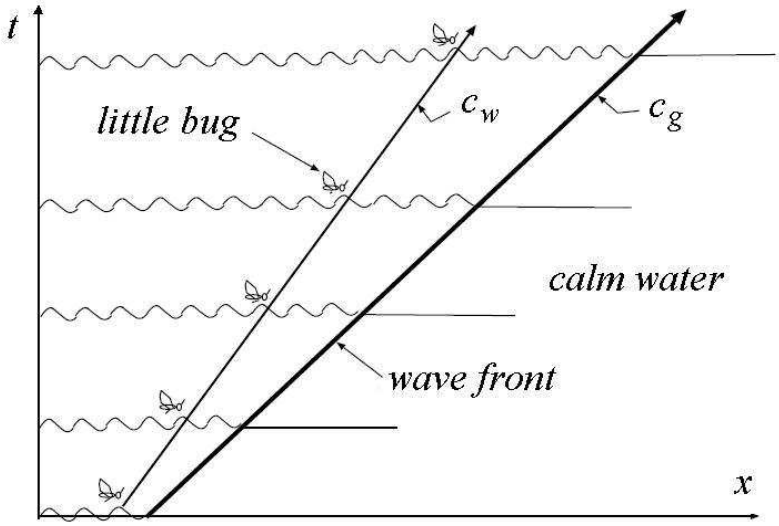

Figure 7.3 Capillary waves move faster than the group wave velocity. v_g=3c/2. A bug on a crest at the front of the wave train would be surprised when waves start appearing in front of the one it is riding as it moves backward in the train. Adapted from (Ananthakrishnan 2005).

List of References

Adam, N. (1937). A Rapid Method for Determining the Lowering of Tension of Exposed Water Surfaces, with some Observations on the Surface Tension of the Sea and of Inland Waters. *Proceedings of the Royal Society of London. Series B, Biological Sciences, 122*(827), 134-139.

Ahrens, C. D. (2007:40). *Meteorology Today: An Introduction to Weather, Climate, and the Environment* Belmont CA, USA: Thompson Brooks/Cole

Alexander, M. (1985). United States Patent No. www.freepatentsonline.com/4512183.html: U. S. Patent.

Alpers, W., & Espedal, H. (Eds.). (2004). *Chapter 11 Oils and Surfactants* Washington, D.C., USA: NOAA/NESDIS; National Oceanic and Atmospheric Administration, Center for Satellite Application and Research.

Alpers, W., & Huhnerfuss, H. (1989). The Damping of Ocean Waves by Surface Films. *Journal of Geophysical Research, 94*(C5), 6251-6265.

Alpers, W., & Hühnerfuss, H. (1988). Radar Signatures of Oil Films Floating on the Sea Surface and the Marangoni Effect. *Journal of Geophysical Research, 93*(C4), 3642-3648.

American Meteorology Society. (2009). Glossary of Meteorology. Retrieved Jan 2009, from http://amsglossary.allenpress.com/glossary/search?id=sensible-heat1

Ananthakrishnan, P. (2005). Suplementary Notes Fall 2005. Unpublished Lecture notes. Florida Atlantic University.

ANCOLD. (2008). Australian Water Statistics *Australian National Committee on Large Dams* Retrieved 2009, from www.ancold.org.au/ www.awa.asn.au/AM/Template.cfm?Section=Water

Andreev, E. G., Gurov, V. V., & Khundzhua, G. G. (1976). *Methods and Implements for registration of a continuous profile of Temperature, Pulsing of components of Flow Velocity and Temperature in the Thin surface Sea Layer*. Paper presented at the 5th Soviet Union Conference on Heat and Mass Exchange, Naukova, Dumka, Kiev, Russia.

AquaArmour. (2010). Product Overview. Retrieved Aug 2010, from http://www.aquaguardiangroup.com/images/stories/product-overview-mar-2010.pdf

Archer, R. J., & La Mer, V. K. (1955). The Rate of Evaporation of Water through Fatty Acid Monolayers. *J. Physical Chemistry, 59*(3), 200.

ASCE (Ed.). (2000). *Guidlines for Instrumentation and Measurements for Monitoring Dam Performance*.

Asheesh, M. (2002). Allocating Gaps of Shared Water Resources (Scarcity Index): Case Study on Palestine-Israel. *Water Resources in the Middle East*, 241-248.

Australian Bureau of Statistics. (2010). Population clock. from http://www.abs.gov.au/ausstats/abs%40.nsf/94713ad445ff1425ca25682000192af2/1647509ef7e25faaca2568a900154b63?OpenDocument

Barger, W., Garrett, W., Mollo-Christensen, E., & Ruggles, K. (1970). Effects of an Artificial Sea Slick upon the Atmosphere and the Ocean. *J. Appl. Meteorol, 9*(3), 396–400.

Barger, W. R., & Garrett, W. D. (1976). *Marking the Sea Surface with Artificial Sea Slicks and Fluorescent Dyes to Aid Search and Rescue or Ocean Dumping Surveillance Operations*. Washington DC.: Naval Research Lab. .

Barnes, G. T., & Feher, A. I. (1980). The Measurement of Temperature Gradients in Water during Evaporation through Monolayer-Free and Monolayer-Covered Surfaces. *J. Colloid Interface Sci., 75*, 584-589.

Barnes, G. T., & Gentle, I. R. (2005). *Interfacial Science*. New York: Oxford University Press.

Barnes, G. T., & Hunter, D. S. (1982). Heat Conduction during the Measurement of the Evaporation Resistances of Monolayers. *Colloid and Interfacial Science, 88*(2), 437 - 443.

Barnes, G. T., & La Mer, V. K. (Eds.). (1962). *The Evaporation Resistances of Monolayers of Long-Chain Acids and Alcohols and their Mixtures*. New York: Academic Press.

Bartholic, J., Runkles, J., & Stenmark, E. (1967). Effects of a Monolayer on Reservoir Temperature and Evaporation. *Water Resour Res, 3*(1), 173-179.

Beard, J., & Wiebelt, J. (1966). Reflectance of Film Covered Water Surfaces as Related to Evaporation Suppression. *Journal of Geophysical Research, 71*, 3835-3838U3831.

Behroozi, F. (2003). United States Patent No. PatentStorm, http://www.patentstorm.us: U. S. Patent.

Behroozi, F., & Behroozi, P. S. (2006). Efficient Deconvolution of Noisy Periodic Interference Signals. *Journal of the Optical Society of America A, 23*(4), 902-905.
Behroozi, P., Cordray, K., Griffin, W., & Behroozi, F. (2007). The Calming Effect of Oil on Water. *American Journal of Physics, 75*(5), 407 - 414.
Birdi, K. S. (1934). *Self-Assembly Monolayer Structures of Lipids and Macromolecules at Interfaces*. New York: Klower Academic/Ptenum Publishers.
Bliss, R. W. (1961). Atmospheric Radiation Near the Surface of the Ground: A Summary for Engineers. *Solar Energy, 5*(3), 103.
Boer, J. H. (1968). *The Dynamical Character of Adsorption* (1st ed.). University of California: Clarendon P. .
Boiten, W. (Ed.). (2000). *Hydrometry*. Brookvfield: A. A. Balklema Publishers VT, USA
BoM. (2009). Average Annual, Monthly and Seasonal Evaporation. *Australian Government Bureau of Meteorology Retrieved 4 Nov 2009 from http://www.bom.gov.au/jsp/ncc/climate_averages/evaporation/index.jsp?period=an*, from http://www.bom.gov.au/jsp/ncc/climate_averages/evaporation/index.jsp?period=an
BoM. (2010). *Australian Government Bureau of Meterology* Retrieved Jan 2010, from http://www.bom.gov.au/sat/glossary.shtml
BOM. (2010). Australia, Climate of our Continent. 2010, from http://www.bom.gov.au/lam/climate/levelthree/ausclim/zones.htm
Bonfillon, A., & Langevin, D. (1993). Viscoelasticity of Monolayers at Oil-Water Interfaces. *Langmuir, 9*(8), 2172-2177.
Boss, & Jumars. (2003). SMS-491: Physical Solutions of Everyday Problems in Aquatic Sciences. Lecture 6: Surface Gravity Waves. from misclab.umeoce.maine.edu/.../Week_6.htm
Botterill, L., & Chapman, B. (2002). *Developing Equitable and Affordable Government Responses to Drought in Australia*.
Bowen, I. S. (1926). The Ratio of Heat Losses by Conduction and Evaporation from any Water Surface. *Physical Review, 27*, 779-787.
Brown, J. (1988). *The Potential for Reducing Open Water Evaporation Losses: A review.* Paper presented at the Hydrology and Water Resources Symposium, ANU Canberra.
Brown, S. (2005). *Gravity, Capillary and Dilational Wave Mode Resonance at a Vsco-Elastic Two-Fluid Interface*. Massachusetts Institute of Technology, Massachusetts
Brutsaert, W. (1982). *Evaporation into the Atmosphere*. Dordrecht, Netherlands Kluwer Academic Publishers Group.
Burington, R. S. (1948). *Handbook of Mathematical Tables and Formulas*: Sandusky, Ohio.
Byrant, E. (Ed.). (1997). *Climate Process and Change*. Cambridge: Cambridge University Press.
Byron, L. (2009). Seepage Through Earth Dams. from http://www.michigan.gov/deq/0,1607,7-135-3313_3684_3723-9536--,00.html
Campbell, J. B. (Ed.). (1996). *Introduction to Remote Sensing* New York: The Guilford Press.
Caseli, L., Masui, D. C., Prazeres, R., Furnel, M., Leone, F. A., Elisabete, M., Zaniquelli, D. . (2005). Adsorption Kinetics and Dilatational Rheological Studies for the Soluble and Anchored Forms of Alkaline Phosphatase at the Air/Water Interface. *Brazilian Chemical Society, 16*(5).
Chang, S. L., McClanahan, M., A., & Kabler, P. W. (Eds.). (1962). *Effect of Bacterial Decomposition of Hexadecanol and Octadecanol in Monolayer Films on the Suppression of Evaporation Loss of Water*. New York: Academic Press Inc.
CityofSydney. (2009). Water Demand. *Retrieved 3 Dec 2009 from http://www.cityofsydney.nsw.gov.au/Environment/Water/CurrentStatus/WaterConservation/WaterDemand.asp*, from Retrieved 3 Dec 2009 from http://www.cityofsydney.nsw.gov.au/Environment/Water/CurrentStatus/WaterConservation/WaterDemand.asp
Clauss, E., Hinzpeter, H., and Mueller-Glewe, J (1970). Messungen zur Temperaturstruktur im Wasser an der Grlnzfliiche Ozean-Atmosphire. *'Meteor' Forsch. Ergebnisse, Reihe B.*, 90-94.
Cleugh, H., Prinsley, R., Bird, P., Brooks, S., Carberry, P., Crawford, M., et al. (2002). The Australian National Windbreaks Program: Overview and Summary of Results. *Australian Journal of Experimental Agriculture, 42*(6), 649-664.
Conover, T. A., & Saylor, J. R. (2006). Infrared Imaging of a Solid Phase Surfactant Monolayer. *Langmuir 22*, 6881-6886.

Craig, I. (2005). *Loss of Storage Water due to Evaporation*. Toowoomba: National Centre for Engineering in Agriculture University of Southern Queensland

Craig, I. (2008). *Loss of Storage Water through Evaporation with Particular Reference to Arid and Semi-arid Zone Pastoralism in Australia*.

Craig, I., Aravinthan, V., Baillie, C., Beswick, A., Barnes, G., Bradbury, R., et al. (2007). Evaporation, Seepage and Water Quality Management in Storage Dams: A Review of Research Methods. *Environmental Health, 7*(3), 84-97.

Craig, I., Green, A., Scobie, M., & Schmidt, E. (2005). *Controlling Evaporation Loss from Water Storages* Toowoomba: USQ.

Cripps, G. (2006). That Dam Seepage *Growcom Water for Profit* Fruit & Vegetable News 25. Retrieved Nov 2009,

, from http://www.growcom.com.au/_uploads/234845WFP_September_06_FV_News.pdf

Crow, F. (1961). Reducing reservoir evaporation. *Agricultural Engineering, 42*(5), 240-243.

Dalton, J. (1802). Experimental essays on the constitution of mixed gases; on the force of steam or vapour from water and other liquids in different temperatures; both in a Torricellian vacuum and in air; on evaporation; and on the expansion of gases by heat. *Memoirs of the Literary and Philosophical Society of Manchester, 5*(11), 535–602.

Daniels, G., & Hover, G. (1994). *The Detection of Oil Slicks at Night with Airborne Infrared Imagers*. Groton CT: Massachusetts Inst of Tech and Lexington Lincoln Lab

Davies, J., & Vose, R. (1965). On the damping of capillary waves by surface films. *Proceedings of the Royal Society of London. Series A, Mathematical and Physical Sciences*, 218-234.

Deaken, E. L., Sheppard, P. A., & Webb, E. K. (1956). Wind Profiles over the Sea, and the Drag at the Sea Surface. *Australian Journal of Physics, 9*, 511.

Deo, A. V., Kulkarni, S. B., Gharpurey, M. K., & Biswas, A. B. (1961). Rate of Spreading and Equilibtirum Spreading Pressure of the Monolayers of n-Fatty Alcohols and n-Alkoxy Ethanols.

Department of the Interior. (1959). *Agencies Report on Lake Hefner, Oklahoma Evaproation Reduction Studies* (No. P.N. 57462-59 8111-4).

DEWHA. (2006). Water consumption per capita. *Retrieved 2 Dec 2009 from http://www.environment.gov.au/soe/2006/publications/drs/indicator/335/index.html*, from http://www.environment.gov.au/soe/2006/publications/drs/indicator/335/index.html

DEWHA. (2010). Market prices for the Murray- Darling Water Basin Water Entitlements. *Water for the Future Policy and Programs* Retrieved Feb 2010, from http://www.environment.gov.au/water/policy-programs/entitlement-purchasing/market-prices.html

Dluhy, R., Ping, Z., Faucher, K., Brockman, J. (1998). Infrared Spectroscopy of Aqueous Biophysical Monolayers. *Thin Solid Films* (327-329), 308-314.

Donlon, C. J., Minnett, P. J., Barton, I. J., Nightingale, T. J., & Gentemann, C. (2002). *The Character of Skin and Subsurface Sea Surface Temperature*: EC- JRC Space Application Institute, Aspra (VA) Italy. Meteorology and Physical Oceanograph Division RSMAS Univeristy of Miami FL. USA. CSIRO Marine Research, Hobart, Australia. Space Science and Technology Department, Rutherford Appleton Laboratory, Chilton UK. Remote Sensing Systems CA USA.

Dorn, V. (1953). Wind Stress on an Artificial pond. *Marine Research, 12*.

Dysthe, D., Rovner, G., Rabin, Y. (1986). Damping of Capillary Waves by Polymeric Monolayers. Comparison with Hydrodynamic Theory. *Physical Chemistry, 90*, 3894-3895.

Eagleman, J. (1967). Pan Evaporation, Potential and Actual Evapotranspiration. *Journal of Applied Meteorology, 6*(3 June), 482-488.

Eagleton, L. C. (1965). *Saline Water Conversion Report for 1965*.

Earnshaw, J., & Hughes, C. (1991). High-frequency capillary waves on the clean surface of water. *Langmuir, 7*(11), 2419-2421.

EEMRU. (2009). Environment and Energy Resources Unit *Retrieved 12 Dec 2009 from http://environ.chemeng.ntua.gr/WSM/Newsletters/Issue4/Indicators_Appendix.htm#Falkenmark*, 2009, from http://environ.chemeng.ntua.gr/WSM/Newsletters/Issue4/Indicators_Appendix.htm#Falkenmark

Einstein, A. (1916). Elementare Theorie der Wasserwellen and des Fluges. *Naturwissenschaften, 4*, 509.

Emery, W., Castro, S., Wick, G., Schluessel, P., & Donlon, C. (2001). Estimating Sea Surface Temperature from Infrared Satellite and In Situ Temperature Data. *Bulletin of the American Meteorological Society, 82*(12), 2773-2785.

Engineering Toolbox. (2005). Relative Humidity of Air. Retrieved Oct 2008, from http://images.google.com.au/imgres?imgurl=http://www.engineeringtoolbox.com/docs/documents/687/saturation-vapor-pressure-diagram.png&imgrefurl=http://www.engineeringtoolbox.com/relative-humidity-air-d_687.html&usg=__jMF50PlsMHkYOqWnjb3a8ISJx-U=&h=418&w=444&sz=12&hl=en&start=2&tbnid=Zw0ZdDoeWjIfVM:&tbnh=120&tbnw=127&prev=/images%3Fq%3Dsaturated%2Bvapour%2Bpressure%26gbv%3D2%26ndsp%3D18%26hl%3Den%26sa%3DN

Engineering Toolbox. (2010). Thermal Conductivity of Some Common Materials. Retrieved Mar 2010, from http://www.engineeringtoolbox.com/thermal-conductivity-d_429.html

Erbil, Y. (Ed.). (2006). *Surface Chemistry of Solid and Liquid Interfaces*. Oxford UK: Blackwell Publishing www.blackwellpublishing.com

Eugster, W., McFadden, J., & Chapin, F. (1997). A Comparative Approach to Regional Variation in Surface Fluxes using Mobile Eddy Correlation Towers. *Boundary-layer meteorology, 85*(2), 293-307.

Ewing, G., & McAlister, E. D. (1960). On the Thermal Boundary Layer of the Ocean. *Science 131*(3410), 1374 - 1376.

Fairall, C. W., Bradley, E. F., Edson, J. B., & Young, G. S. (1996). Bulk parametrization of air-sea fluxes for tropical global atmosphere coupled-ocean atmosphere response experiment. . *J. Geophys. Res*(101), 3747-3764.

FAO. (2007). Coping with Water Scarcity- Challenge of the Twenty-First Century. *Retrieved 11Jan 2009 from http://www.fao.org/nr/water/docs/escarcity.pdf*, from http://www.fao.org/nr/water/docs/escarcity.pdf

Filippov, A. T. (2000). *The Versatile Soliton*. Boston: Birhauser, Hamilton Printing Company.

Fingas, M. F., & Brown, C. E. (2000). *Review of Oil Spill Remote Sensing.* Paper presented at the Seventh International Conference of Remote Sensing, Ottawa, Ontario, Canada.

Fingas, M. F., Brown, C. E. (Ed.). (2007). *Oil spill environmental forensics: fingerprinting and source identification*. San Diego, California: Academic Press, Elsevier.

Fitzgerald, L. (1963). Wind Induced Stresses on Water Surfaces: A Wind Tunnel Study. *Australian Journ. Phys, 16*(4), 475.

Fitzgerald, L., & Vines, R. (1963). Retardation of Evaporation by Monolayers: Practical Aspects of the Treatment of Large Water Storages. *Australian Journal of Applied Science, 14*, 340-346.

Fitzgerald, L. M. (1964). The Effect of Water Damping on the Surface Velocity of Water in a Wind Tunnel. *Australian Journal of Physics, 17*, 184-188.

Foulds, E., & Dressler, R. (1968). Performance of Monolayer Blends of Odd and Even Carbon Chain Alcohols in Water Evaporation Suppression. *Industrial & Engineering Chemistry Product Research and Development, 7*(1), 75-79.

Francis, J. (1954). Wind stress on a water surface. *Quarterly Journal of the Royal Meteorological Society, 80*(345), 438-443.

Frenkiel, J. (1965). *Evaporation Reduction. Physical and Chemical Principles and a Revew of Experiments. Water planning for Israel, Tel Aviv and New York*

Fritschen, L. J. (1965). Accuracy of Evapotranspiration Determinations by the Bowen Ratio Method. *Hydrological Sciences Journal, 10*(2), 38-48.

Gabler, R., Petersen, J., & Trapasso, M. (Eds.). (2007). *Essentials of Physical Geography* Belmont CA USA: Thomson Higher Education.

Gade, M. (2002). *Measurements at the Edges of Molecular Slicks*. Hamburg: University of Hamburg. Hamburg Institute of Oceanography.

Gade, M. (2005). Molecular Surface Films - Wave Damping and Radar Backscattering. *Research in the Lab* Retrieved Mar 2010, from http://www.ifm.zmaw.de/forschung/fernerkundung/laborexperimente/monomolecular-surface-films/?no_cache=1&sword_list%5B%5D=backscattering

Gade, M., Alpers, W., Huhnerfuss, H., & Lange, P. (1998). Wind Wave Tank Measurements of Wave Damping and Radar Cross Sections in the Presence of Monomolecular Surface Films. *Journal of Geophysical Research, 103*, 3167-3178.

Gade, M., Alpers, W., Huhnerfuss, H., Masuko, H., & Kobayashi, T. (1998). *Imaging of Biogenic and Anthropogenic Ocean Surface Films by the Multifrequency Multipolarization SIR-C/X-SAR*: J. Geophys. Res.

Gainer, J. L., Beard, J. T., & Thomas, R. R. (1969). *Water Evaporation Suppression*. Blacksburg, Virginia: Water Resources Research Center, Virginia Polytechnic Institute.
Garrett, W. (1965). Collection of slick-forming materials from the sea surface. *Limnology and Oceanography, 10*(4), 602-605.
Garrett, W. (1971). Retardation of Water Drop Evaporation with Monomolecular Surface Films. *Journal of Atmospheric Sciences, 28*, 816-819.
Garrett, W. D., & Barger, W. R. (1970). Factors Affecting the Use of Monomolecular Surface Films to Control Oil Pollution on Water. *Environmental Science & Technology, 4*(2), 123-127.
Garrett, W. D., & Zisman, W. A. (1970). Damping of Capillary Waves on Water by Monomolecular Films of Linear Polyorganosiloxanes. *The Journal of Physical Chemistry, 74*(8), 1796-1805.
Gates, D. (1980:268). *Biophysical Ecology*. New York: Springer - Verlag.
GDH Hassall. (2010). Murray Darling Basin Water Entittlements - Summary of Market Prices for Approved Transfers. *Market prices for Murray Darling Water Entitlements* from http://www.environment.gov.au/water/policy-programs/entitlement-purchasing/pubs/market-prices-mar10.pdf
Gentemann, C. L., & Minnett, P. J. (2008). Radiometric Measurements of Ocean Surface Thermal Variability. *Journal of Geophysical Research, 113*(C08017).
Gericke, A., Simon-Kutscher, J., & Hühnerfuss, H. (1993). Influence of the Spreading Solvent on the Properties of Monolayers at the Air Water Interface. *Langmuir, 9*, 3115-3321.
Ghumman, M. A. (1971). *Study of Emulsions, Their Production and Industrial Uses; Chapter 2 "To check the evaporation of Water"* University Of The Punjab, Lahore, Pakistan.
Gladyshev, M., & Sushchik, N. (1994). The effect of the monomolecular layer of fatty acid on the temperature of surface water film. *Atmospheric and Oceanic Physics, 30*(1).
Gladyshev, M. I. (1988). Investigations of the Water Surface Film Temperature in a Laboratory Vessel of Small Volume. *Vodnyie Resursy*(4), 69-73.
Gladyshev, M. I. (2002). *Biophysics of the Surface Microlayer of Aquatic Ecosystems*. London: IWA Publishing, Alliance House.
Goldacre, R. J. (1949). Surface Films on Natural Bodies of Water. *Journal of Animal Ecology, 18*(1), 36-39.
Goodrich, F. C. (1962). On the Damping of Water Waves by Monomolecular Films. *The Journal of Physical Chemistry, 66*(10), 1858-1863.
Gottifredi, J., & Jameson, G. (1968). The Suppression of Wind-Generated Waves by a Surface Film. *Journal of Fluid Mechanics 32*(03), 609-618.
Gottifredi, J., & Jameson, G. (2006). The suppression of wind-generated waves by a surface film. *Journal of Fluid Mechanics, 32*(03), 609-618.
Grassl, H. (1976). The Dependence of the Measured Cool Skin of the Ocean on Wind Stress and Total Heat Flux *Bound-Layer Meteor. , 10*, 465-474.
Grossman, R. L., Bean., B. R., & Marlatt, W. E. (1969). Airborne Infrared Radiometer Investigation of Water Surface Temperature With and Without an Evaporation- Retarding Monomolecular Layer,. *Geophys. Res, 74*, 2471.
Grundy, F. (Ed.). (1962). *Some Problems of Maintaing as Monolmolecular Film on Reservoirs Affected by Winds*. New York: Academic Press.
Gugliotti, M., Rodrigues, T.S., Baptista, M. Sl., Politi, M. J. (2004). Large Increase in the Heat Transfer through Monolayers Detected by Beam Deflection. *Langmuir* (20), 5648-5650.
Gurney, R. J., Foster, J. L., & Parkinson, C. L. (1993). *Atlas of Satellite Observations related to Global Change*. London, Great Britain Cambridge University Press
Hale, M., & Mitchell, J. (1997). Sea surface microlayer and bacterioneuston spreading dynamics. *Marine ecology progress series. Oldendorf, 147*(1), 269-276.
Ham, J. (2001). *Measuring Seepage losses from Waste Treatment Lagoons:* : Kansas Water Resources Research Institute Annual Technical Report: A simplified water balance approach for use by Government Agencies, Consultants and Industry.
Hancock, N., Symes, T. (2009). *EvapCalc – A Modest-Cost Technique for Real-Time Measurement of Evaporaiton (and Seepage) from Farm Dams* Paper presented at the IWER2009 International Workshop on Evaporation from Reservoirs.
Handler, R. A., Smith, G. B., & Leighton, R. I. (2000). *The Thermal Structure of an Air- Water Interface at Low Wind Speeds*: Naval Research Laboratory, Remote Sensing Division, Washington DC USA.
Harkins, W. (1952). *The physical chemistry of surface films*: Reinhold.

Hasse, L. (1971). The Sea Surface Temperature Deviation and the Heat Flow at the Sea-Air Interface. *Boundary-Layer Meteorology, 1*(3), 368-379.
Heavens, O. S. (1955). *Optical Properties of Thin Solid Films*. London, England: General Publishing Company, Canada. Originally published by Butterworths Scientific Publications London.
Heikkila, R., Kwong, C., & Cornwell, D. (1970). Stability of Fatty Acid Monolayers and the Relationship between Equilibrium Spreading Pressure, Phase Transformations, and Polymorphic Crystal Forms. *The Journal of Lipid Research, 11*(3), 190.
Helfer, F., Zhang, H., & Lemckert, C. (2009). *Evaporation Reduction by Windbreaks: Overview, Modelling and Efficiency*. City East Qld.: Griffith University.
Hengstermann, T., & Reuter, R. (1990). Lidar fluorosensing of mineral oil spills on the sea surface. *Applied Optics, 29*(22), 3218-3227.
Herzig, M. (2007). Isotherms. University of Queensland.
Holsoft's Physics Resources Pages. (2001). Online Calculators. *Holsoft Educational Software and Utilities* from http://physics.holsoft.nl/physics/ocmain.htm
Hühnerfuss, H. (2006). Basic Physicochemical Principles of Monomolecular Sea Slicks and Crude Oil Spills. *Marine Surface Films*, 21-35.
Hühnerfuss, H., Alpers, W., Lange, P., & Walter, W. (1981). Attenuation of Wind Waves by Artificial Surface Films of Different Chemical Structure. *Geophysical Research Letters, 8*(11), 1184-1186.
Hühnerfuss, H., Walter, W., & Kruspe, G. (1977). On the Variability of Surface Tension with Mean Wind Speed. *Journal of Physical Oceanography, 7*(4), 567-571.
IFAS. (2009). Centre for Aquatic and Invasive Plants. Institute of Food and Agricultural Sciences. University of Florida from http://plants.ifas.ufl.edu/
International Commision on Illumination. (2010). CIE Central Bureau,. from http://www.cie.co.at/index.php/Publications
Ivanov, A., He, M., & Fang, M. (2002). Oil Spill Detection with the RADARSAT SAR in the Waters of the Yellow and East China Sea: A case study. from www.gisdevelopment.net/aars/acrs/2002/sar/011.pdf
Jarvis, N. (1962). The effect of monomolecular films on surface temperature and convective motion at the water/air interface. *Journal of Colloid Science, 17*(6), 512-522.
Jarvis, N., Garrett, W., Scheiman, M., & Timmons, C. (1967). Surface chemical characterization of surface-active material in seawater. *Limnology and Oceanography, 12*(1), 88-96.
Jarvis, N. L. (1962). *The Effects of Monomolecular Films on the Surface Temperature and Convection Motion at the Water/Air Interface*. Washington D.C.: U.S. Naval Research Laboratory.
Jarvis, N. L., Timmons, C. O., & Zisman, W. A. (1962). *The Effect of Monomolecular Films on the Surface Temperature of Water*. New York: Academic Press.
Jeffreys, H. (1925). On the formation of water waves by wind. *Proceedings of the Royal Society of London. Series A, Containing Papers of a Mathematical and Physical Character, 107*(742), 189-206.
Jennison, I. (2003). *Methods for Reducing Evapoation from Storages used from Urban Water Supplies- Final Report from GHD*. Brisbane Qld. : Department of natural resources and mines.
Jiles, D. (2001). *Introduction to the Electronic Properties of Materials* Neil Thornes Ltd. Cheltenham UK.
Jones, F. E. (1992). *Evaporation of Water with Emphasis on Applications and Measurements*. Michigan USA. : Lewis Publishers.
Kaiser, R. (1972). 3635819: United States Patent Office.
Karantzalos, K., & Argialas, D. (2008). Automatic Detection and Tracking of Oil Spills in SAR Imagery with Level Set Segmentation. *International Journal of Remote Sensing, 29*(21), 6281-6296.
Karantzalos, K., & Argialas, D. (2008N). Automatic detection and tracking of oil spills in SAR imagery with level set segmentation. *International Journal of Remote Sensing, 29*(21), 6281-6296.
Karman, V. (1930). Mechanical Simitude and Turbulence. *Nachrichten von der Gesellschaft der Wissenschaften zu Gottingen. Translated by National Advisory Committee for Aeronautics* Retrieved May 2010, Technical Memorandum No 611, from http://ntrs.nasa.gov/archive/nasa/casi.ntrs.nasa.gov/19930094805_1993094805.pdf
Katsaros, K. B. (1980). The Aqueous Thermal Boundary Layer. *Boundary-Layer Meteorology* (18), 107-127.
Katsaros, K. B., Garrett, W.D. . (1982). Effects of Organic Surface Films on Evaporation and Thermal Structure of Water in Free and Forced Convection *Int. J. Heat Mass Trans, 25*, 1661-1670.

Katsaros, K. B., Liu, W. T., Businger, J. A., & Tillman, J. A. (1977). Heat Transport and Thermal Structure in the Interfacial Boundary Layer Measured in an Open Tank of Water in Turbulent Free Convection. *Fluid Mechanics, 83*, 311-335.

Kaye, G. W. C., & Laby, T. H. (1973). *Tables of Physics and Chemical Constants and Some Mathematical Functions*. New York: Longman.

Kenyan, K. E. (1983). On the Depth of Wave Influence,. *Journel of Physical Oceanography, 13*.

Kenyon, K. E. (1998). Capillary Waves Understood by an Elementary Method. *Journal of Oceanography, 54*, 343-346.

Keulegan, G. H. (1951). Wind Tides in Small. Closed Channels. *Journal of Research of the National Bureau of Standards, 46*, 358-381.

Kolevzon, V. (1999). Dilational viscosity of Langmuir monolayers. *Physica A: Statistical Mechanics and its Applications, 271*(1-2), 1-8.

Konda, M., Imasato, N., Nishi, K., & Toda, T. (1994). Measurement of the Sea Surface Emissivity. *Journal of Oceanography, 50*(1), 17-30.

Korenowski, G., Saylor, J., Wagenen, E., Kelley, J., Anderson, M., & Edwards, E. (2006). Imaging surfactant concentration distributions at the air/water interface. *Marine Surface Films*, 165-173.

Krause, F., & Lange, W. (1965). Aqueous Solubilities of n-Dodecanol, n-Hexadecanol, and n-Octadecanol by a New Method. *The Journal of Physical Chemistry, 69*(9), 3171-3173.

KSV. (2009). Surface and Interfacial tension., 2009, from http://www.ksvinc.com/LB.htm#isotherms

Kurzeja, R. J., & Pendergast, M. M. (2002). *Comparison of MTI Water Temperatures with Ground Truth Measurements at Lake Crater, OR* (No. WSRC-TR-2002-00415): US Department of Energy, NTIS, Westinghouse Savannah River Co., SMP Enterprises.

La Mer, V., Healy, T., & Aylmore, L. (1964). The Transport of Water Through Monolayers of Long-Chain n-Paraffinic Alcohols. *Journal of Colloid Science, 19*(8), 673-684.

La Mer, V., & Robbins, M. (1958). The Effect of the Spreading Solvent on the Properties of Monolayers. *The Journal of Physical Chemistry, 62*(10), 1291-1295.

La Mer, V. K. (1962). *Retardation of Evaporation by Monolayers pg 19*

La Mer, V. K., & Aylmore, L. A. (1961). *Evaporation Resistance as a Sensitive Measure of the Purity and Molecular structure of Monolayers* Paper presented at the Proceedings National. Academy of Sceince Columbia University.

La Mer, V. K., & Barnes, G. T. (1959). *The Effects of Spreading Technique and Purity of Sample on the Evaporation Resistance of Monolayers.* Paper presented at the National Academy of Sciences of the United States of America.

La Mer, V. K., & Healey, T. W. (1965). Evaporation of Water: Its Retardation by Monolayers. *Science, New Series, American Association for the Advancement of Science, 148*(3666), 36-42.

Lai, R. (1977). Evaporation from a Warm, Wavy Surface: A Laboratory Study. *Journal of Physical Oceanography, 7*(3).

Lamb, H. (1906). *Hydrodynamics* (3rd ed.). London: Cambridge University Press.

Lamb, H. (1932). *Hydrodynamics* (Sixth ed.). London: Cambridge University Press.

Langmuir, I., and Schaefer, V. (1943). Rates of evaporation of water through compressed monolayers on water. *J. Franklin Inst, 235*(119).

Langmuir, I., & Langmuir, D. B. (1927). The effect of Monomolecular Films on the Evaporation of Ether Solutions. *The Journal of Physical Chemistry 31* (11), 1719-1733.

Langmuir, I., & Schaefer, V. (1939). Properties and Structure of Protein Monolayers. *Chemical Reviews, 24*(2), 181-202.

Langmuir, I., & Schaefer, V. (1943). *Franklin Inst, 235*, 119.

Lapham, G. S., Dowling, D. R., & Schultz, W. W. (2001). Linear and Nonlinear Gravity-Capillary Water Waves with a Soluble Surfactant. *Experiments in Fluids, 30*(4), 448-457.

Lawrence, P., Meigh, J., & Sullivan, C. (2002). The Water Poverty Index: An International Comparison. . *Keele International Research Papers. Retrieved 19 Aug 09 from http://www.keele.ac.uk/depts/ec/wpapers/kerp0219.pdf*, from http://www.keele.ac.uk/depts/ec/wpapers/kerp0219.pdf

Lighthill, J. (2005). *Waves in Fluids*. Cambridge UK: Cambridge University Press.

Linacre, E. (1997). Penman's Equation for Lake Evaporation. from http://www-das.uwyo.edu/~geerts/cwx/notes/chap04/penman.html

Lösche, M. (2008). Intensity of Fluorescent Activity (Professor of Physics ed.). Pittsburgh, PA: Carnegie Mellon University.
Lucassen, J. (1968). Longitudinal capillary waves. Part 1.—Theory. *Transactions of the Faraday Society, 64*, 2221-2229.
Lucassen, J. (1968). Longitudinal capillary waves. Part 2.—Experimental. *Transactions of the Faraday Society, 64*, 2230-2235.
MacRitchie, F. (1969). Evaporation Retarded by Monolayers. *Science 163*, 929-931.
Makin, V., & Kudryavtsev, V. (2002). Impact of Dominant Waves on Sea Drag. *Boundary-Layer Meteorology, 103*(1), 83-99.
Mangarella, P., Chambers, A., Street, R., & Hsu, E. (1973). Laboratory Studies of Evaporation and Energy Transfer Through a Wavy Air-Water Interface. *Physical Oceanography* (3), 93-101.
Mansfield, W. (1959). The Influence of Monolayers on Evaporation from Water Storages. III. The Action of Wind, Wave, and Dust Upon Monolayers. *Austral. J. Appl. Sci, 10*, 73.
Mansfield, W. (Ed.). (1962). *Aspects of Evaporation Control*. New York: Academic Press.
Marlatt, W. E., & Grossman, R. L. (1968). *An Investigation of Water Surface Temperature by an Airborne Infrared Radiometer: Lake Hefner. Technical Paper No. 119*. Oklahoma: Department of Atmospheric Science. Colorado State University.
Marple, D. T. F., & Vanderslice, V. A. (1960). Reflectivity of Fatty Acid Monolayers on Water. *J. Phys. Chem, 64*, 1231–1234.
Massel, S. R. (1996). *Ocean surface waves: their physics and prediction* (Vol. 11). Hackensack NJ USA: World Scientific Publishing.
McAlister, E. D., & McLeish, W. (1969). Het Transfer in the Top Millimeter of the Ocean. *Journal of Geophysical Research, 74* (13), 3408-3414.
McAlister, E. D., & McLeish, W. (1970). A Radiometric System for Airborne Measurement of the Total Heat Flow from the Sea. *Applied Optics, 9* (12), 2697-2705.
McArthur, I. K. H. (1962). Cetyl Alcohol Monolayers for Water Conservation: Methods of Application and the Influence of Wind. Australia: CSIRO
McJannet, D., Cook, F., Knight, J., & Burn, S. (2008). Evaporation Reduction by Monolayers: Overview, Modelling and Effectiveness: CSIRO: Water for a Healthy Country National Research Flagship.
McKenna, S., & Bock, E. (2006). Physicochemical effects of the marine microlayer on air-sea gas transport. *Marine Surface Films*, 77-91.
McKeown, W., Bretherton, F., Huang, H. L., Smith, W. L., & Revercomb, H. L. (1995). Sounding the Skin of Water: Sensing Air-Water Interface Temperature Gradients with Interferometry *Journal of Atmospheric and Oceanic Technology, 12*, 1313-1327.
McMahon, C., Craig, I., Turnbull, D., Schmidt, E., & Hancock, N. (2008). Laboratory Study of Wind Stress on Surface Film Materials, 2007-2008. National Centre for Engineering in Agriculture, Publication 1002040/2, USQ
Mendelson, R., Brauner, R. W., & Gericke, A. (1995). External Infrared Reflection Absorption Spectrometry of Monolayer Films at the Air Water Interface. *Physical Chemistry, 46*, 305-334.
Miller, R. (2003). *Applications and Advantages of the Capillary Waves Method*. Germany: Max Planck Institute of Colloids and Interfaces.
Mobasheri, M. R. (2006). Reformation Time for the Thermal Skin Layer of the Ocean. *International Journal of Remote Sensing, 27*(23 December), 5285-5299. Retrieved from http://www.informaworld.com/smpp/title~content=t713722504. doi:10.1080/01431160600836026
Nave, N. (2009). Relative Humidity. *Hyperphysics*, from http://hyperphysics.phy-astr.gsu.edu/hbase/hframe.html
Nave, N. (2009). Thin films. *Hyperphysics*, from http://hyperphysics.phy-astr.gsu.edu/hbase/phyopt/thinfilm.html
Navon, U., & Fenn, J. B. (1971). Effect of Monomolecular Films on Natural Convection in Water. *AIChE Journal. American Institute of Chemical Engineers, 17*(1), 137-140.
NCEA. (2010). Ready Reckoner - Economic Ready Reckoner. Evaporation Mitigation Systems. *National Centre for Engineering in Agriculture* Retrieved Feb 2010, from http://www.readyreckoner.ncea.biz/#
Netprocanopies. (2010). Netprocanopies. from www.netprocanopies.com
Nima Technology. (2009). Langmuir and Langmuir-Blodgett Deposition from http://www.nima.co.uk/langmuir-and-langmuir-blodgett-troughs#ProductRange

Noe, E. R., & Dressler, R. G. (1967). Performance of Edd-and Even-Chain Pure Alcohol Monolayers in Water Evaporation Retardation. . *l & E C Product Research and Development, 6*(2), 132-136.
Nova Scotian Institute of Science. (1956). *Proceedings of the Nova Scotian Institute of Science* (Vol. 24-26). Halifax.
Novus Automation Inc. (2008). .Humidity and Temperature. from http://www.novusautomation.com
NPSI. (2005/4 April). Controlling Evaporation Losses from Farm Dams. *Factsheet*
Nutting, G., & Harkins, W. (1939). Pressure--Area Relations of Fatty Acid and Alcohol Monolayers. *Journal of the American Chemical Society, 61*(5), 1180-1187.
NWC. (2008). Water use in Australia. Retrieved July 2008, from http://www.nwc.gov.au/www/html/236-water-use-in-australia.asp
O'Brien, R., Feher, A., Li, K., & Tan, W. (1976). The Effect of Monolayers on the Rate of Evaporation of H_2O and Solution of O_2 in H_2O. *Canadian Journal of Chemistry, 54*(17), 2739-2744.
O'brien, R. N. (1998). United States Patent No. www.freepatentsonline.com: U. S. Patent.
O'Neil, R. A., Neville, R.A. and Thompson, V. . (1983). *The Arctic Marine Oilspill Program (AMOP) Remote Sensing Study*. Ottawa, Ontario, .
Oertel, H., Prandtl, L. (2004). *Prandtl's Essentials of Fluid Mechanics*. New York: Springer-Verlag Inc.
Ohmura, A. (1982). Objective Criteria for Rejecting Data for Bowen Ratio Flux Calculations. *Journal of Applied Meteorology, 21*, 595-598.
Oxford Reference Online. (2009). "evaporation". *A Dictionary of Physics* Retrieved 1 June 2010 from <http://www.oxfordreference.com/views/ENTRY.html?subview=Main&entry=t83.e1035>
Penman, H. L. (1948). Natural Evaporation from Open Water, Bare Soil and Grass. *Proc. Roy. Soc A,, 193,*, 120-145.
Penny, G. W. (1945). Heat Transfer. *Scientific American 248*(Feb), 101-105.
Perez, E., & Wolfe, J. (1994). A Simple, Cheap, Clean, Reliable, Linear, Sensitive, Low-Drift Transducer for Surface Pressure. *Langmuir, 10*(3), 974-975.
Phaovattana, V., Daigo, K. (1995). *Study on Evporation Control for Water Conservation Measures by Floating Cover Method*. Thailand.
Pigeat, P., Rouxel, D., & Weber, B. (1998). Calculation of Thermal Emissivity for Thin Films by a Direct Method. *Physical Review B, 57*(15), 9293-9300.
Pogorzelski, S., & Kogut, A. (2001). Static and dynamic properties of surfactant films on natural waters. *Oceanologia, 43*(2), 223-246.
Ramey, V. (2004). Plant management in Florida waters from http://plants.ifas.ufl.edu/guide/evaptran.html
Rasmusson, E., & Carpenter, T. (1982). Variations in Tropical Sea Surface Temperature and Surface Wind Fields Associated with the Southern Oscillation/El Niño. *Monthly Weather Review, 110*(5), 354-384.
Rayleigh. (1847). *On the theory of Oscillatory Wave*.
Recreation, A. G. C. a. (2010). Australian Weather and the Seasons. Retrieved 2010, from http://www.cultureandrecreation.gov.au/articles/weather/
Reddi, L. N. (2003). *Seepage in soils: principles and applications* Holeboken, New Jersey, USA: John Wiley & Sons.
Rideal, E. K. (1924). On the Influence of Surface Films on the Evaporation of Water. *Journal of Physical Chemistry, 38*, 1244.
Robinson, L. C. (1973:91). *Physical Principles of Far-Infrared Radiation* (Vol. 10). New York USA: Academic Press
Robinson, P., & Davies, J. (1972). Laboratory Determinations of Water Surface Emissivity. *Journal of Applied Meteorology, 11*(8), 1391-1393.
Rosano, H., & Mer, V. (1956). The Rate of Evaporation of Water through Monolayers of Esters, Acids and Alcohols. *The Journal of Physical Chemistry, 60*(3), 348-353.
Ruggles, K. W. (1970). The Vertical Mean Wind Profile Over the Ocean for Light to Moderate Winds *Journal of Applied Meteorology, 9*, 389-395.
Rus, B. (2003). Comparative Study of Monolayer Fatty Acids at the Air/Water Interface. *Leonardo Electronic Journal of Practices and Technologies, 3*, 111-117.
Salisbury, J., & D'Aria, D. (1994). Emissivity of Terrestrial Materials in the 3-5 μm Atmospheric Window. *Remote Sensing of Environment, 47*(3), 345-361.
Saunders, P. M. (1967). The Temperature at the Ocean Air Interface *Atmospheric Science, 24*, 269-273.

Saylor, J. R., Flack, K. A., Schultz, M. P., Smith, G. B. (2002). The Correlation Between Surface Temperature and Subsurface Velocity during Evaporative Convection. *Experiments in Fluids Springer-Verlag*
(32), 570-579.
Saylor, J. R., Smith, G. B., & Flack, K. A. (2000). The Effect of a Surfactant Monolayer on the Temperature Field of a Water Surface Undergoing Evaporation. *International Journal of Heat and Mass Transfer 43*, 3073-3086.
Saylor, J. R., Smith, G. B., & Flack, K. A. (2000). Infrared Imaging of the Surface Temperature Field of Water During Film Spreading. *Physics of Fluids, 12*(3), 597-602.
Saylor, J. R., Smith, G. B., & Flack, K. A. (2001). An Experimental Investigation of the Surface Temperature Field During Evaporative Convection. *Physics of Fluids, 2*(13), 428-439.
Schooley, A. (1971). Diffusion Sublayer Thickness Over Wind-Disturbed Water Surfaces. *Journal of Physical Oceanography, 1*(3), 221-223.
Schulman, J., & Teorell, T. (1938). On the Boundary Layer at Membrane and Monolayer Interfaces. *Transactions of the Faraday Society, 34*, 1337-1342.
Sebba, P., & Briscoe, H. V. A. (1940). The Evaporation of Water Through Unimolecular Films. *Chem. Soc. London*, 106-114.
Segal, L., & Burstein, L. (2010). Retardation of Water Evaporation by a Protective Float. *Water resources management, 24*(1), 129-137.
Segelstein, D. (1981, Aug 2009). Refractive index as a function of wavelength. *Master of Science Thesis* Retrieved Sep 2009, from http://www.philiplaven.com/p20.html; http://www.philiplaven.com/Segelstein.txt
Shih, W., & Andrews, A. (2008). *Modeling of Thickness Dependent Thermal Contrast of Native and Crude Oil Covered Water Surfaces.* Paper presented at the Geoscience and Remote Sensing Symposium.
Sigma Aldrich. (2008). 2009, from http://www.sigmaaldrich.com
SILO. (2010). Chapter 4 - Determination of ETo. *Crop evapotranspiration - Guidelines for computing crop water requirements - FAO Irrigation and drainage paper 56* Retrieved Aug 2010, from http://www.longpaddock.qld.gov.au/silo/evap/index.html
Singh, V., & Xu, C. (1997). Evaluation and Ggeneralization of 13 Mass-Transfer Equations for Determining Free Water Evaporation. *Hydrological Processes, 11*(3), 311-323.
Sinnamon, B. F., Dluhy, R.A, Barnes, G.T. (1999). Reflection-Absorption FT-IR Spectroscopy of Pentadeconoic acid at the Air/Water Interface. *Colloids and Surfaces, 146*, 49-61.
Skidmore, E., & Hagen, L. (1970). Evaporation in Sheltered Areas as Influenced by Windbreak Porosity. *Agricultural Meteorology, 7*, 363-374.
Smith, C. C., Lof, G., Jones, R. . (1994). Measurement and Analysis of Evaporation from an Inactive Outdoor Swimming Pool. *Solar energy, 53*(1), 3-7.
Smith, J. W. (1909). Recent Evaporation Investigations. *The Ohio Naturalist, The Biological Club of the Ohio University, 9*(3).
Smith, W., Rao, P., Koffler, R., & Curtis, W. (1970). The Determination of Sea-Surface Temperature from Satellite High Resolution Infrared Window Radiation Measurements. *Monthly Weather Review, 98*, 604-611.
Solcomhouse. (2009). Exxon Valdez Oil Spill. 2009, from http://www.solcomhouse.com/valdez.htm
Somasundaran, P. (2006). *Encyclopedia of Surface and Colloid Science* (Vol. Volume 5, pp. 3243).
Spaulding, M. (Ed.). (1999). *Drift Currrent Under the Action of Wind and Waves*. New York: Oxford Univeristy Press. The Institute of Mathematics and its Applications
Spillane, K., & Hess, G. (1978). Wind-Induced Drift in Contained Bodies of Water. *Journal of Physical Oceanography, 8*(5), 930-935.
Steinhart, J. S. a. S. R. H., S. R. . (1968). Calibration Curves for Thermistors. *Deep Sea Res*(15), 497-503.
Strub, P., & Powell, T. (1987). Surface temperature and transport in Lake Tahoe: inferences from satellite (AVHRR) imagery. *Continental Shelf Research, 7*(9), 1001-1013.
Suarez, M., Emery, W., & Wick, G. (1997). The Multi-Channel Infrared Sea Truth Radiometric Calibrator (MISTRC). *Journal of Atmospheric and Oceanic Technology, 14*(2), 243-253.
Taft, D., Egging, D., & Kuhn, H. (1995). Sheen Surveillance: An Environmental Monitoring Program Subsequent to the 1989 Exxon Valdez Shoreline Cleanup. *Exxon Valdez oil spill: fate and effects in Alaskan waters*, 215-238.

Tailby, S., & Portalski, S. (1961). The Optimum Concentration of Surface Active Agents for the Suppression of Ripples. *Chemical Engineering Research and Design, 39*(a), 328-336.
Takashi, A., & Kunio, W. (1989). The Mechanism of Heat Transport in Thermal Convection at High Rayleigh Numbers. *Physics of Fluids A: Fluid Dynamics, 1*(5), 861-867.
Takeda, A. (1963). Wind Pofiles Over Sea Waves *The Journal of the Oceanographical Society of Japan, 19*(3), 137-142.
Tanny, J., Cohen, S., Assouline, S., Lange, F., Grava, A., Berger, D., et al. (2008). Evaporation From a Small Water Reservoir: Direct Measurements and Estimates. *Hydrology*(351), 218- 229.
The Centre For Water Research. (2006). DYRESM. from http://www.cwr.uwa.edu.au/software1/models1.php?mdid=2
Tiblin, L. O., Florey, Q. L., & Garstka, W. U. (1962). Laboratory and Field Reservoir Evaporation Eduction Investigations Being Performed by the Bureau of Reclamation. In V. La Mer (Ed.), *Retardation of Evaporation by Monolayers: Transport processes*. New York: Academic Press.
Troy, D. (2006). *Remington: The Science and Practice of Pharmacy* (21st ed.). Maryland, USA: Lippincot Williams & Wilkins.
Ultimate Products (Aust) Pty Ltd. (2009). Liquid anti-evaporation film. 2009, from www.aquatain.com.au
Valenzuela, G. (1978). Theories for the Interaction of Electromagnetic and Ocean Waves- A review *Boundary-Layer Meteorology, 13*(1-4), 61-85.
Van Dijk, A. (2003). De principles of surface flux physics. *Report Dept. Meteorology and Air Quality, Wageningen University*.
Van Dorn, W. (1953). Wind Stress on an Artificial Pond. *Journal of Marine Research, 12*(3), 249-276.
Viehmann, W., & Eubanks, A. (1972). Effects of Surface Contamination on the Infrared Emissivity and Visible-Light Scattering of Highly Reflective Surfaces at Cryogenic Temperatures(Simultaneous Measurement of Infrared Emissivity and Visible Llight Scattering of Contaminant Films on Highly Reflective, Stainless Steel Substrates at Cryogenic Temperatures). *Space Simulation p 489-502(SEE N 72-22250 13-11)*.
Vines. (1959). The Damping of Water Waves by Surface Films. *CSIRO Australia*.
Vines, R. G. (Ed.). (1962). *Evaporation control : A method of treating large water storages.* New York: Academic Press.
Vogel, V., & Moebius, D. (1989). Resonance of Tansverse Capillary and Longitudinal Waves as a Tool for Monolayer Investigations at the Air-Water Interface. *Langmuir, 5*(1), 129-133.
Volino, R. J., & Smith, G. B. (1999). Use of Simultaneous IR Temperature Measurements and DPIV to Investigate Thermal Plumes in a Thick Layer Cooled from Above. *Experiments in Fluids Springer-Verlag* (27), 70-78.
Wahlquist, A. (2008). *Thirsty Country. Options for Australia*. Sydney, Australia: Jacama Books. Allen & Unwin.
Wang, Q., Feder, A., Mazur, E. . (1994). Capillary Wave Damping in Heterogeneous Monolayers. *J. Phys. Chem. , Department of Physics and Division of Applied Sciences, Harvard University, Cambridge, Massachusetts*(98), 12720-12726.
Wangersky, P. (1976). The surface film as a physical environment. *Annual Review of Ecology and Systematics, 7*, 161-176.
Ward, A., & Trimble, S. (2004). *Enivonmental Hydrology*: Lewis Publishers
Watts, P. J. (1983). *Evaporation from an Agricultural Catchment : A Field and Theoretical Study of Evaporation.* University of Melbourne.
Weast, R. (Ed.). (1974). *Handbook of Chemistry and Physics*. Cleveland, Ohio, USA: CRC Press
Wells, P., Butler, J., & Hughes, J. (1995). *Exxon Valdez oil spill: fate and effects in Alaskan waters*.
Wieliczka, D. M., Weng, S., & Querry, M. R. (1989). Wedge Shaped Cell for Highly Absorbent Liquids: Infrared Optical Constants of Water. *Applied Optics, 28*, 1714-1719.
Williams, J. P., Mayberry, W. R., Payne, W. J. (1966). Metabolism of Linear Alcohols with Various Chain Lengths by a Pseudomonas Species. *Applied Microbiology, 14*(2), 156-160.
Wolbeer, H. J. (1963). *The calculated efficiency of monolayers in relation to increased water temperature*: Associate Research Officer, Saskatchewan Research Council.
WSAA. (2009). Water Services Association of Australia. *WSAA Media centre Facts and Figures* from https://www.wsaa.asn.au/Media/Facts/Pages/default.aspx
Wu, J. (1971). An Estimation of Oceanic Thermal-Sublayer Thickness. *Journal of Physical Oceanography, 1*, 284-286.

Wu, J. (1971). Evaporation Retardation by Monolayers: Another Mechanism. *Science, New Series, American Association for the Advancement of Science, 174*(No. 4006), 283-285.
Wu, J. (1975). Wind-Induced Drift Currents. *Journal of Fluid Mechanics, 68*(01), 49-70.
Wu, J. (1982). Wind-Stress Coefficients over Sea Surface from Breeze to Hurricane. *Journal of geophysical research, 87*(C12), 9704-9706.
Wu, J. (1988). On Nondimensional Correlation Between Roughness Length and Wind-Friction Velocity. *Journal of Oceanography, 44*(5), 254-260.
Wullschleger, S., Meinzer, F., & Vertessy, R. (1998). A Review of Whole-Plant Water Use Studies In Tree. *Tree Physiology, 18*(8-9), 499.
www.aquatain.com. (2008). Liquid anti-evaporation film. *Ultimate Products (Aust) Pty Ltd* Retrieved July-09, from www.aquatain.com.au
www.aquatain.com.au. (2009). Liquid anti-evaporation film. *Ultimate Products (Aust) Pty Ltd* Retrieved July-09, from www.aquatain.com.au
www.flexiblesolutions.com. (2009). Water$aver Application Rates and Coverage. Feb 2010, from http://www.flexiblesolutions.com/products/watersavr/
Yiasoumi, B. (2004). Leaking Farm Dams. *Ag Facts*, from http://www.dpi.nsw.gov.au/__data/assets/pdf_file/0004/164038/leaking-dams.pdfj
Yokoyama, R. a. S. T. (1991). Estimation of Sea Surface Temperature via AVHRR of NOAA and Comparison with Fixed Buoy Data. *Int. J. Rem. Sens*(12,), 2513-2528.
Zhang, Y. (1999). Moderate Resolution Imaging Spectrometer Emmisivity Library. *MODIS UCSB Emissivity Library* from http://www.icess.ucsb.edu/modis/EMIS/html/em.html
Zhu, F., Miao, R., Xu, C., & Cao, Z. (2007). Measurement of the Dispersion Relation of Capillary Waves by Laser Diffraction. *American Journal of Physics, 75*, 896.
Zisman, W. (1941). The Spreading of Oils on Water Part I. Ionized Molecules Having Only One Polar Group. *The Journal of Chemical Physics, 9*, 534.